

Design of Ka-Band Reflectarray for Space

Submitted by

Tan Xue Wen (A0139082E)

Department of Electrical & Computer Engineering

In partial fulfillment of the
requirements for the Degree of
Bachelor of Engineering
National University of Singapore

ABSTRACT

This dissertation will be presenting the process of designing the Ka-Band reflectarray antenna which is widely used in satellite application. There is high demand for such antenna due to its ease of fabrication and installation on any flat surface as opposed to a parabolic bowl antenna, while providing high gain. The design process can be broken down into two parts: element design & system design. Several element designs and reflectarray configurations were investigated to gain comprehensive understanding on the topic. The end product of this project is a Ka-band reflectarray with a circular aperture consisting of 51×51 square ring patch elements, operating at 28 GHz range. The elements are printed on a 60mil Rogers 4003C substrate, backed by a ground plane. The element grid size is 4.4mm ($\sim 0.411\lambda_0$), the square ring patch element can achieve up to about 400° of reflection phase variation by varying their size. The proposed reflectarray displays a peak gain of 33.94 dB with an aperture efficiency of 57.14% and a 1-dB gain bandwidth of 6%. The reflectarray is fed by an off-set pyramidal horn (LB-28-15) angled at 17.283° with a F/D ratio of 0.9. The proposed reflectarray design was also fabricated and tested in the microwave chamber / compact range to validate the theoretical design of the reflectarray. Lastly for exploration, a dual frequency/band reflectarray was further studied to overcome the narrow bandwidth characteristic (which is beyond the scope of this project). The author has also programmed an automated reflectarray designer software to provide a teaching platform for newcomer with zero experience in reflectarray.

ACKNOWLEDGMENTS

The author would like to dedicate this page to Prof. Chen Zhi Ning, Dr. Chia Tse Tong and Dr. Li Teng to specially thank them for their time and support throughout this project.

Prof. Chen Zhi Ning has given the author an opportunity to work on this wonderful project and funding on the fabrication of the antenna. Prof. Chen has been a great mentor who gives critical and constructive advice to the author since the start of the project. The author picked up this project because he was touched by Prof. Chen's teaching (EE2011) 2 years ago.

Dr. Chia Tse Tong kickstarted the entire project by introducing the author to the concept of reflectarray. Dr. Chia had been providing round-the-clock support whenever the author had doubts. He proof-read the author's writings throughout the entire FYP journey which is beyond his job-scope. In addition, he provided the author a workspace in Temasek lab. The author is extremely grateful for Dr. Chia unwavering guidance and hope to work with him again in the future if given the opportunity.

Lastly to Dr. Li Teng who supported the author on his last sprint for the fabrication and testing of the antenna. The fabricated antenna is a huge success thanks to him.

TABLE OF CONTENTS

ABSTRACT	i
ACKNOWLEDGMENTS	ii
LIST OF FIGURES	v
LIST OF TABLES	ix
LIST OF SYMBOLS AND ABBREVIATIONS	x
1 Introduction	1
1.1 Project Overview	1
1.2 Project Flowchart	3
2 Background	4
2.1 Antenna Fundamentals	4
2.2 Antenna Parameters	5
3 Literature Review	9
3.1 Reflectarray Antenna	9
3.2 Analysis and Design of Reflectarray	12
3.3 Phase Tuning Approaches for Reflectarray Element	17
4 Reflectarray – Element Design	21
4.1 Square Patch Element – Single Resonator	21
4.2 Square Patch Element – Multi-layering	22
4.3 Single Layer Multi-Resonating Element (Chosen)	25
5 Reflectarray – Center Feed Design	28
5.1 System Design – Pyramidal Horn Theory	28
5.2 System Design – LB-28-15 Feed	29
5.3 Reflectarray F/D and Phase Distribution	32
5.4 System Design – Element Mapping	33
5.5 System Design – AUTOCAD Script Automation	34
5.6 Simulation Result	35

6	Reflectarray – Offset Feed Design	45
6.1	Feed Position & Phase Distribution	46
6.2	Offset Configuration with Tilted Beam	51
7	Reflectarray – with a Splash Plate Feed	54
7.1	Design Approach for a Splash Plate	54
7.2	Narrow Beamwidth Splash Plate	59
8	Fabrication & Measurement Results	62
9	Conclusion and Future Work	65
10	Bonus & Exploration Work	66
10.1	Dual Frequency/Band Reflectarray for 5G Communication (28/38GHz)	66
10.2	Automated Reflectarray Design App	73
10.3	Radiation Analysis Techniques	74
	References	75
	Appendix A – Reflectarray Automation App Algorithm	77
	Appendix B – Health & Safety	87

LIST OF FIGURES

FIGURE 1: ANTENNA AS A TRANSITION DEVICE [2].	4
FIGURE 2: EXAMPLE OF RADIATION PATTERN IN 2D & 3D [2].	8
FIGURE 3: THE FIRST REFLECTARRAY ANTENNA USING WAVEGUIDE TECHNOLOGY [3].	9
FIGURE 4: COMPARISON BETWEEN REFLECTARRAY AND PARABOLIC REFLECTOR ANTENNA.	10
FIGURE 5: DIFFERENTIAL SPATIAL PHASE DELAY OF REFLECTARRAY: PHASE DIFFERENCE BETWEEN TWO PATHS S1 AND S2 FROM THE FEED TO THE REFLECTARRAY ELEMENTS.	11
FIGURE 6: GEOMETRY OF THE REFLECTARRAY [4].	13
FIGURE 7: VISUALIZATION OF THE RE-RADIATED WAVE.	13
FIGURE 8: PHASES ON THE APERTURE WITH AN OFFSET FEED AND OFF-BROADSIDE BEAM: (A) SPATIAL DELAY, (B) PROGRESSIVE PHASE, (C) PHASE DISTRIBUTION ON THE REFLECTARRAY ANTENNA, AND (D) PHASE DISTRIBUTION ON THE CONTINUOUS APERTURE. [4]	14
FIGURE 9: RADIATION PATTERN FOR DIFFERENT Q.	15
FIGURE 10: EXAMPLE OF EFFICIENCIES VS F/D PLOT.	16
FIGURE 11: WORKING MECHANISM OF THE PHASE-DELAY LINE.	17
FIGURE 12: APERTURE COUPLED PATCHES WITH SLOTS AND DELAY LINE [8].	18
FIGURE 13: EXAMPLE OF REFLECTARRAY USING VARYING ELEMENT SIZE.	19
FIGURE 14: MULTILAYER STRUCTURE – 3 LAYERS (LEFT) [9]; MULTILAYER ELEMENT – 2 LAYERS (RIGHT).	19
FIGURE 15: LEFT) SINGLE RESONATING ELEMENT; MIDDLE) DOUBLE RESONATING ELEMENT; RIGHT) TRIPLE RESONATING ELEMENT.	20
FIGURE 16: MODEL FOR THE SINGLE PATCH ELEMENT.	21
FIGURE 17: PHASE SHIFT VS R1 (LEFT); RETURN LOSS VS R1 (RIGHT) FOR SINGLE PATCH ELEMENT.	22
FIGURE 18: MODEL FOR 2-LAYER SQUARE PATCH ELEMENT.	23
FIGURE 19: PHASE SHIFT VS R1 (LEFT); RETURN LOSS VS R1 (RIGHT) FOR 2-LAYER SQUARE PATCH ELEMENT.	23
FIGURE 20: MODEL OF 2-LAYER SQUARE PATCH WITH DIFFERENT SIZE RATIO. $R_2 = K_1 \times R_1$ & PHASE SHIFT WITH DIFFERENT K_1 @ $\Theta = 0^\circ$.	24
FIGURE 21: PHASE SHIFT VS R1 (LEFT); RETURN LOSS VS R1 (RIGHT) FOR 2-LAYER SQUARE PATCH ELEMENT @ $K_1 = 0.7$.	25
FIGURE 22: MODEL OF SQUARE RING PATCH ELEMENT: $R_2 = K_1 \times R_1$, $W = K_2 \times R_1$.	26
FIGURE 23: (LEFT) VARYING K_1 @ $K_2 = 0.1$; (RIGHT) VARYING K_2 @ $K_1 = 0.6$, BOTH @ $\Theta = 0^\circ$.	26
FIGURE 24: PHASE SHIFT VS R1 (LEFT); RETURN LOSS VS R1 (RIGHT) FOR SQUARE RING PATCH ELEMENT @ $K_1 = 0.6$, $K_2 = 0.2$.	27

FIGURE 25: PYRAMIDAL HORN AND COORDINATE SYSTEM [2].	28
FIGURE 26: LB-28-15 SCHEMATIC DRAWING [11].	30
FIGURE 27: LB-28-15 RADIATION PATTERN A) DATASHEET [11] ; B) CST SIMULATED RESULT.	31
FIGURE 28: 3D RADIATION PATTERN OF THE LB-28-15 & Q VALUE FOR LB-28-15.	31
FIGURE 29: THEORETICAL F/D PLOT FOR D = 224.4MM & Q = 6.4.	33
FIGURE 30: CENTER FEED A) RAW PHASE DISTRIBUTION PLOT; B) NORMALIZED PHASE DISTRIBUTION PLOT BY 360°.	33
FIGURE 31: (A) DATASET CATEGORIZATION; (B) FINALIZED DIMENSION MAPPING.	34
FIGURE 32: ELEMENT DRAWING AUTOMATION PROCESS.	35
FIGURE 33: SYMMETRY PLANES FOR CENTER-FED REFLECTARRAY.	36
FIGURE 34: 3D RADIATION PATTERN FOR THE SQUARE RING PATCH ELEMENT DESIGN @ 28GHZ.	36
FIGURE 35: 2D RADIATION PATTERN FOR THE SQUARE RING PATCH ELEMENT DESIGN @ 28GHZ.	37
FIGURE 36: MAXIMUM REALIZED GAIN VS FREQUENCY FOR SQUARE RING PATCH ELEMENT.	38
FIGURE 37: 3D RADIATION PATTERN FOR THE SINGLE PATCH ELEMENT DESIGN @ 28GHZ.	38
FIGURE 38: 2D RADIATION PATTERN FOR THE SINGLE PATCH ELEMENT DESIGN @ 28GHZ.	39
FIGURE 39: MAXIMUM REALIZED GAIN VS FREQUENCY FOR SINGLE PATCH ELEMENT.	40
FIGURE 40: ILLUSTRATION OF PARABOLA WITH DEFINING PARAMETERS [12].	41
FIGURE 41: PARABOLIC REFLECTOR DESIGN WINDOW.	42
FIGURE 42: 3D RADIATION PATTERN FOR THE PARABOLIC BOWL REFLECTOR ANTENNA @ 28GHZ.	42
FIGURE 43: 2D RADIATION PATTERN FOR THE PARABOLIC BOWL REFLECTOR ANTENNA @ 28GHZ.	43
FIGURE 44: MAXIMUM REALIZED GAIN VS FREQUENCY FOR PARABOLIC BOWL REFLECTOR ANTENNA.	44
FIGURE 45: APERTURE BLOCKAGE IN FRONT-FED REFLECTARRAY SYSTEMS: (A) SYMMETRIC, (B) OFFSET [4].	45
FIGURE 46: GEOMETRY OF THE OFFSET CONFIGURATION.	46
FIGURE 47: OFFSET FEED A) RAW PHASE DISTRIBUTION PLOT, B) NORMALIZED PHASE DISTRIBUTION PLOT BY 360°.	47
FIGURE 48: DATASET CATEGORIZATION FOR OFFSET.	47
FIGURE 49: SYMMETRY PLANES FOR OFFSET-FED REFLECTARRAY.	48
FIGURE 50: 3D RADIATION PATTERN FOR SQUARE RING PATCH ELEMENT DESIGN - OFFSET FED CONFIGURATION @ 28GHZ.	48
FIGURE 51: 2D RADIATION PATTERN FOR THE SQUARE RING PATCH ELEMENT DESIGN - OFFSET FED CONFIGURATION @ 28GHZ, E-PLANE (TOP), H-PLANE (BOTTOM).	49
FIGURE 52: MAXIMUM REALIZED GAIN VS FREQUENCY FOR OFFSET FED REFLECTARRAY.	49

FIGURE 53: 3D RADIATION PATTERN FOR SQUARE RING PATCH ELEMENT DESIGN CENTER FED WITH STRUCTURE @28GHZ.	50
FIGURE 54: 2D RADIATION PATTERN FOR SQUARE RING PATCH ELEMENT DESIGN CENTER FED WITH STRUCTURE @28GHZ.	50
FIGURE 55: GEOMETRY OF THE OFFSET CONFIGURATION FOR TITLED BEAM.	51
FIGURE 56: OFFSET FEED WITH TITLED BEAM @ 17° PHASE DISTRIBUTION.	52
FIGURE 57: 3D RADIATION PATTERN FOR SQUARE RING PATCH ELEMENT DESIGN - OFFSET FED WITH TITLED BEAM AT -17° @ 28GHZ.	52
FIGURE 58: 2D RADIATION PATTERN FOR SQUARE RING PATCH ELEMENT DESIGN - OFFSET FED WITH TITLED BEAM AT -17° @ 28GHZ.	53
FIGURE 59: VISUALIZATION OF THE SPLASH PLATE FEED CONFIGURATION.	54
FIGURE 60: G.T.D MODEL [13].	55
FIGURE 61: GEOMETRY OF THE DESIGNED SPLASH PLATE.	56
FIGURE 62: RADIATION PATTERN OF THE SPLASH PLATE.	56
FIGURE 63: F/D PLOT FOR THE SPLASH PLATE CONFIGURATION.	57
FIGURE 64: 3D RADIATION PATTERN FOR SQUARE RING PATCH ELEMENT DESIGN WITH SPLASH PLATE FEED @ 28GHZ.	58
FIGURE 65: 2D RADIATION PATTERN FOR SQUARE RING PATCH ELEMENT DESIGN WITH SPLASH PLATE FEED @ 28GHZ.	58
FIGURE 66: GEOMETRY OF THE NARROW BEAMWIDTH SPLASH PLATE.	59
FIGURE 67: RADIATION PATTERN OF THE NARROW-BEAMWIDTH SPLASH PLATE.	60
FIGURE 68: F/D PLOT FOR THE NARROW BEAMWIDTH SPLASH PLATE CONFIGURATION.	60
FIGURE 69: 3D RADIATION PATTERN FOR SQUARE RING PATCH ELEMENT DESIGN WITH NARROW BEAMWIDTH SPLASH PLATE FEED @ 28GHZ.	61
FIGURE 70: 2D RADIATION PATTERN FOR SQUARE RING PATCH ELEMENT DESIGN WITH NARROW BEAMWIDTH SPLASH PLATE FEED @ 28GHZ.	61
FIGURE 71: MODEL OF THE REFLECTARRAY WITH THE HOLDING STRUCTURE.	62
FIGURE 72: FABRICATED REFLECTARRAY ANTENNA TESTED IN MICROWAVE CHAMBER (LEFT) & COMPACT RANGE (RIGHT).	63
FIGURE 73: MEASURED VS SIMULATED RESULT @ 28GHZ.	63
FIGURE 74: MEASURED MAXIMUM GAIN OVER FREQUENCIES.	64
FIGURE 75: REFLECTING SURFACE GEOMETRY OF A SINGLE-LAYER DUAL-FREQUENCY REFLECTARRAY ANTENNA.	67
FIGURE 76: GEOMETRY OF THE (A) 28 GHZ CROSS DIPOLE & (B) 38 GHZ SQUARE RING PATCH PHASING ELEMENT, $R_2 = K_1 \times R_1$, $W = K_2 \times R_1$.	68
FIGURE 77: REFLECTED PHASE RESPONSE VERSUS DIMENSION A) DIPOLE (L_1) & B) SQUARE RING PATCH (R_1).	69

FIGURE 78: F/D CURVE FOR THE PROPOSED DESIGN.	70
FIGURE 79: PHASE DISTRIBUTION CURVE FOR A) 28 GHZ & B) 38 GHZ.	70
FIGURE 80: SCHEMATIC VIEW OF THE DUAL-FREQUENCY REFLECTARRAY.	71
FIGURE 81: A) SIMULATED RADIATION PATTERNS AT 28 GHZ AND 38 GHZ; B) SIMULATED GAIN AND APERTURE EFFICIENCY IN FREQUENCY BAND.	72
FIGURE 82: 3D RADIATION PATTERN FOR BOTH 28GHZ AND 38GHZ STACKED TOGETHER.	72
FIGURE 83: GRAPHICS USER INTERFACE OF THE REFLECTARRAY DESIGN APPLICATION.	73
FIGURE 84: ARRAY THEORY VS CST SIMULATION RADIATION PATTERN.	74

LIST OF TABLES

TABLE 1: FREQUENCY VS GAIN OF LB-28-15 HORN ANTENNA [11].

44

LIST OF SYMBOLS AND ABBREVIATIONS

U	Radiation Intensity
f	Frequency
G	Gain
η_s	Spillover Efficiency
η_i	Illumination Efficiency
η_a	Aperture Efficiency
P	Power
E	Electric field
H	Magnetic field
A_e	Effective Aperture Area
λ	Wavelength
λ_0	Wavelength in free space
R_i	Displacement from feed to element i
k_0	Wavenumber in free space
φ_R	Required phase compensation by the phasing element
θ_o	Desired reflected beam in Theta direction
ϕ_o	Desired reflected beam in Phi direction
q	Q-Value
φ_{ref}	Reference phase
D	Diameter of aperture
D_0	Aperture Blockage Diameter

3D	3 Dimension
5G	5th Generation
AutoCAD	Auto Computer-Aided Design
BW	Bandwidth
CST MWS	Computer Simulation Technology Microwave Studio
dB	Decibel
dBi	Decibel Isotropic
EM	Electromagnetic
F/D	Focal to Diameter Ratio
FBP	Feed Beam Point
FNBW	First-Null Beamwidth
FSS	Frequency Selective Surface
FYP	Final Year Project
G.T.D	Geometrical Theory of Diffraction
HF	High Frequency
HFSS	High Frequency Structure Simulator
HPBW	Half Power Beamwidth
Hz	Hertz
IEEE	Institute of Electrical and Electronics Engineers
MATLAB	Matrix Laboratory
MIMO	Multiple-Input and Multiple-Output
NUS	National University of Singapore
PCB	Printed Circuit Board

PTFE	Polytetrafluoroethylene
RA	Reflectarray
RF	Radio Frequency
TEM	Transverse Electric & Magnetic
VSWR	Voltage Standing Wave Ratio

1 INTRODUCTION

1.1 PROJECT OVERVIEW

The project assigned for the Final Year Project (FYP) is on the study of “Design of Ka-Band Reflectarray for Space”. The project is mainly research in nature that deals with studies of the reflectarray operating in Ka-Band frequency. Ka-Band refers to the range of 26.5 – 40 GHz, which is often used for satellite communication. With the upcoming development in 5G mobile network communications, a Ka-Band reflectarray will be highly relevant because of the overlap in frequency band.

The reflectarray is widely used on satellite due to its ease of fabrication and installation on flat surfaces as opposed to a parabolic dish reflector antenna, while providing high gain. Unlike the parabolic dish reflector antenna that uses physical curvature to compensate for the phase difference, the reflectarray antenna uses an array of phasing elements to perform such a function. For this project, a 28 GHz reflectarray was designed and fabricated with high gain and aperture efficiency. In this project, CST Microwave Studio (CST WMS) suite is used to design and simulate the reflectarray antenna. CST MWS is a specialized tool for 3D electromagnetic simulation. It provides an insight into the EM characteristics of the high frequency (HF) designs [1].

The reflectarray design is split into two parts: the element design and the system design. At the element design stage, the main goal is to derive a phasing element (commonly known as the unit cell) with the ability to achieve 360° phase variation, with gentle dimension to phase change and minimal return loss. The dimension to phase transition must not be too drastic as there are limitations on the manufacturing precision. A unit cell phase can be tuned by varying the size of the element, by adding a delay line or rotating. Having a bad element design (inadequate phase variation and high return loss) will result in low-gain. The system design stage is where the position

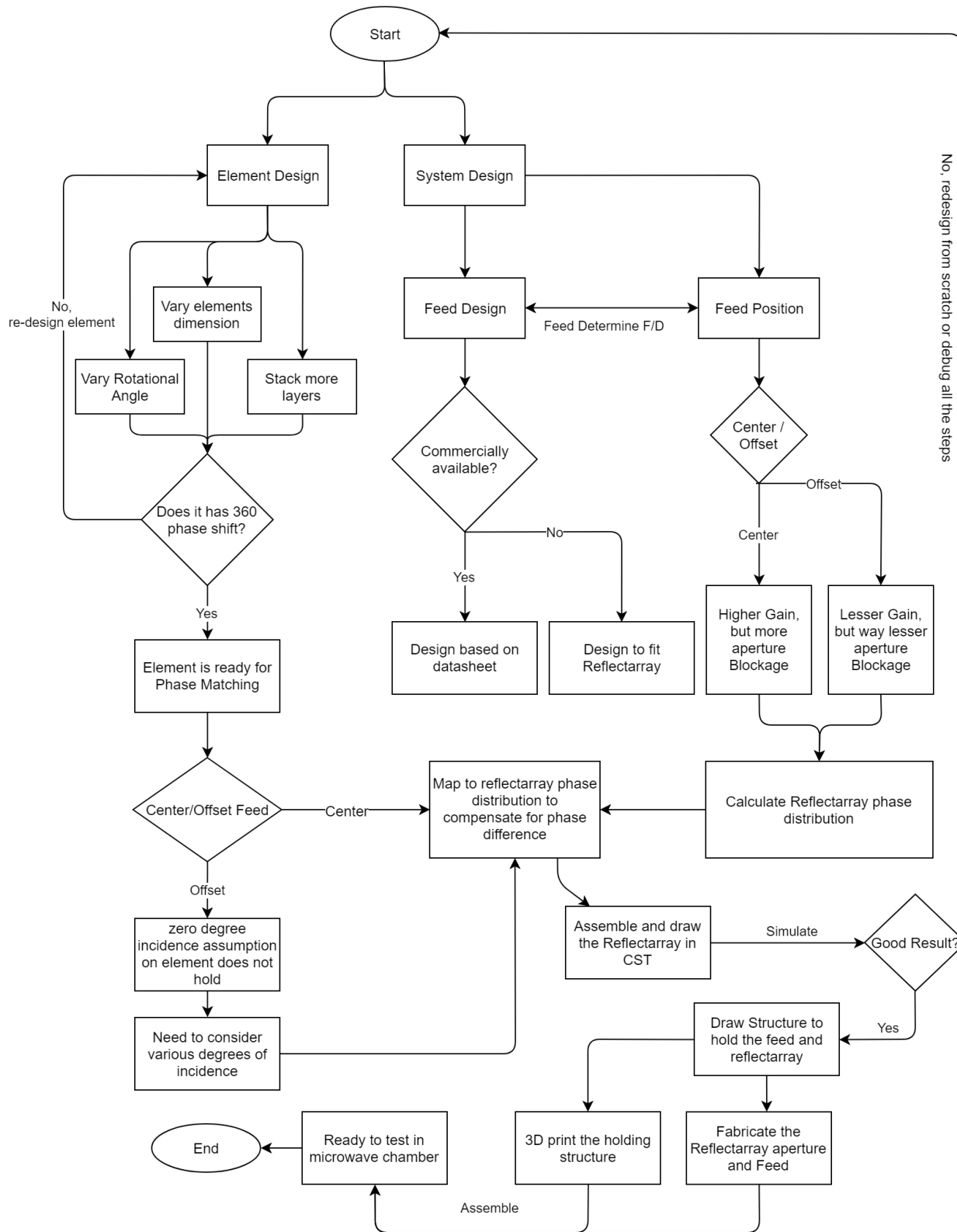
of the feed is considered: offset or center feed. The system can also be designed to operate in either far or near-field depending on its application. To achieve decent efficiency in a reflectarray, the F/D ratio is typically chosen between 0.7 and 1. However, the F/D ratio largely depends on the beamwidth of the feed. The F/D ratio is selected to achieve -10 dB radiation taper at the edges of the reflectarray aperture or by aperture efficiency analysis approach. Hence, the feed also plays a significant role in a working reflectarray. For this project, a commercially available feed (LB-28-15) is used.

After the element and system designs are finalized, the entire reflectarray is rendered using AUTOCAD for automated drawing and passed to CST for simulation. When a satisfactory result is achieved, the antenna is sent for fabrication where measurement in a microwave chamber/compact range is performed to validate the design.

The flow of this dissertation is as follows: literature review to cover the important aspect to designing a reflectarray, element designs to investigate on the different types of element, system designs to study on the different reflectarray configuration, fabrication and testing of the antenna to validate the theoretical design. Exploratory works are also carried out in the bonus section on a dual frequency/band reflectarray. An automated reflectarray design software programmed by the author to provide a teaching platform for newcomers is also presented.

The end product of this FYP is a working fabricated reflectarray antenna with a gain of 33.94 dB, an aperture efficiency of 57.14% and well-controlled sidelobe level at around -20 dB. It has been tested and proven in the compact range.

1.2 PROJECT FLOWCHART



2 BACKGROUND

2.1 ANTENNA FUNDAMENTALS

An antenna can be thought as a network between circuit and free space as it transforms electrical signals into electromagnetic signals when it transmits information while transforming electromagnetic signals back to electrical signals when it is receiving information through free space as shown in Figure 1.

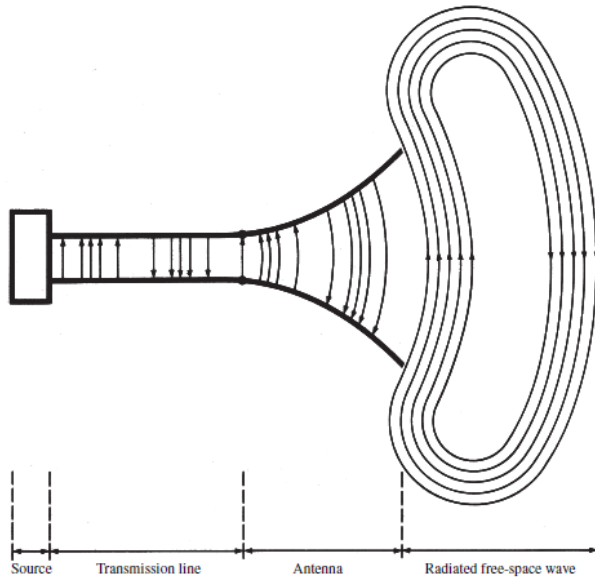


Figure 1: Antenna as a transition device [2].

Antennas can be categorized into two types: Isotropic and Directional. Examples of Isotropic antenna will be the Dipole and Monopole antenna. These antennas tend to have a wider beamwidth and can capture EM signals in an extremely wide angle (usually near 360°), lightweight and simple to design. However, the disadvantages are the extremely low gain and directivity of the antenna. Hence, these antennas are unsuitable for far-distance communication as the signals will become too weak. This is where the directional antenna comes into play. Examples of directional antennas are Yagi-Uda, aperture, array and reflector antenna.

2.2 ANTENNA PARAMETERS

Antenna parameters describe the performance and characteristics of an antenna. They are usually given to antenna engineers as the design requirement by the client. Key parameters are defined as below:

2.2.1 Radiation Pattern

A radiation pattern is a graphical representation of the radiation property of the antenna as a function of space coordinates [2]. Radiation pattern describes how the power is radiated out from the antenna and the scale is usually in logarithmic scale to highlight extremely small/big values. Radiation pattern can be plotted in two ways: 3 or 2 dimensional, as shown in Figure 2. Other than main lobe, the other lobes (known as side-lobes and back-lobe) are undesirable and should be minimized.

2.2.2 Directivity

Directivity describes how “focused” the antenna is to a specific direction. For example, an ideal isotropic antenna has a directivity of 1 (0dB) because it is not specifically tuned to transmit/capture power in a desired direction, but a parabolic dish reflector antenna can have a directivity as high as 30+ dBi (usually a pencil beam shape). A more formal definition is described as below:

$$D = \frac{U_{max}}{U_{avg}} \quad (1)$$

Where U_{max} is the maximum radiation intensity of the main beam and U_{avg} is the average radiation intensity over all space.

2.2.3 3dB Beamwidth

3dB Beamwidth is also known as Half Power Beamwidth (HPBW) as the 3dB refers to half. It is defined as the angular separation in which the magnitude of the radiation is reduced to 50%. Another convention that is also used is the First-Null Beamwidth (FNBW), which refers to angular separation in which the magnitude is zero. This property is usually related to directivity as smaller beamwidth usually means a very highly directed beam, however this is not always true if the antenna is badly designed.

2.2.4 Bandwidth

Bandwidth describes the range of frequency that the antenna can operate before it becomes unacceptable ($VSWR > 1.5$). The larger the bandwidth, the antenna can operate on a larger frequency range vice versa.

$$BW_{broadband} = \frac{f_{upper}}{f_{lower}} \quad (2)$$

$$BW_{narrowband} = \frac{f_{upper} - f_{lower}}{f_{center}} \quad (3)$$

Bandwidth is an important parameter to the entire RF design because it describes the sensitivity and tolerance of the antenna to frequency change. The gain might drop a lot with a small change around its operating frequency if the bandwidth is narrow.

2.2.5 Antenna Efficiency and Gain

Antenna efficiency is the ratio between input power and the output power. The input power is the power supplied to the antenna and the output power is the power radiated out. If the antenna can translate 100% of the input power to output power, means the antenna is ideal (lossless), and hence the antenna efficiency is 100% (which is usually not the case)

$$\eta_{rad} = \frac{P_{rad}}{P_{in}} \quad (4)$$

The gain of the antenna is related to the antenna efficiency and directivity by:

$$G = \eta_{rad} D \quad (5)$$

This gain is usually known as the IEEE gain in simulation software (HFSS or CST). There is also another gain that is more commonly used which is the realized gain. Contrary to the IEEE gain, realized gain includes loss from impedance and polarization mismatch. Thus, it is a more accurate representation of the antenna gain. In this project, realized gain is selected over IEEE gain when calculating the aperture efficiency of the antenna.

2.2.6 Effective Aperture Area & Aperture Efficiency

Effective Aperture Area is defined as the amount of useful area of the antenna that captures or transmits the EM waves. For example, if the antenna has a big area, but unable to transmit/capture the EM wave effectively, this means the effective aperture area of this antenna is low. Effective Aperture Area, A_e affects the directivity of an antenna directly. Aperture Area is related to directivity as follows:

$$D = \frac{4\pi A_e}{\lambda^2} \quad (6)$$

Another similar parameter used to measure the performance of the antenna is the aperture efficiency parameter. Aperture efficiency gives a visualization of the ratio of effective area over the real physical area. Often realized gain is used in place of directivity in order to find A_e as it accounts for matching loss, which is more realistic.

$$e_a = \frac{A_e}{A_{physical}} = \frac{G\lambda^2}{4\pi A_{physical}} \quad (7)$$

Aperture efficiency is usually calculated to determine whether an antenna is well designed.

2.2.7 Polarization

Polarization refers to the orientation of the electric field oscillations. It can be linear, circular or elliptical (usually if the circular is not perfect). A circular polarization may be desired to overcome polarization mismatch (e.g. a receiver antenna may be in the wrong orientation relative to the polarization of the incident field).

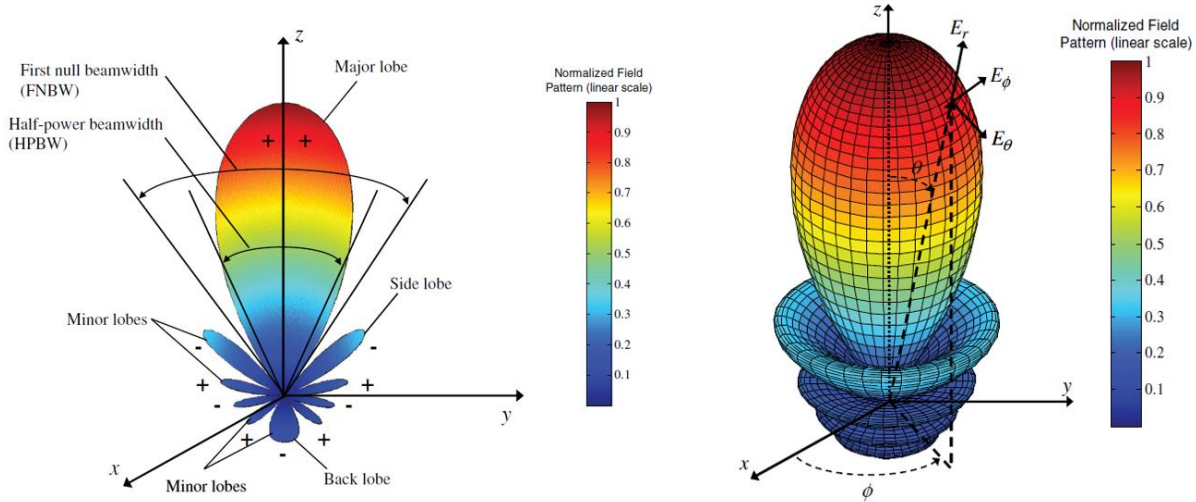


Figure 2: Example of radiation pattern in 2D & 3D [2].

3 LITERATURE REVIEW

3.1 REFLECTARRAY ANTENNA

3.1.1 Introduction

The very first reflectarray dates back to as early as 1963, where waveguides were used as the phasing elements. Its major drawback was its massive size and bulkiness as shown in Figure 3. Reflectarray antenna only gained attention after there was a breakthrough in printed microstrip antenna where elements were shrunk to a layer of thin metal making this idea more practical and affordable.

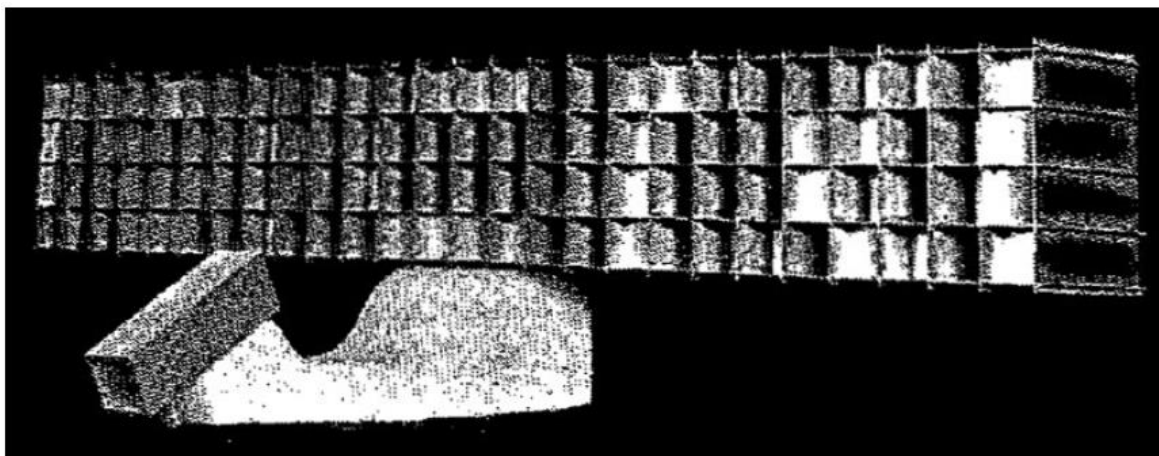


Figure 3: The first reflectarray antenna using waveguide technology [3].

The modern reflectarray can be thought as an amalgamation of both a parabolic reflector and a microstrip array antenna to counteract their limitations. The parabolic reflector is difficult and costly to manufacture due to the precision in making the parabolic shape, especially at higher frequencies. In addition, the parabolic reflector is incapable of achieving wide-angle electronic beam scanning. [4]

The microstrip array antenna is capable of sweeping wide-angle beam but the phase shifters required to perform such a function are extremely expensive. The phase shifters making up the beamformer are inefficient, often requiring amplifiers to compensate for the power loss. In addition,

microstrip patch array also suffers energy loss from the feeding network, which can be complicated to design. [4]

The reflectarray, on the other hand, combines the advantages of both the parabolic reflector and the array antenna to overcome the challenges of manufacturing the parabolic and need of phase shifters in an array antenna to attain a low cost but high gain and wide-angle beam-sweeping antenna.

As the name suggests, the reflectarray antenna is made up of array of elements (in this case the microstrip patch) that replaces the dish of a parabolic reflector. Its working mechanism is similar to the parabolic reflector with a feed antenna that will scatter EM waves on the reflector (made up of microstrip patches) which will be re-radiated back to space in a desired direction/angle. Figure 4 shows an illustration of the working mechanism of a reflectarray antenna with a parabolic reflector as comparison.

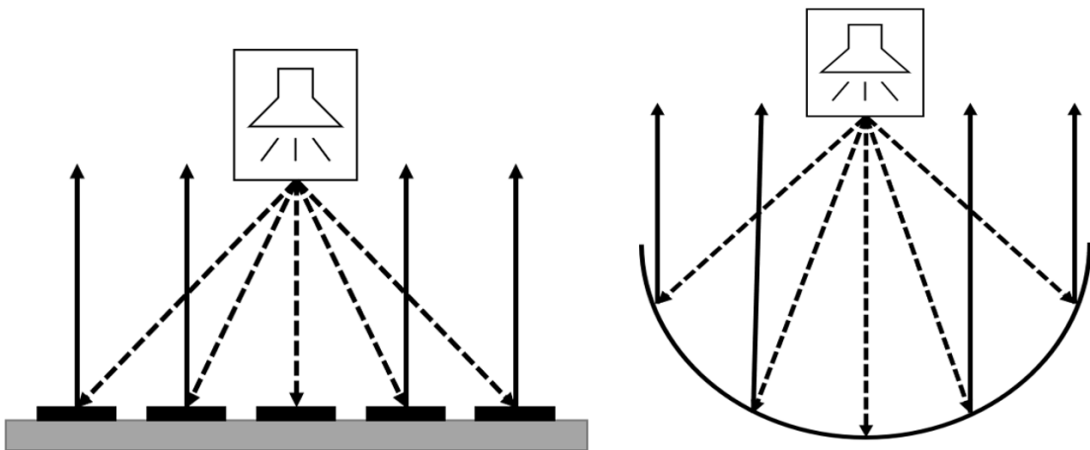


Figure 4: Comparison between reflectarray and parabolic reflector antenna.

In order to get a better idea, the following analogy can be made: In a parabolic reflector, the path difference is compensated by the curvature of the reflector dish so that each EM wave travels at the same distance when it hits the reflector; thus, each EM wave will have the same phase and is reflected in the same direction. The reflectarray works in similar manner, by introducing

phase delay when the EM wave hits the microstrip patch (or phasing element) to compensate for the path/phase difference [5]. There are various methods to fine tune the phasing element for such application, which will be discussed in the chapter 3.3.

The advantage of a reflectarray is the ability to achieve good efficiency of more than 50 percent (usually) without the need of power divider that is found in microstrip patch array. In addition, it is able to scan wide-angle using low-loss electronic phase shifters or by rotating the elements (if rotational elements are used). Moreover, compared to the parabolic dish, it is much more portable because the reflectarray aperture is foldable/collapsible and conformal to flat surfaces. Most importantly, it is cheaper than the parabolic dish since precision manufacturing can be avoided through printed circuit board (PCB) technology. [4]

However, despite its desirable traits, there are several shortcomings for the reflectarray antenna. First and foremost is its bandwidth. Since the elements are designed for a specific frequency, the reflectarray suffers from a narrow bandwidth characteristic. The bandwidth is limited by two factors: the bandwidth of the phasing elements and the differential spatial phase delay (refers to Figure 5). [6]

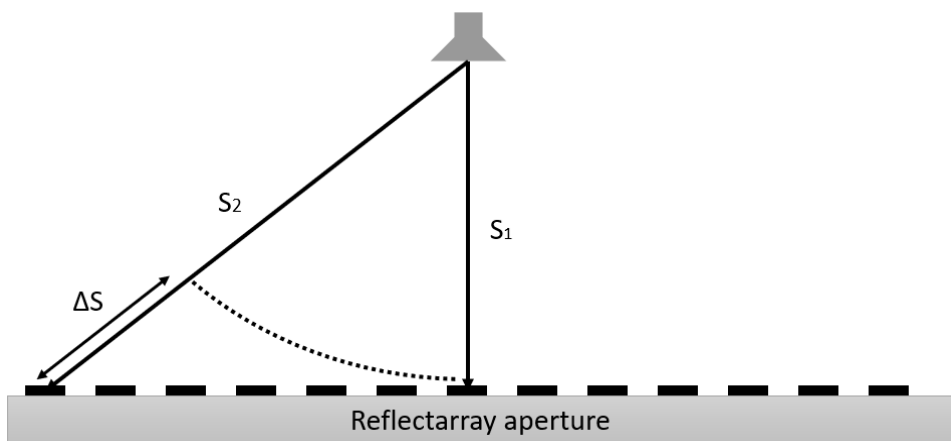


Figure 5: Differential spatial phase delay of reflectarray: phase difference between two paths S1 and S2 from the feed to the reflectarray elements.

3.2 ANALYSIS AND DESIGN OF REFLECTARRAY

A reflectarray antenna design can be broken down into two parts: the system design and the element design. The system design stage includes the study of the phase distribution of the reflectarray and feed position while the element design stage entails the design of phasing elements to meet the phase compensation needs of the reflectarray.

3.2.1 Phase Shift Distribution

The phase shift distribution plot describes the compensation requirement of each phasing element. Typically, the phase difference is directly related to the distance between the feed and element, the further the feed to the element, the more phase difference there is as compared to the nearest element. The nearest element refers to the element closest to the feed phase center, which is usually used as the phase reference for other elements.

The position of the feed also greatly affects the gain of the reflectarray antenna. A common practice will be setting the feed radiation level at the edge of the reflectarray at -10 dB (normalized to the peak of the feed radiation). However, for this dissertation an analytical approach is used instead as introduced in [7].

From Figure 6 and Figure 7, the required element phase shift can be derived by adding the spatial phase from feed phase center to that element, $-k_0 R_i$ and the phase shift introduced by the element. The resulting equation is given in (8).

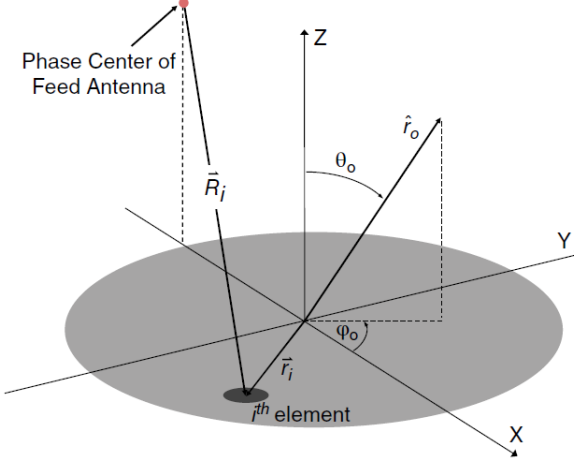


Figure 6: Geometry of the reflectarray [4].

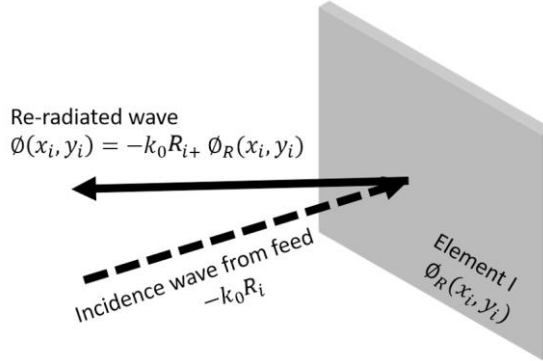


Figure 7: Visualization of the re-radiated wave.

$$\phi(x_i, y_i) = -k_0 R_i + \phi_R(x_i, y_i) \quad (8)$$

The negative sign came from using the $e^{j\omega t}$ convention. R_i refers to the distance from the feed phase center to the element i and $\phi_R(x_i, y_i)$ refers to the phase that the element introduces.

Next, to scan this collimated beam in any direction (θ_o, ϕ_o) , a progressive phase can be added to the aperture in the form of:

$$\begin{aligned} \phi_{pp} &= -k_0 \vec{r}_i \cdot \hat{r}_o \\ \phi_{pp} &= -k_0 (x_i \sin \theta_o \cos \phi_o + y_i \sin \theta_o \sin \phi_o) \end{aligned} \quad (9)$$

Equating equations 8 and 9, the phase distribution equation is derived:

$$\phi_R(x_i, y_i) = k_0 (R_i - (x_i \cos \phi_o + y_i \sin \phi_o) \sin \theta_o) \quad (10)$$

The reflectarray is somewhat similar to the parabolic reflector antenna, but the reflectarray consists of discrete compensation as such the phase distribution is pixelated unlike the parabolic reflector which is continuous (see Figure 8).

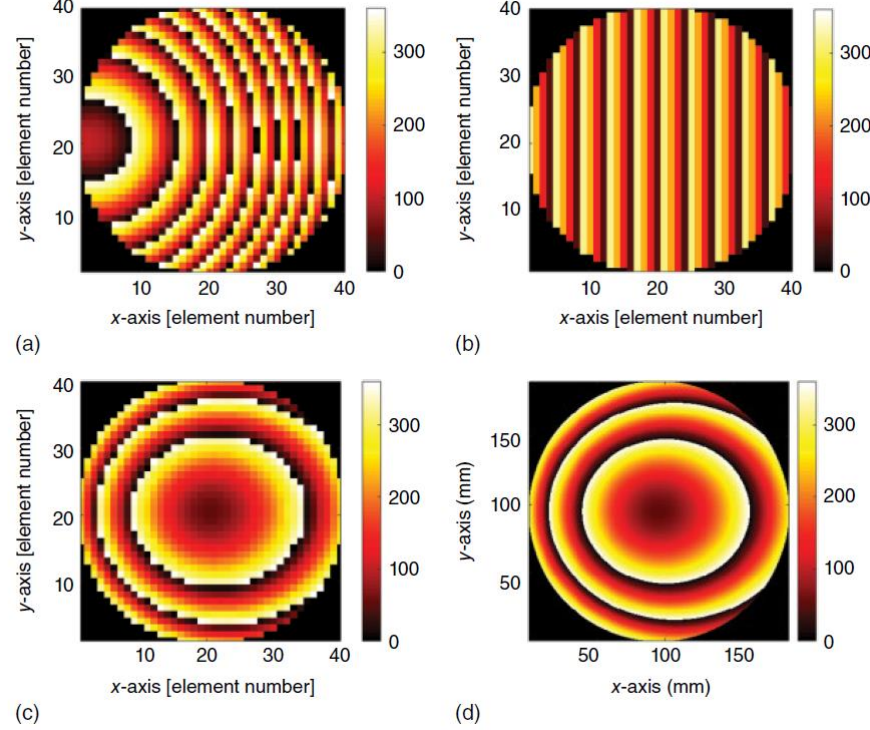


Figure 8: Phases on the aperture with an offset feed and off-broadside beam: (a) spatial delay, (b) progressive phase, (c) phase distribution on the reflectarray antenna, and (d) phase distribution on the continuous aperture. [4]

3.2.2 Optimal Focal Length to Diameter Ratio (F/D) by Analytical Methods

The common practice for selecting the F/D of a reflectarray is usually the -10 dB edge taper of the feed, so that there is a balance between spillover efficiency and illumination efficiency. There is an analytical approach on determining the F/D of the reflectarray. According to [7], the feeding beam is assumed to have a normalized power pattern of:

$$U_f(\theta, \phi) = \begin{cases} \cos^{2q} \theta & (0 \leq \theta \leq \frac{\pi}{2}) \\ 0 & \text{elsewhere} \end{cases} \quad (11)$$

The shape of the radiation pattern is determined by the q value of the feed. The larger the q value, the narrower the beamwidth (see Figure 9).

Next, the radiation pattern of the scattering element is similarly assumed to be given by:

$$U_e(\theta, \phi) = \begin{cases} \cos^{2q_e} \theta_e & (0 \leq \theta \leq \frac{\pi}{2}) \\ 0 & \text{elsewhere} \end{cases} \quad (12)$$

Most of the time, the q_e value of the scattering element can be safely assumed to be one.

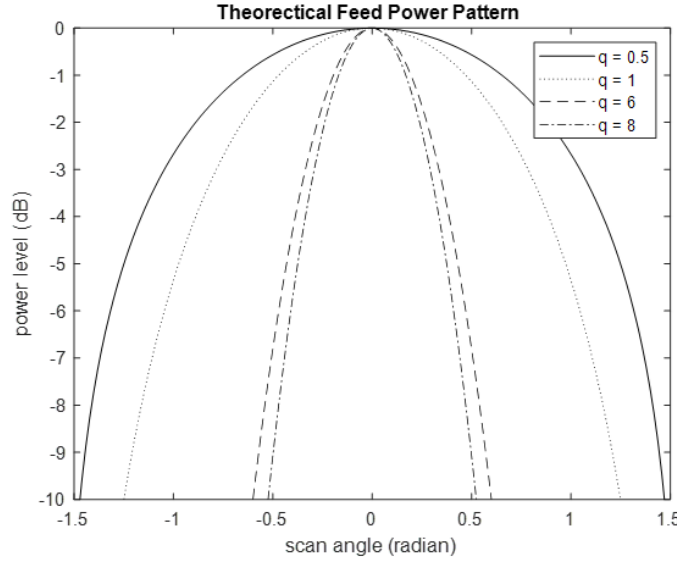


Figure 9: Radiation pattern for different q .

Spillover efficiency and illumination efficiency are needed to be found first before the calculation of the theoretical peak aperture efficiency. Spillover efficiency is defined as the ratio of the power captured by the reflectarray aperture to the total radiated power of the feed, given mathematically by

$$\eta_s = \frac{\int \int \vec{P}(\vec{r}) \cdot d\vec{s}}{\sum \int \int \vec{P}(\vec{r}) \cdot d\vec{s}} \quad (13)$$

The illumination efficiency is a measure of how close the realized aperture distribution is to uniform illumination. Mathematically, it is given by

$$\eta_i = \frac{1}{A_a} \frac{\left| \iint_A I(x, y) dA \right|^2}{\iint_A |I(x, y)|^2 dA}, \quad (16)$$

where A_a is the aperture area and $I(x, y)$ is the amplitude distribution over the aperture.

After numerically obtaining the spillover and illumination efficiencies, the aperture efficiency is a product of the former two efficiencies:

$$\eta_a = \eta_s \eta_i \quad (18)$$

The three efficiencies are plotted in Figure 10 for a circular reflectarray aperture of diameter 224.4 mm with a center-fed feed of $q = 6.4$. The optimal F/D in this case is around 0.9. Although the above analysis is only applicable for center-fed reflectarray, it provides a useful starting point for offset-fed configurations.

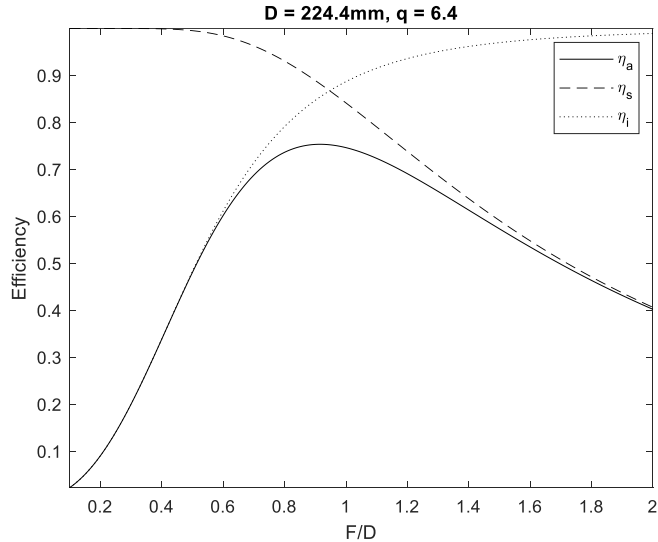


Figure 10: Example of efficiencies vs F/D plot.

3.3 PHASE TUNING APPROACHES FOR REFLECTARRAY ELEMENT

The phasing elements are the building blocks of the reflectarray aperture. Without a good phasing element design, one can expect the reflectarray to be extremely inefficient with low gain. There are three ways to tune the phase of phasing element: adding a delay line to the element, varying the element size and rotating the element for circular polarized design.

3.3.1 Elements with Phase/Time-Delay Line

In this approach, the incident wave is first captured by the element, then the signal enters the delay-line, gets reflected at the end of the line, re-enters the element and is re-radiated [5]. The idea is demonstrated in Figure 11.

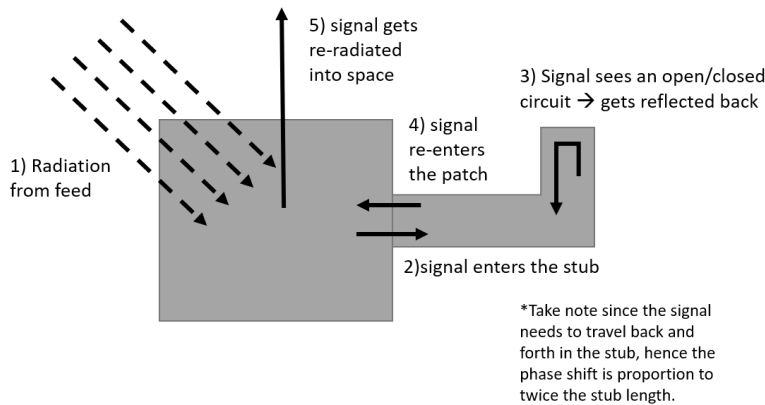


Figure 11: Working mechanism of the Phase-Delay line.

The phase shift is proportional to the length of the stub, which can be expressed as

$$\phi_{delayline} = 2kl \quad (19)$$

where k is the propagation constant of the signal along the stub and l is the length of the stub. The equation is quite intuitive, the longer the phase delay because the wave has to travel a longer distance.

The advantage of this element is the ease of fabrication with current printed circuit technology. The design is also fairly straightforward. However, the flaws include the

accommodation of the stubs, as there may be insufficient space on the surface; the stubs may introduce spurious radiation. Since the wave has to travel along the stub (more often than not is not lossless), there will be deterioration in electrical performance. However, there are several ways to overcome some of these challenges. One way is by having multiple layers, one for the patches and one for the stubs. This technique is often known as the *Aperture-Coupled Patches with slots and lines of variable length*. [8] [9] This idea is demonstrated in Figure 12, where there are element layer and phase shifting layer.

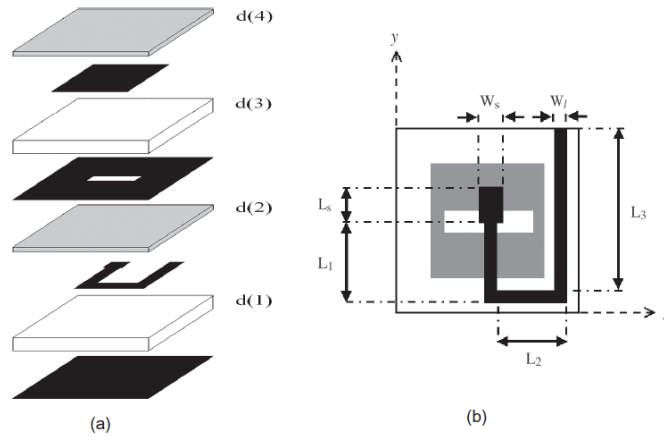


Figure 12: Aperture Coupled Patches with slots and delay line [8].

The delay line can be broken down into two parts: stub and variable length delay line. The stub is used for matching impedance to the patch while the variable length delay line will be responsible for shifting the phase. Due to the additional layer, there will be space for the stubs. In addition, the phase response is relatively linear as compared to the variable size patch and the spurious radiation from the stubs is absorbed and eliminated by the ground plane. However, it is bulkier due to multiple layers.

3.3.2 Varying Element Size

Elements of different size will operate at different resonance frequency. Making use of this property, each element can be phase tuned by varying the size as shown in Figure 13. In an ideal

case, a single resonance can provide a complete cycle of 360° but in reality, the common practice is to use more than one resonant element to achieve a complete cycle. Typically, for a substrate with thickness of less than $1/10$ wavelength, a phase shift above of 300° is attainable for a single resonant element [4].

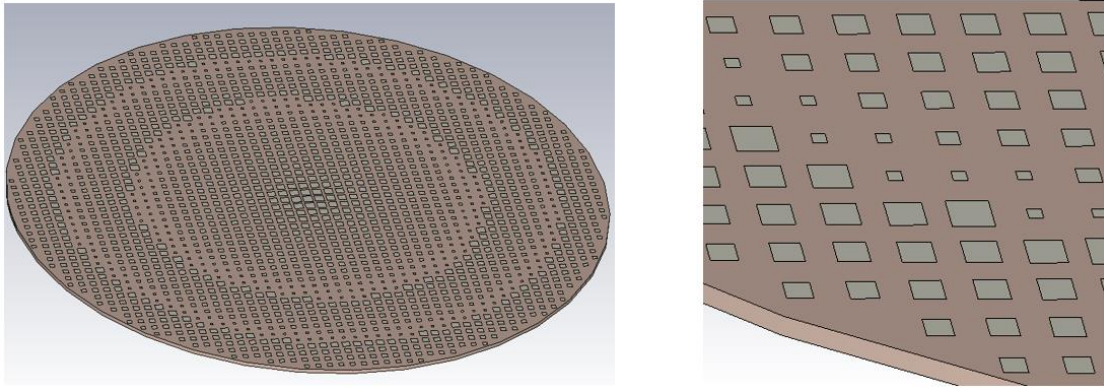


Figure 13: Example of reflectarray using varying element size.

Phasing element with less than a full cycle is usually undesirable because it is unable to fully compensate for the phase difference, resulting in a less focused beam and a lower gain reflectarray. There are a few strategies to mitigate this shortcoming. Stacking several layers of patches is one way to create an element with a complete cycle. This well-known technique is commonly known as multi-layering as shown in Figure 14.

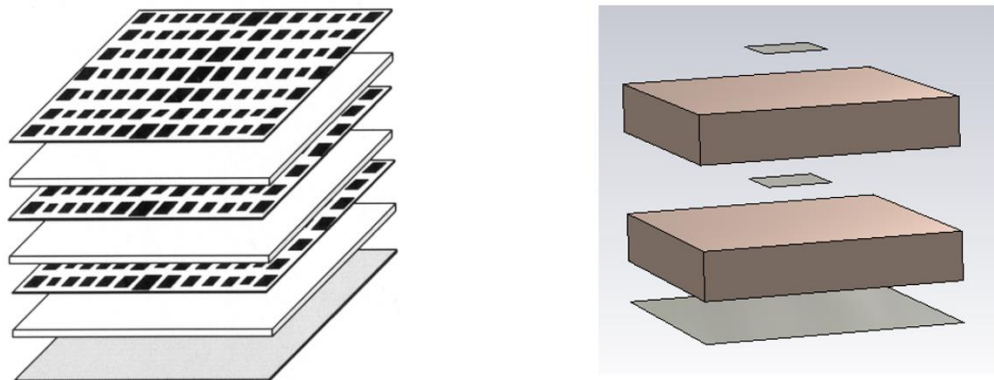


Figure 14: Multilayer structure – 3 layers (left) [9]; Multilayer element – 2 layers (right).

Another way is to introduce multiple resonating elements [10] in the design. Instead of using only a single patch, introducing a square ring surrounding the square patch or using double

ring elements can help to achieve a full cycle (see Figure 15 for examples). In an ideal case, one element can achieve 360° and two elements can achieve 720° . However, in reality, the phase variation achieved is lesser than the ideal case.

To achieve phase linearity and lower sensitivity to dimension change, a thicker substrate can be used. This is particularly important, as the fabrication of the antenna may not be able to meet the strict demand for the physical dimension of the elements. The next chapter will investigate and experiment with various element designs.

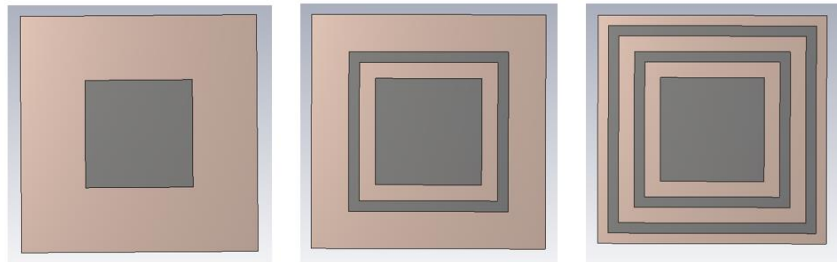


Figure 15: Single resonating element (left); Double resonating element (middle); Triple resonating element (right).

4 REFLECTARRAY – ELEMENT DESIGN

In this project, the element size is 4.4×4.4 mm or $2\lambda/5$ (within the $1/2 - 1/3 \lambda$ range [4]) at 28 GHz. Rogers4003C, a commercially available substrate, is used as the substrate. There are a few design constraints such as having the **smallest space and width at 0.1mm** due fabrication precision limitation.

4.1 SQUARE PATCH ELEMENT – SINGLE RESONATOR

This is the most basic element for reflectarray where variable square patches are used to fine-tune the phase of each element as shown in Figure 16. The length of the patch varies from 1 to 3.57 mm. A simple square patch element is expected to have less than 360° of phase shift. In reality, the single patch element is rarely used. However, we will use it as a reference for other elements to show the importance of a full cycle phase variation.

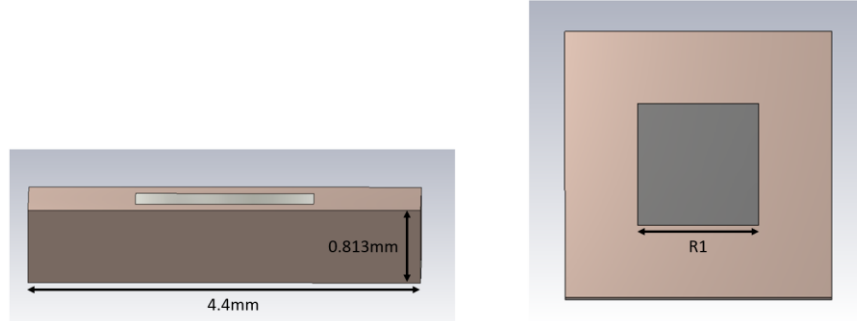


Figure 16: Model for the single patch element.

The element is simulated in the CST software where for the incident angle varying from 0° to 60° . At each incident angle, the dimension R1 is varied to determine the reflection phase and the reflection loss. The results are shown in Figure 17. As expected, a single patch resonator element is unable to provide a full cycle of 360° . At $\theta=0^\circ$, the maximum phase variation is around 250° only. The following sections will explore more element designs that will overcome the challenge faced by the single resonator.

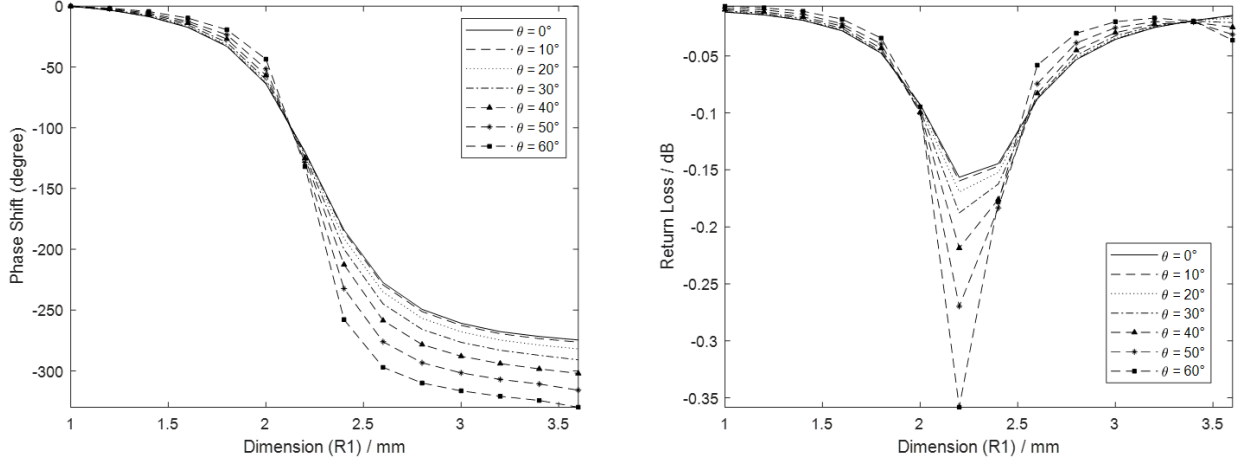


Figure 17: Phase Shift vs R_1 (left); Return Loss vs R_1 (right) for single patch element.

4.2 SQUARE PATCH ELEMENT – MULTI-LAYERING

As discussed in the previous chapter, multi-layering is one of the most common ways to increase the phase shift. By stacking the elements on top of one another, we can effectively increase the phase shift by approximately two times. This is the most convenient method to increase the phase shift, as it does not require complicated design.

Figure 18 illustrates the “2-layer element” which is constructed by stacking up the square patch element seen in Section 4.1. As there are two layers, the design can be thought as having two resonators per element; hence, it should be able to provide more than 360° phase variation as shown in Figure 19. Even though the phase variation is over 400° , this design is not feasible for usage. When R_1 is around 2.2 to 2.4, the phase is extremely sensitive to dimensional change. Some dimensional deviation will result in a big difference in phase shift. This will require a very strict precision demand on the fabrication of the reflectarray antenna.

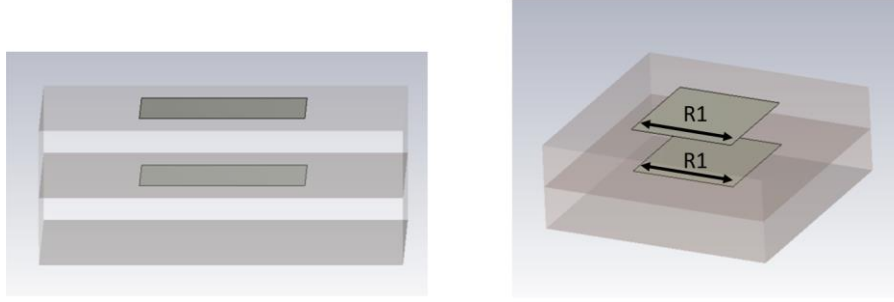


Figure 18: Model for 2-layer square patch element.

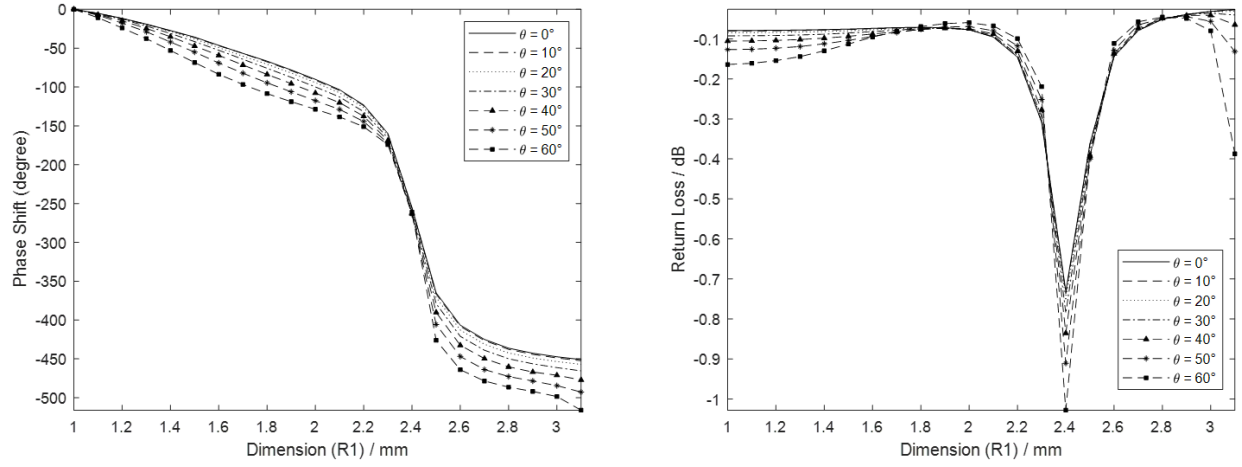


Figure 19: Phase Shift vs $R1$ (left); Return Loss vs $R1$ (right) for 2-layer square patch element.

Since this element can achieve such wide range of phase variation, there are a few ways to make the phase gradient gentler at the cost of phase range. The first way is to use thicker substrates. A common practice that is similar to this approach is to use air gap instead of thickening the substrate to cut cost. Some designers will use foam as a substitute to air gap as they have similar properties.

Another way is by making the sizes of top and bottom patch different. In this example, different proportions will be explored in order to find the optimal proportion for the design (see Figure 20). The reason why this method will work is that when the top and bottom have a different proportion, they will have different resonating frequencies. If the top and bottom are exactly the same size, they will have the same frequency response, which in turn amplify the resonating frequency change causing the steep phase gradient as seen above.

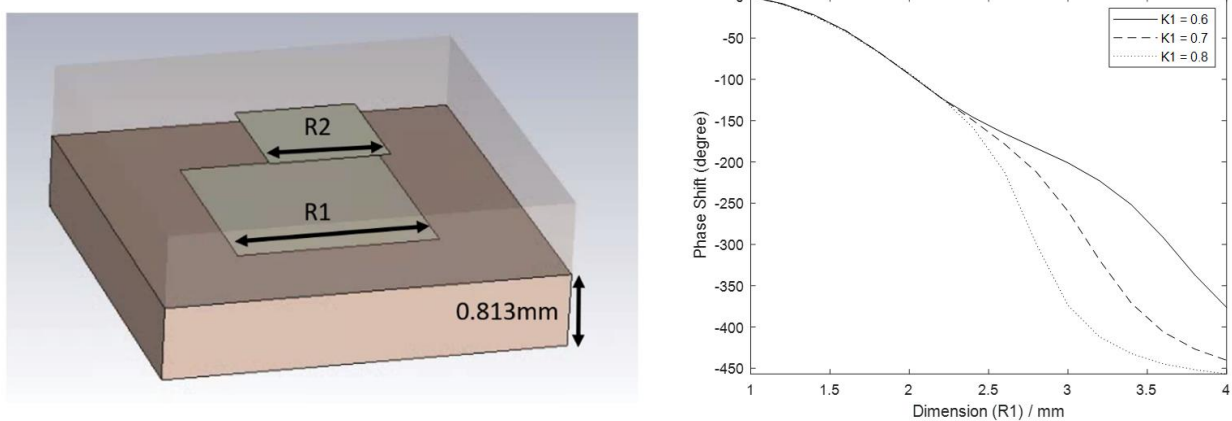


Figure 20: Model of 2-layer square patch with different size ratio. $R2 = K1 \times R1$ & Phase shift with different $K1$ @ $\theta = 0^\circ$.

Based on the simulation results in Figure 20, $K1 = 0.8$ becomes too steep after $R1 = 2.5\text{mm}$. For $K1 = 0.6$, even though the gradient is quite gentle, it barely reaches 360° . Hence, $K1=0.7$ with 360° phase range and a gentle slope is the most suitable choice for this design.

Compared to the previous design which had the same size for both top and bottom layers, this is a much better design with good linearity and slow changing phase variation while achieving a full cycle. Multilayer reflectarray is more common in situation where the elements are not possible to fabricate because it is too small as in mm-wave designs.

Figure 21 shows the phase and loss of the latest design for different incident angles up to 60° . The phase range remains more than 360° for all incident angles. The loss is worst for incident angle of 60° , but it is still less than 1 dB.

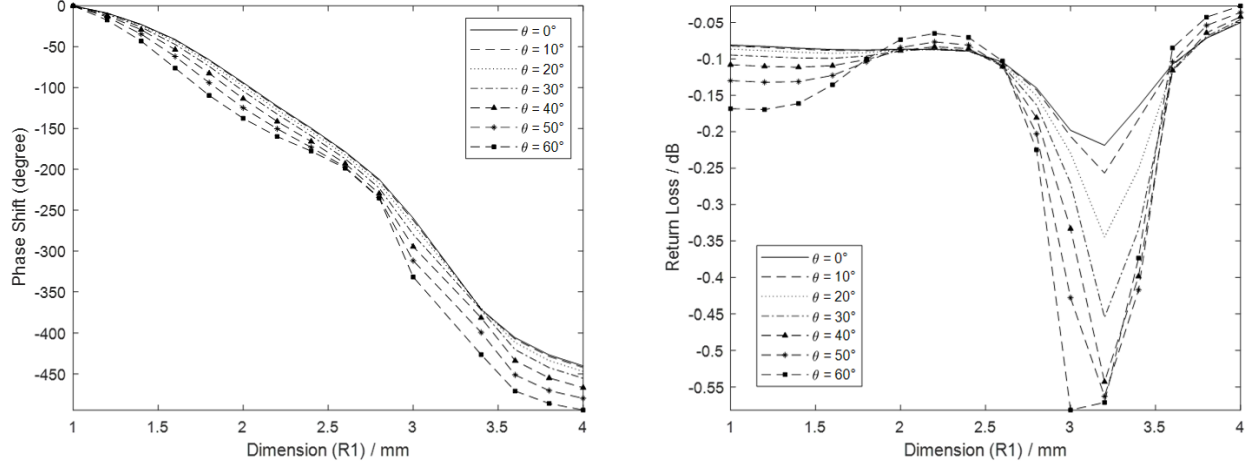


Figure 21: Phase Shift vs R_1 (left); Return Loss vs R_1 (right) for 2-layer square patch element @ $K_1 = 0.7$.

4.3 SINGLE LAYER MULTI-RESONATING ELEMENT (CHOSEN)

As shown previously, having multiple resonating elements can help to achieve a full cycle. The single layer multi-resonating element approach involves an element where two or more resonators are printed on a single layer as seen in Figure 15. Most reflectarray designers favour this approach as it only requires a single layer, making the design less costly than the multi-layer design while achieving a similar outcome. The combinations are usually: double square rings, double circular rings or a ring surrounding a patch.

The square ring patch design is able to achieve a phase shift of more than 360° . It has two degree of freedom, the relative size of the inner patch, the width of the outer ring. This section will explore the different dimensionality of the double square ring patch to derive the optimized parameters for the phasing element (see Figure 22).

From Figure 23, $K_1=0.6$ is selected as $K_1 = 0.4$ is definitely out due to its insufficient phase shift and $K_1 = 0.5$ barely made it. $K_1 = 0.7$ has too steep a gradient for R_1 between 2 to 3 mm @ $K_2 = 0.2$.

For K2, any choice of the three values in Figure 23 is acceptable as the three curves are quite similar @ $K1 = 0.6$. $K2 = 0.1$ is chosen due to the fabrication precision limitation. If $K2=0.075$ is used, the smallest W will be 0.075 mm, which is beyond the fabrication limit of 0.1 mm. For $K2 = 0.125$, the gradient is slightly steeper than $K2 = 0.1$.

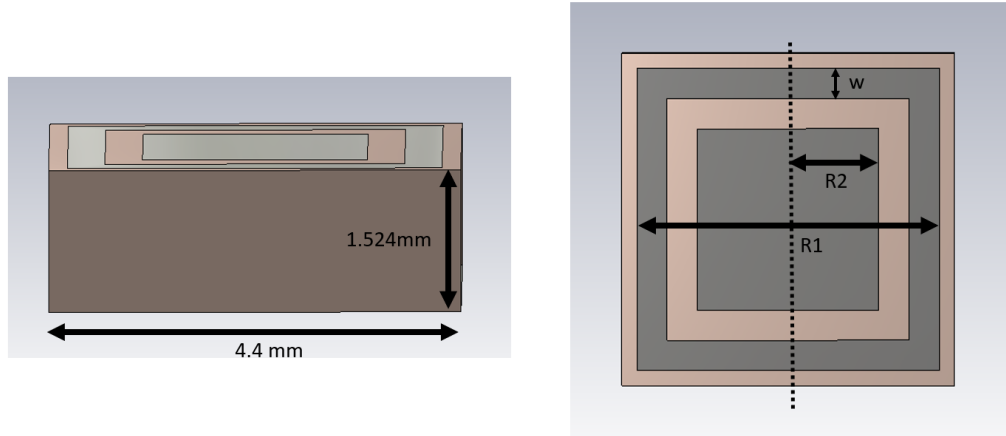


Figure 22: Model of square ring patch element: $R2 = K1 \times R1$, $W = K2 \times R1$.

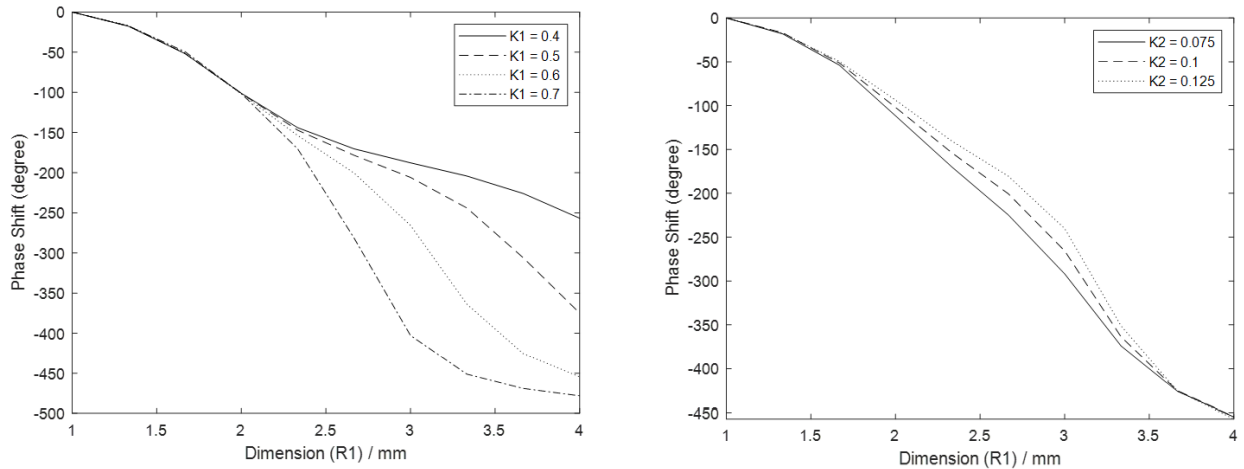


Figure 23: Varying $K1$ @ $K2 = 0.1$ (left); Varying $K2$ @ $K1 = 0.6$ (right), Both @ $\theta = 0^\circ$.

Figure 24 shows phase and loss variation for the selected design. The phase response over incident angles is acceptable while the return loss is negligible (less than 0.4 dB). Compared to the multi-layer element, this single-layer element generally has a gentler gradient especially for 0° incidence angle. From the fabrication perspective, it is cheaper to fabricate a single-layer PCB and

is also easier to assemble. Overall, after exploring the options, the multi-resonant element is the most suitable for this project and will be chosen as the representative element.

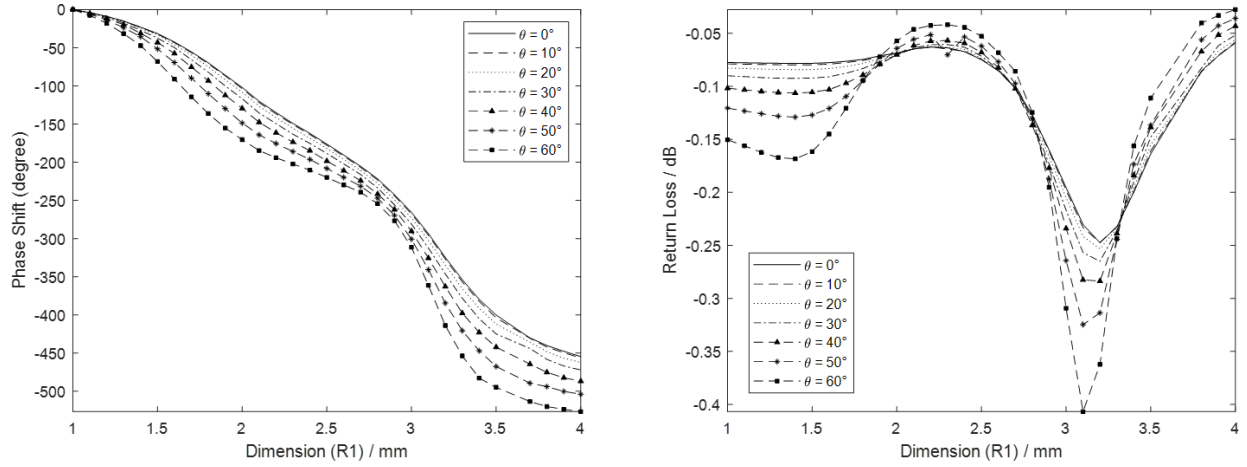


Figure 24: Phase Shift vs R_1 (left) ; Return Loss vs R_1 (right) for square ring patch element @ $K_1 = 0.6$, $K_2 = 0.1$.

5 REFLECTARRAY – CENTER FEED DESIGN

5.1 SYSTEM DESIGN – PYRAMIDAL HORN THEORY

The knowledge behind creating a pyramidal horn is not required in this project because in order to cut cost, commercially available horn in the lab is used instead hence designing one is optional. However, there are times when the designer has to create his/her pyramidal horn to fit into the reflectarray design and some horns may not be available and has to be fabricated from scratch. This section will explore the theory of pyramidal horn design.

The characteristics of a horn antenna can be adjusted using the following parameters: start point (a, b), end point (a₁, b₁) and length of horn antenna (p_h & p_e) as shown in Figure 25.

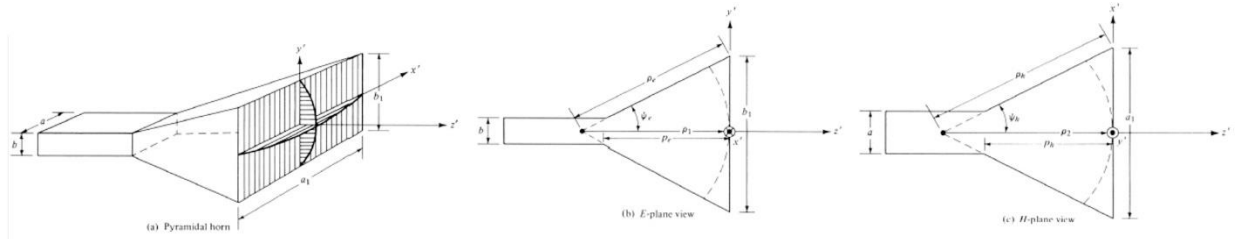


Figure 25: Pyramidal horn and coordinate system [2].

The gain of the horn antenna can be expressed as

$$G_0 = \frac{1}{2} \frac{4\pi}{\lambda^2} (a_1 b_1) \approx \frac{2\pi}{\lambda^2} \sqrt{3\lambda\rho_h} \sqrt{2\lambda\rho_e} \quad (20)$$

Equation 20 is further manipulated into the following:

$$\left(\sqrt{2\chi} - \frac{b}{\lambda}\right)^2 (2\chi - 1) = \left(\frac{G_0}{2\pi} \sqrt{\frac{3}{2\pi}} \frac{1}{\sqrt{\chi}} - \frac{a}{\lambda}\right)^2 \left(\frac{G_0^2}{6\pi^3} \frac{1}{\chi} - 1\right) \quad (21)$$

where

$$\frac{\rho_e}{\lambda} = \chi \quad (22)$$

$$\frac{\rho_h}{\lambda} = \frac{G_0^2}{8\pi^3} \left(\frac{1}{\chi}\right)$$

Equation 21 is also known as the horn-design equation.

The first step is to find the value of χ which satisfies equation 21. The starting value for the iteration is $\chi(tiral) = \frac{G_0}{2\pi\sqrt{2\pi}}$ and will stop when χ is found. Using this χ value, ρ_e and ρ_h can be found with equation 22.

The values of a_1 and b_1 can be found using the following formula (equation 23):

$$a_1 = \sqrt{3\lambda\rho_h} = \frac{G_0}{2\pi} \sqrt{\frac{3}{2\pi\chi}} \lambda \quad (23)$$

$$b_1 = \sqrt{2\lambda\rho_e} = \sqrt{2\chi}\lambda$$

Values of P_e and P_h (length of the horn) can be calculated using:

$$P_h = (a_1 - a) \left[\left(\frac{\rho_h}{a_1} \right)^2 - \frac{1}{4} \right]^{1/2} \quad (24)$$

$$P_e = (b_1 - b) \left[\left(\frac{\rho_e}{b_1} \right)^2 - \frac{1}{4} \right]^{1/2}$$

Regarding about the G_0 value, the higher the G_0 value, the smaller the beamwidth of the horn, hence the magnitude at the edge will also be reduced. However, the equations are not perfect and still requires a lot of tweaking before getting the desired radiation pattern. There is an algorithm for horn antenna design that is written in MATLAB in [2].

5.2 SYSTEM DESIGN – LB-28-15 FEED

This project will be using a commercially available 26.5 – 40.0 GHz standard gain horn antenna from A- Info: LB-28-15 [11]. This horn is suitable for this project as it has a q value of

6.4 hence the beamwidth is not too narrow or wide and it operates in the Ka-Band. The horn will be used in the C Type configuration as shown in Figure 26.

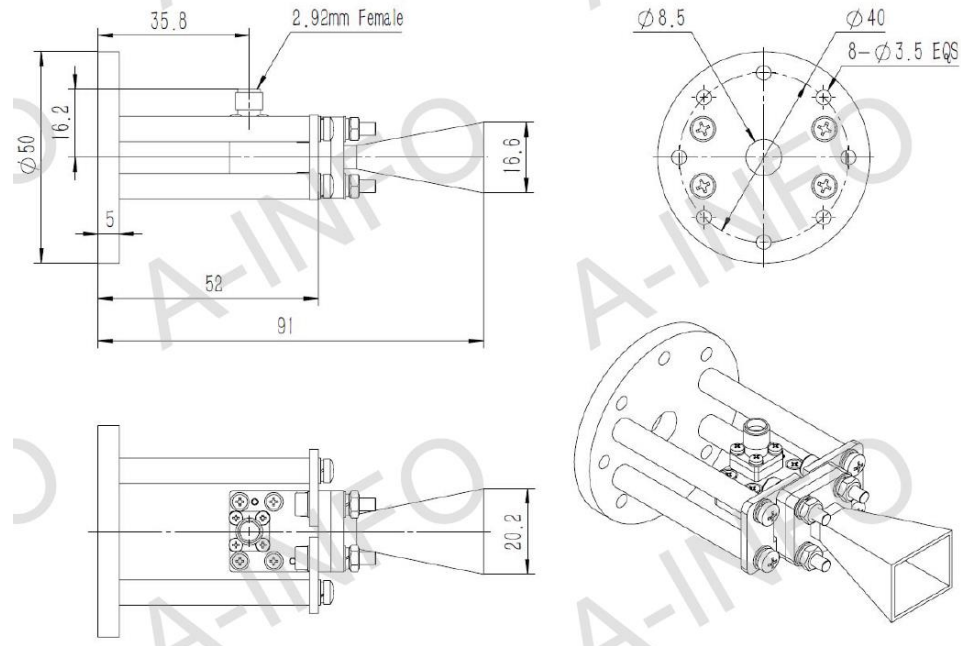


Figure 26: LB-28-15 schematic drawing [11].

The horn is modelled in CST using the schematic drawing given by [11]. To check whether the model is drawn correctly, there is a sample radiation pattern provided by the manufacturer for the frequency @ 28 GHz to check against the CST simulated radiation pattern in Figure 27. Comparing the datasheet radiation pattern and CST simulated result, the radiation pattern is more or less the same, but the most important thing is that the beamwidth is similar, as this will affect the F/D analysis later.

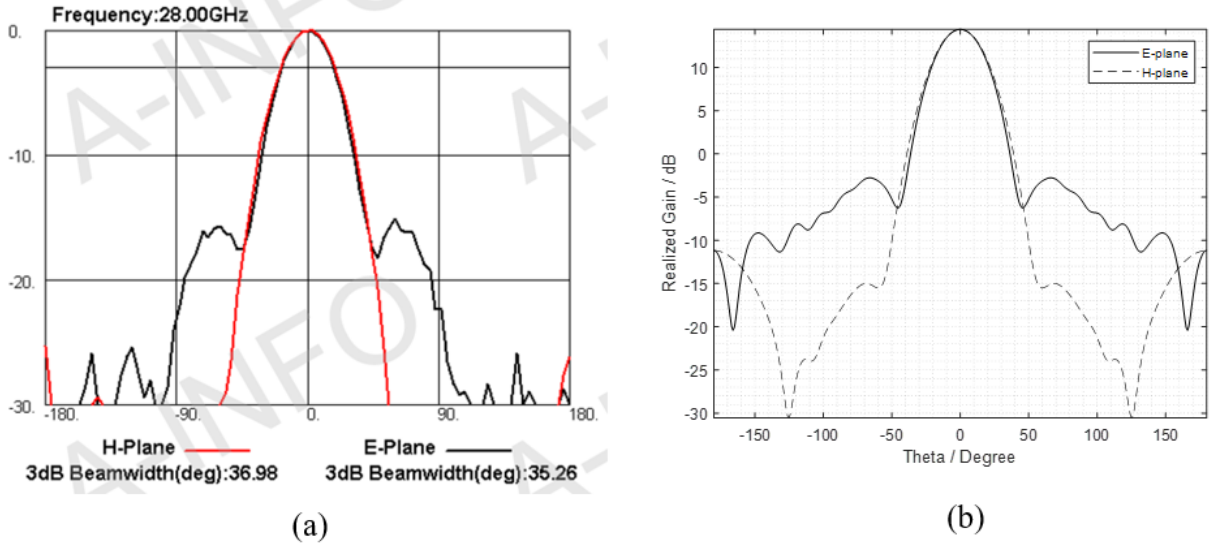


Figure 27: LB-28-15 radiation pattern a) Datasheet [11] ; b) CST simulated result.

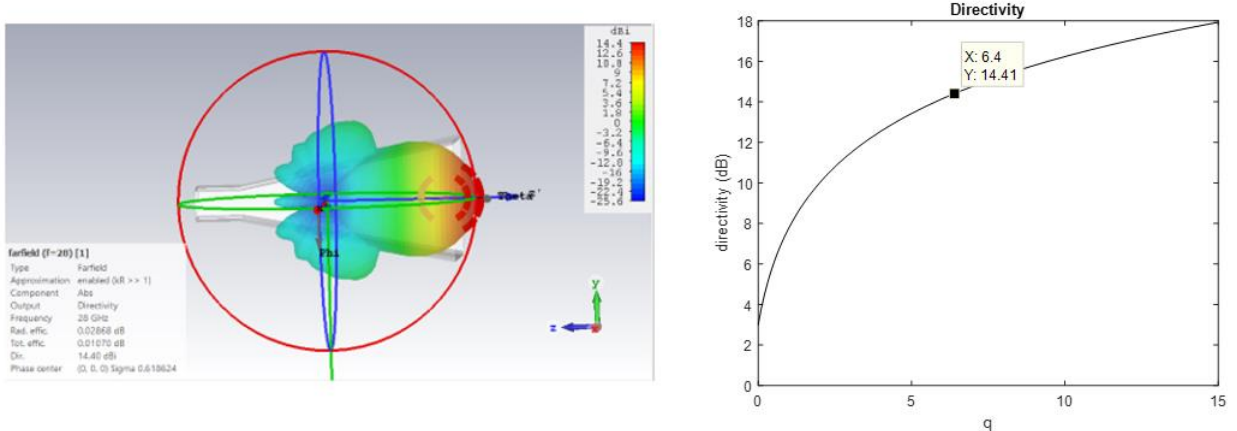


Figure 28: 3D radiation pattern of the LB-28-15 & q value for LB-28-15.

The directivity of the horn can be computed by

$$D = \frac{U_{\max}}{U_{\text{avg}}} = \frac{4\pi U_{\max}}{P_{\text{rad}}} = \frac{4\pi U_{\max}}{\int_{\phi=0}^{2\pi} \int_{\theta=0}^{\pi} U(\theta, \phi) \sin \theta d\theta d\phi} \quad (25)$$

where $U(\theta, \phi)$ is from (11). This equation is solved in MATLAB and plotted for a range of q values as shown in Figure 28. The LB-28-15 pyramidal horn is found to have a q-value of 6.4. In addition, it is found that the phase center of LB-28-15 is at 1.861 mm away from the aperture opening.

The next step is to find out the optimal position for the pyramidal horn feed. Often, designers will use -10 dB taper for their design as it is able to strike a good balance between the spillover and illumination efficiency. But for this dissertation, an analytical approach is used to calculate the optimal feed position.

5.3 REFLECTARRAY F/D AND PHASE DISTRIBUTION

Before calculating the F/D ratio, the reflectarray size has to be determined first. To avoid a reflectarray that is too bulky to test, the number of elements is chosen to be 51×51 , giving a diameter of $51 \times 4.4 \text{ mm} = 224.4 \text{ mm}$. The overall physical size will be acceptable and at the same time achieve good gain. Using (13), (16) and (18), where $D=224.4\text{mm}$ and $q=6.4$, the following plot in Figure 29 is obtained. According to Figure 29, the peak efficiency is at around an F/D of 0.9. Hence, the pyramidal horn's phase center will be placed at 201.96mm ($224.4 * 0.9$) directly above the center of the reflectarray.

The phase-shift distribution plot is required to calculate the amount of phase-shift needed for each element to direct the beam in a desired direction. Using (10), the required phase of each cell on the reflectarray is computed via a MATLAB script. A phase distribution of the reflectarray is shown in Figure 30. The plot on the right is after taking modulus of 360° of the plot on the left.

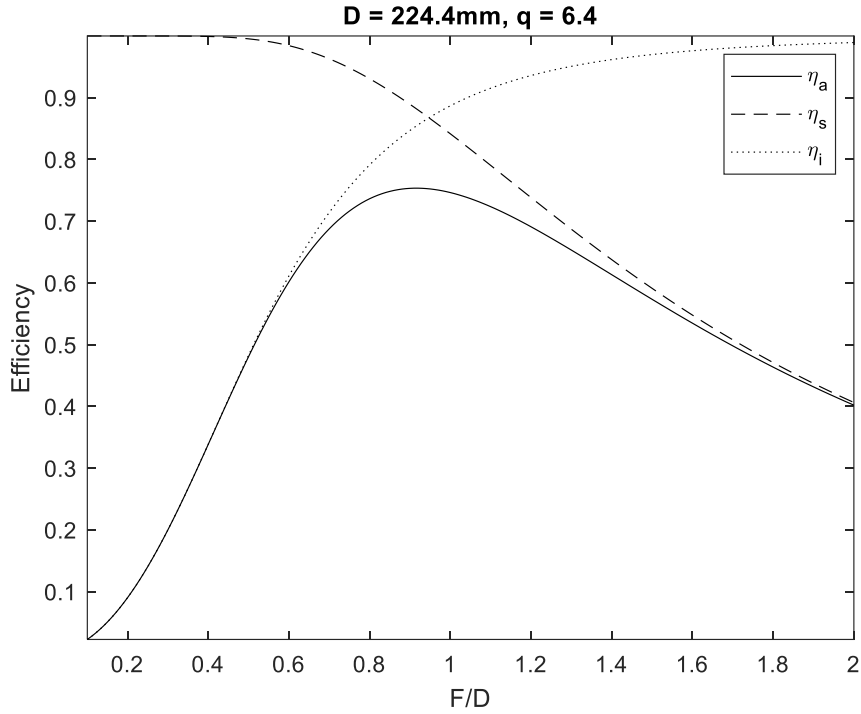


Figure 29: Theoretical F/D plot for $D = 224.4\text{mm}$ & $q = 6.4$.

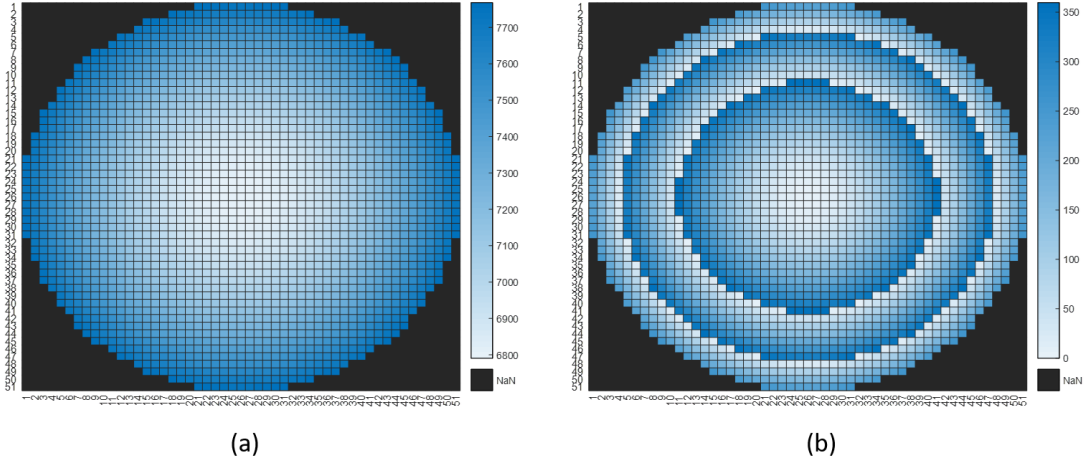


Figure 30: Center feed a) Raw phase distribution plot; b) Normalized phase distribution plot by 360° .

5.4 SYSTEM DESIGN – ELEMENT MAPPING

The mapping process is to determine the physical dimension for the element design corresponding to its desired phase. The best dimension determination is found using the spline function in MATLAB. Although the 0° incident angle phase curve can be used to determine all

the element dimensions, it is preferable and more accurate to use the phase curve corresponding closest to the actual incident angle at the element.

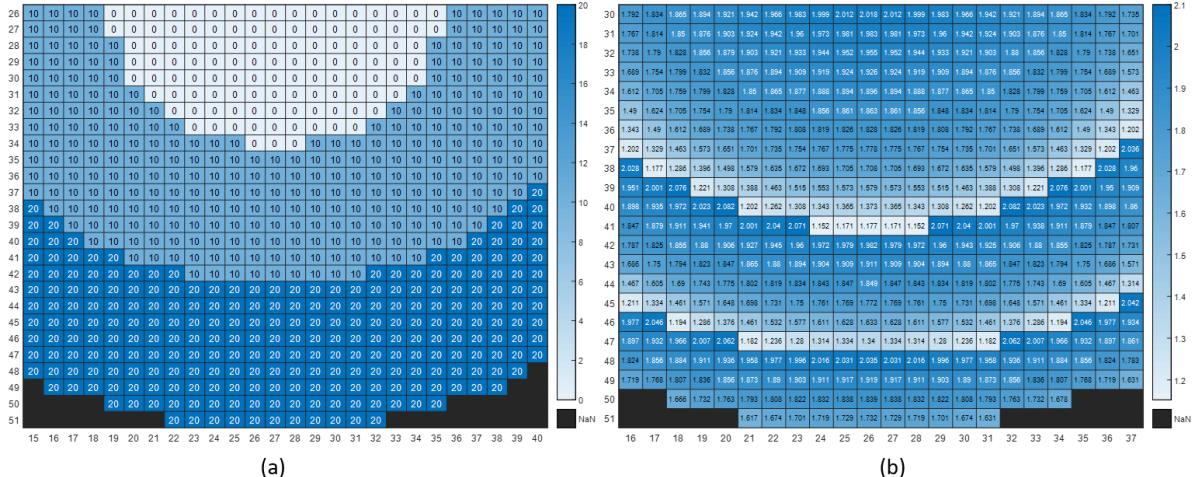


Figure 31: (a) Dataset categorization; (b) Finalized dimension mapping.

Figure 31(a) shows a section of the reflectarray grouped into different incident angle bins for dimension mapping. As the element moves away from the center of the reflectarray, the incident angle deviates from 0° . Hence, a different phase curve corresponding to the incident angle has to be used for dimension mapping. Figure 31(b) shows the finalized dimensions for the element generated from the relevant phase curve.

5.5 SYSTEM DESIGN – AUTOCAD SCRIPT AUTOMATION

Drawing 2000+ elements manually is not an easy feat. Hence, there must be some automation to make the task more efficient. Firstly, MATLAB is utilized to churn out all necessary results that includes the dimensions and coordinates of the elements in a tabular format (Matrix). Next, MATLAB is used to print out the commands in SCR format that is compatible with the AUTOCAD scripting format. The AUTOCAD will run the SCR file to create a 2D surface of the reflectarray elements before the result is exported as DXF format for CST to import. Since the

imported DXF format is a 2D surface, the substrates and ground plane have to be added. The horn feed (from the previous section) is also imported to complete the reflectarray simulation model.

Figure 32 summarizes the automation process.

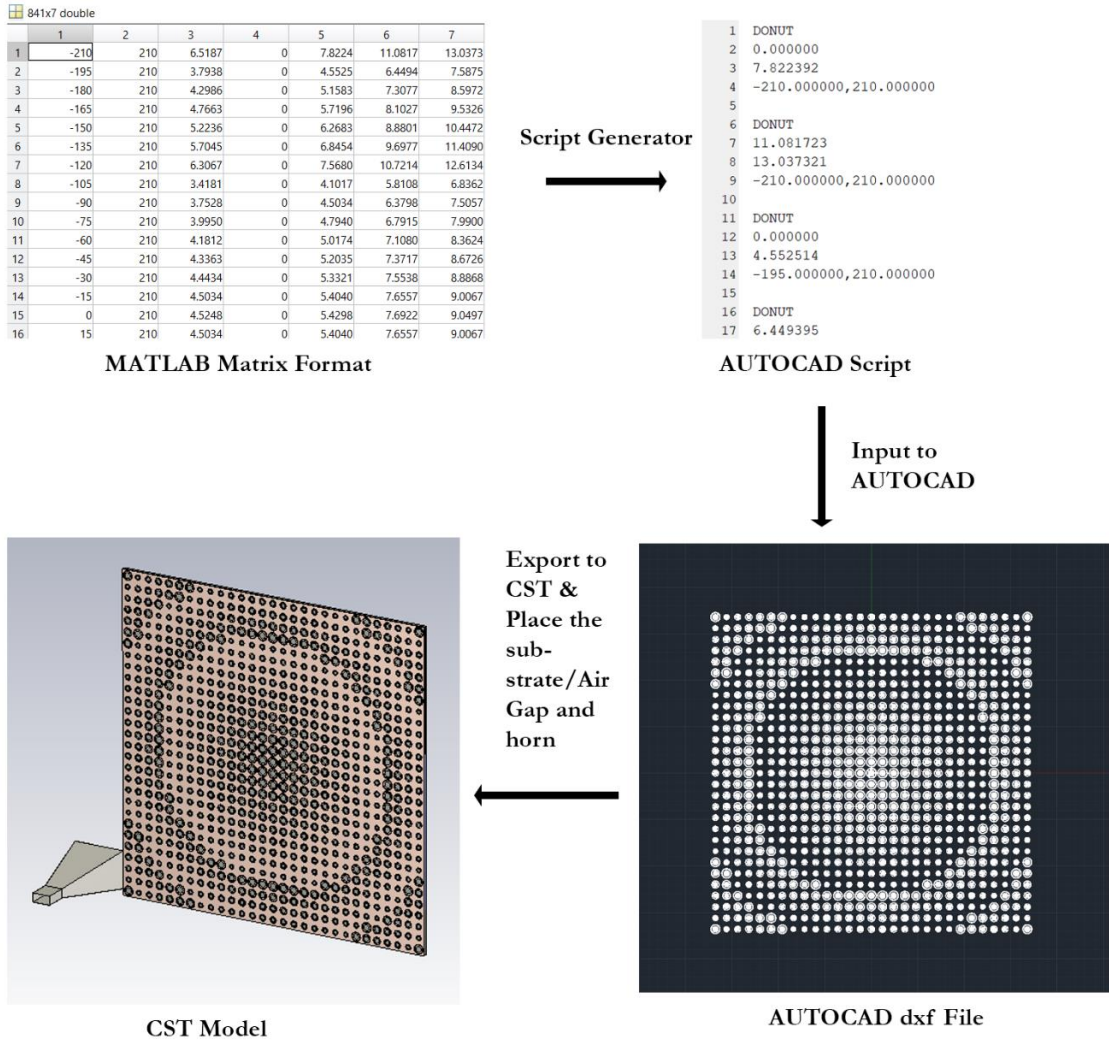


Figure 32: Element drawing automation process.

5.6 SIMULATION RESULT

Fortunately, there are ways to simulate the reflectarray more efficiently in CST by making use of the symmetry property function. For center-fed case, using symmetry in the XZ and YZ planes means the simulation time can be cut down by up to four times. Following the TEM convention for the horn, the symmetry planes are as shown in Figure 33.

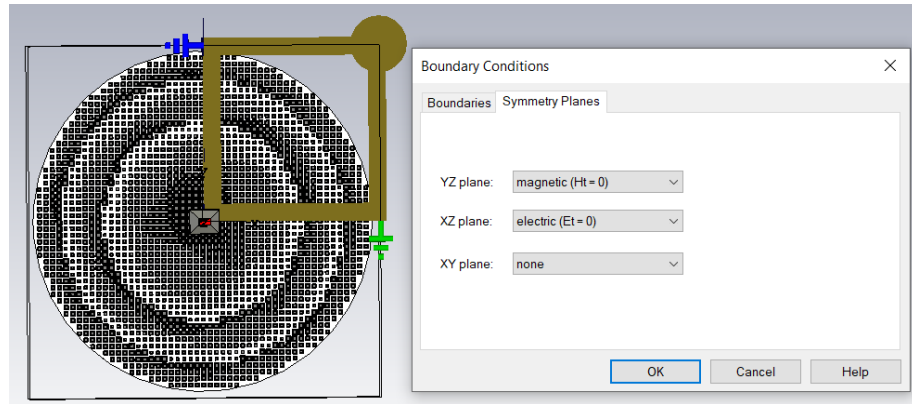


Figure 33: Symmetry planes for center-fed reflectarray.

5.6.1 Square Ring Patch Element Design

Figure 34 and Figure 35 show the radiation patterns for the center-fed reflectarray with square ring patch element design.

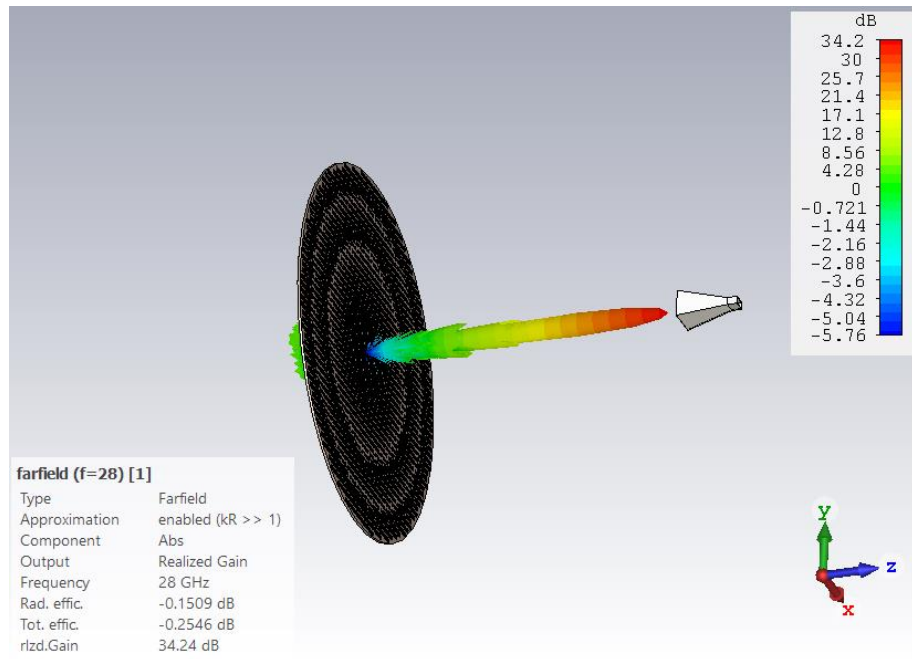


Figure 34: 3D radiation pattern for the square ring patch element design @ 28GHz.

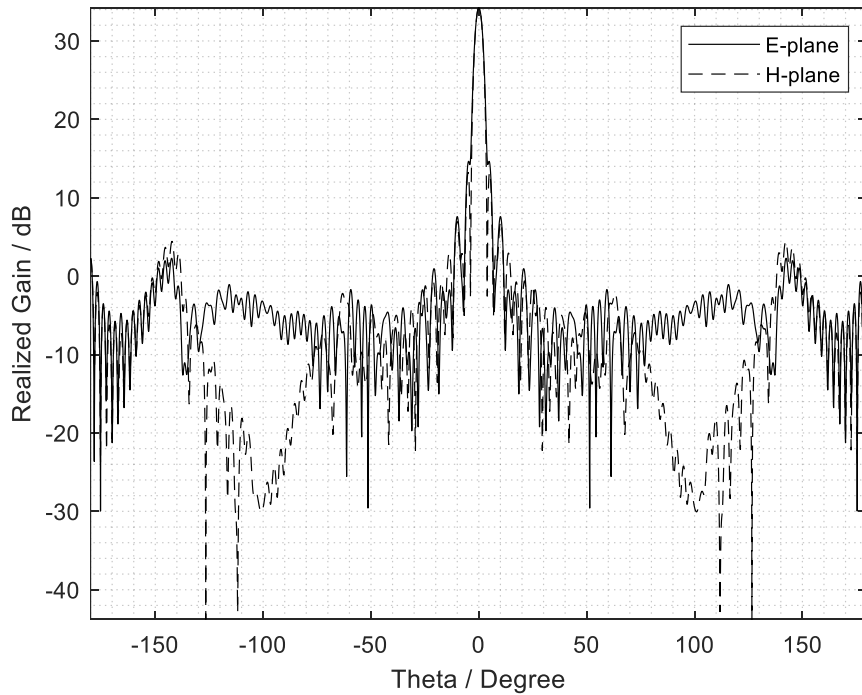


Figure 35: 2D radiation pattern for the square ring patch element design @ 28GHz.

The realized gain is 34.24 dB and the 3-dB beamwidth 3° . The radiation pattern is a pencil beam with a very small beamwidth. The aperture efficiency of this reflectarray design is 61.3%, which is acceptable for this type of antenna. The sidelobe level in the E-plane ($\phi=90^\circ$) is -19.6 dB while at H-plane ($\phi=0^\circ$) is -21 dB.

From Figure 36, the reflectarray has a useable 1-dB bandwidth from 26.5 to 29.5 GHz, or about 5.36%. This value is typical of most reflectarrays.

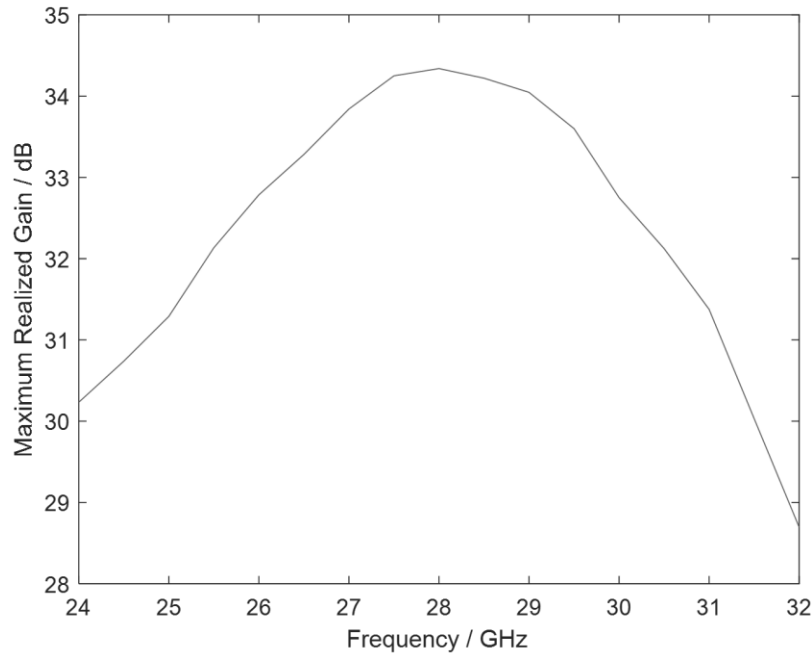


Figure 36: Maximum Realized Gain vs Frequency for square ring patch element.

5.6.2 Square Patch Comparison

In order to better understand why having a full cycle phase shift element is important, a reflectarray using the single layer square patch element is also simulated. Figure 37 and Figure 38 show the radiation patterns for the single layer square patch reflectarray.

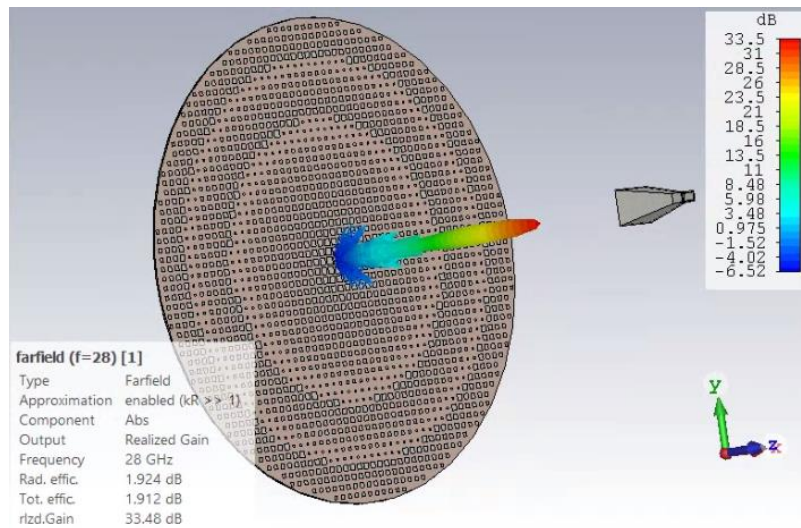


Figure 37: 3D radiation pattern for the single patch element design @ 28GHz.

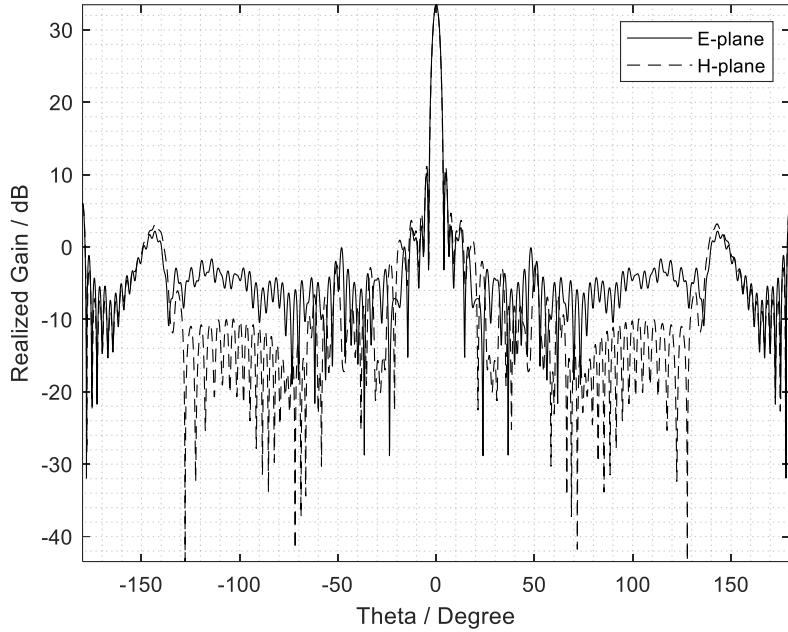


Figure 38: 2D radiation pattern for the single patch element design @ 28GHz.

The realized gain of this reflectarray is 33.5 dB which is slightly lower than 34.24 dB for the square ring patch reflectarray. Its 3-dB beamwidth is 3° , which is the same as the former design since the beamwidth is a function of the aperture. The aperture efficiency of this square patch reflectarray design is 52%, which is 9% lower than the square ring patch reflectarray. The sidelobe levels of the square patch reflectarray in the E-plane and H-plane are -23.3 dB and -22.3 dB, respectively. These levels are about 3.7 and 1.3 dB lower than that of the square ring patch reflectarray. Similar to the square ring patch element design, the square patch design (see Figure 39) has about 5.4% (1-dB) bandwidth.

It is expected that the square patch will have a lower gain compared to the ring patch elements as the square patch does not have the sufficient phase shift to completely compensate for the phase difference (refer to chapter 3.1). The square patch can only compensate up to around 260 degrees at 0° incidence. To minimize the phase discrepancy, the phase mapping is centered at around 180° to compensate for the middle phase range, with the maximum and minimum phases

compensated by the biggest/smallest element. However, the square patch version did very well against the square ring patch element model as it only lose out 0.74 dB even with its simple element design.

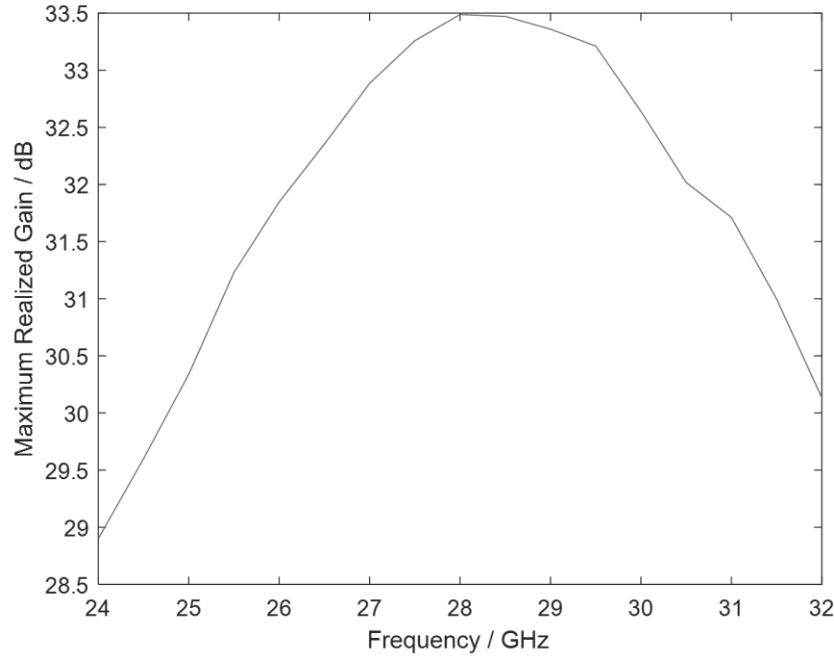


Figure 39: Maximum Realized Gain vs Frequency for single patch element.

5.6.3 Comparing to a Center Fed Parabolic Reflector Antenna

This section will compare the performance of the parabolic reflector and a reflectarray. Unlike the reflectarray, the parabolic reflector does not compensate the phase difference with elements. Instead, it compensates by the physical curvature so that the phase compensation is continuous instead of discrete as in a reflectarray. The same pyramidal horn (LB-28-15) is also placed at the same position for the parabolic reflector at 0.9 F/D as shown in Figure 42. The diameter is also 224.4mm to match the reflectarray size.

The following paragraphs provide some theory related to the parabolic reflector. The equation of the parabola is as follows in xz -plane:

$$x^2 = 4F(F - z), \quad |x| \leq \frac{D}{2} \quad (26)$$

where F is the focal length and D is the diameter of the parabolic reflector (see Figure 40).

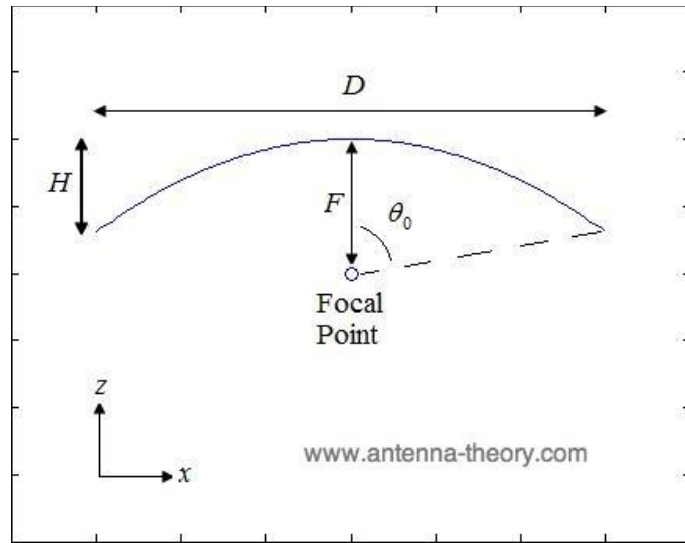


Figure 40: Illustration of parabola with defining parameters [12].

The diameter (D) and focal length (F) are related by the following two equations:

$$\begin{aligned} \frac{F}{D} &= \frac{1}{4 \tan(\theta_0 / 2)} \\ F &= \frac{D^2}{16H} \end{aligned} \quad (27)$$

Using CST macro function (see Figure 41), the parabola can be simply be drawn out by inputting the parameters, where D = 224.4mm and the focal length is 0.9 * 224.4mm (the F/D from the reflectarray parameters).

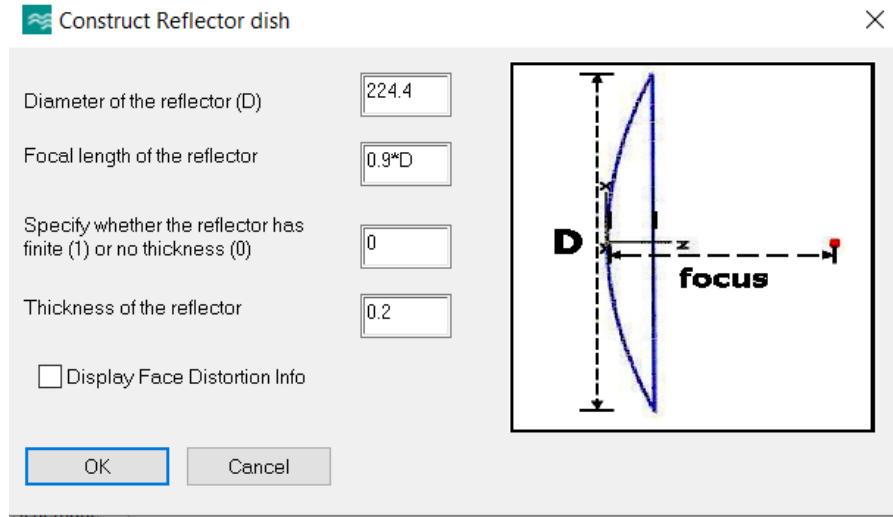


Figure 41: Parabolic reflector design window.

Figure 42 and Figure 43 show the radiation patterns for the parabolic reflector antenna. The realized gain is 35 dB and the 3-dB beamwidth is 3°. The aperture efficiency is 73%, which is normal for a parabolic reflector antenna. The sidelobe levels in the E-plane and H-plane are -22.5 dB and -21.4 dB, respectively. The sidelobe levels are below -20 dB for both planes.

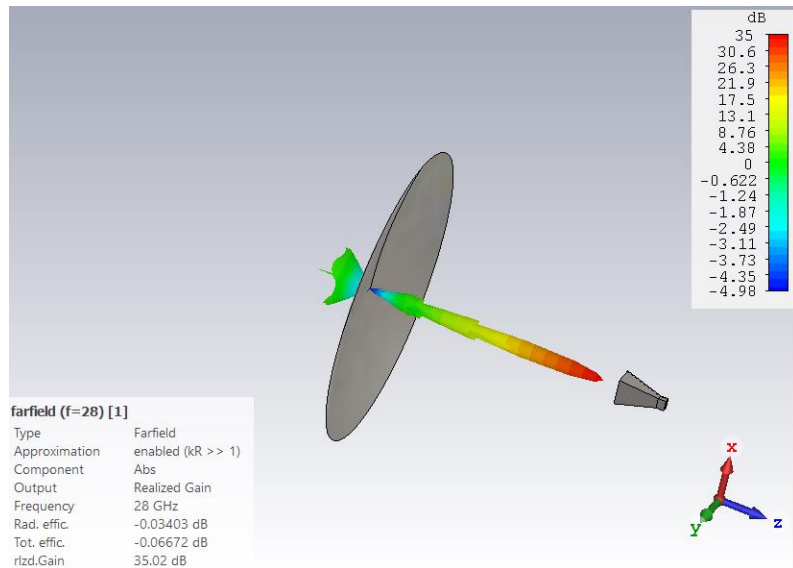


Figure 42: 3D radiation pattern for the parabolic bowl reflector antenna @ 28GHz.

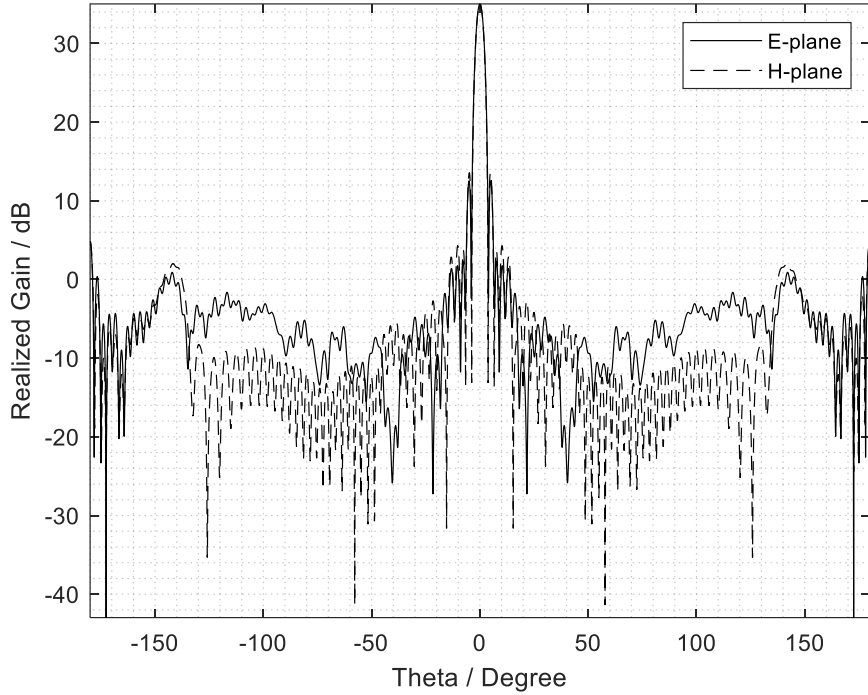


Figure 43: 2D radiation pattern for the parabolic bowl reflector antenna @ 28GHz.

Not surprisingly, the parabolic reflector antenna's performance is superior over the reflectarray antenna. Its efficiency of 73% is more than 10% higher than the square ring patch reflectarray (61.3%). One reason is that the phase compensation in the reflectarray antenna is discrete whereas it is continuous in the parabolic reflector antenna (refer to Figure 8d). In addition, the parabolic reflector is just pure metal, so that there is no dielectric loss.

Unlike the reflectarray antenna, the bandwidth of the parabolic reflector antenna is not limited by the frequency of the incident wave. From (26) and (27), frequency is not a parameter in the design of the parabolic reflector. According to Figure 44, it can be quite misleading that as the frequency increases, the gain increases. Theoretically, the parabolic reflector has infinite bandwidth, but the feed's finite bandwidth will eventually limit the increase in the gain of the parabolic reflector antenna. Table 1 shows the characteristics of the LB-28-15 horn at different frequency.

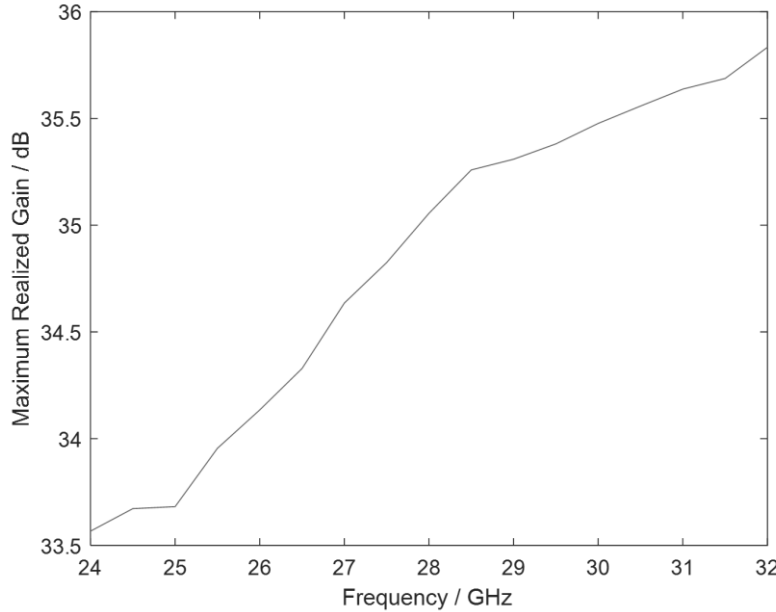


Figure 44: Maximum Realized Gain vs Frequency for parabolic bowl reflector antenna.

Table 1: Frequency vs Gain of LB-28-15 horn antenna [11].

Frequency (GHz)	Gain (dB)	Antenna Factor (dB/m)
26.5	13.63	45.04
27.0	13.68	45.15
27.5	13.91	45.08
28.0	13.97	45.18
28.5	14.17	45.12
29.0	14.09	45.37
29.5	14.04	45.57
30.0	14.42	45.33
30.5	14.83	45.06
31.0	15.11	44.92
31.5	15.41	44.76
32.0	15.26	45.05
32.5	14.97	45.48
33.0	15.42	45.16

Frequency (GHz)	Gain (dB)	Antenna Factor (dB/m)
33.5	15.34	45.37
34.0	15.37	45.46
34.5	15.62	45.34
35.0	15.60	45.49
35.5	15.65	45.57
36.0	15.92	45.41
36.5	15.83	45.63
37.0	15.91	45.66
37.5	15.94	45.75
38.0	16.11	45.69
38.5	16.29	45.62
39.0	16.35	45.68
39.5	16.21	45.93
40.0	16.39	45.86

Overall, the properties of the reflectarray antenna are quite similar to the parabolic reflector antenna except for the bandwidth. Although its aperture efficiency is inferior compared to that of the parabolic reflector antenna, the reflectarray is easy to fabricate and can be installed on any flat surfaces. In addition, it is also collapsible unlike the parabolic reflector.

6 REFLECTARRAY – OFFSET FEED DESIGN

In the previous configuration, the biggest flaw in the center-fed reflectarray antenna is the aperture blockage by the feed. The effect will become even more prominent when the supporting structures of the feed are also included. The undesirable effects of aperture blockage are increased sidelobe level and reduction in antenna gain. These effects will worsen if the aperture blockage is increased.

In Figure 45(a), the aperture blockage is a function of D_0 / D where D_0 is the blockage diameter and D is the aperture diameter. If this blockage ratio is lesser than 0.2, the blockage will not affect the radiation pattern significantly, as seen in the simulated results for the center-fed reflectarray in Chapter 5 (note that the supporting structure of the feed has not been accounted for).

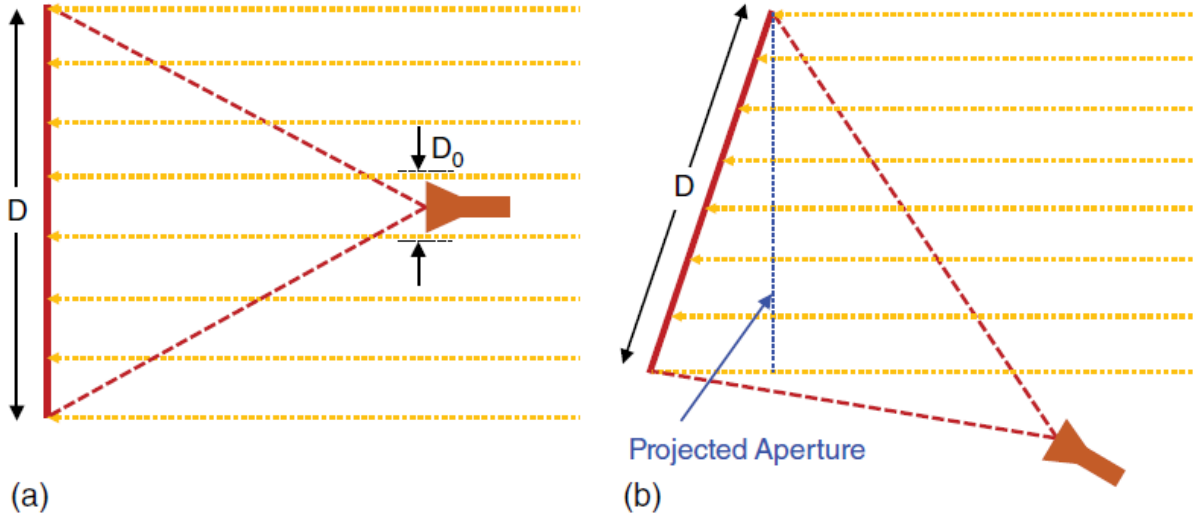


Figure 45: Aperture blockage in front-fed reflectarray systems: (a) symmetric, (b) offset [4].

An offset feed configuration does not result in an increased gain but a reduced gain. As seen in Figure 45(b), even for the same physical aperture, the projected aperture is smaller. Nevertheless, this is still a good trade-off as it totally eliminates aperture blockage which can be beneficial for large aperture.

6.1 FEED POSITION & PHASE DISTRIBUTION

In this study, the same F/D ratio of 0.9 is used. The geometry of the offset-fed reflectarray is shown in Figure 46. Note that the feed is not totally offset to the point where there is zero aperture blockage.

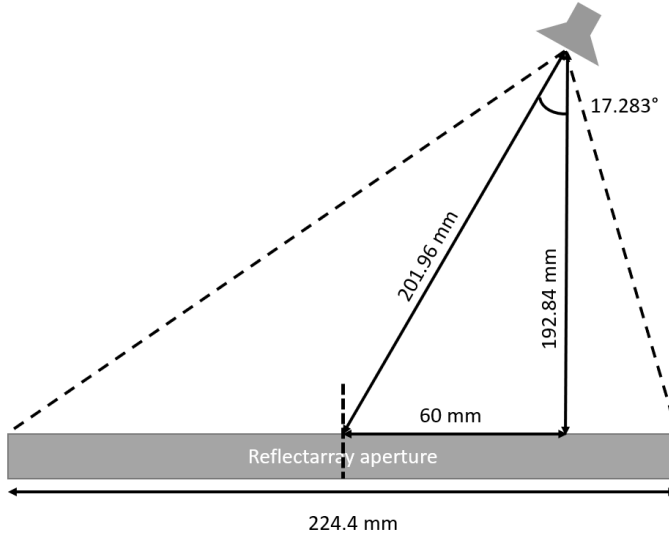


Figure 46: Geometry of the offset configuration.

Using (10), the phase distribution plots are obtained as shown in Figure 47 for the desired beam direction at $(0^\circ, 0^\circ)$. Similarly, the element mapping is done and drawn in CST for simulation. Note that the element used here is the square ring patch element. As this is an offset configuration, the element on the far side away from the horn will have a steeper incidence angle than the one nearer to the feed. From Figure 48, the farthest elements have an incidence angle of more than 40° , which was not the case for the center-fed configuration.

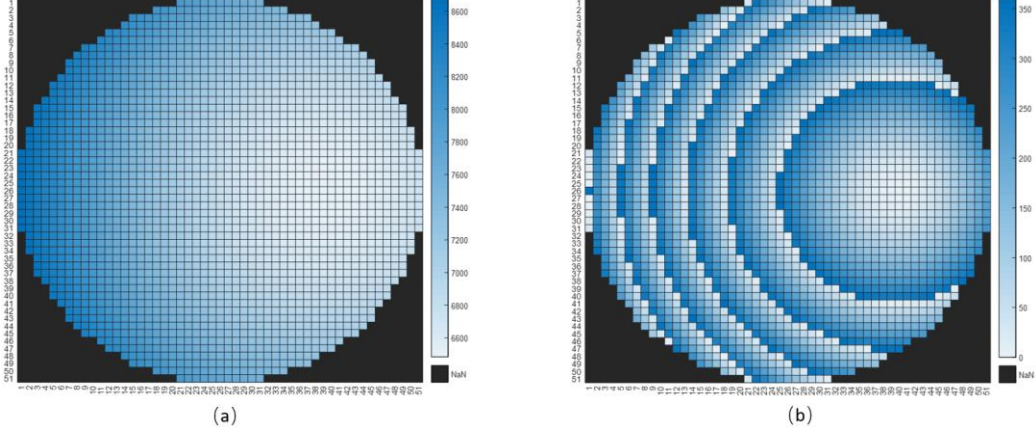


Figure 47: Offset feed a) Raw phase distribution plot, b) Normalized phase distribution plot by 360° .

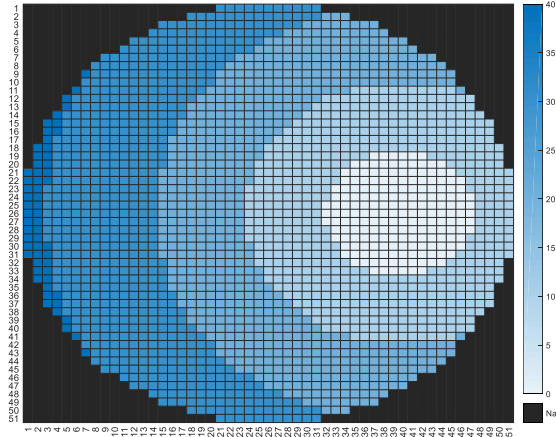


Figure 48: Dataset categorization for offset.

Since the reflectarray is now only symmetrical in one plane (YZ) (see Figure 49), the runtime is longer than that for the center-fed configuration. In addition, as the time-domain solver in CST cannot handle a “tilted” port, the waveguide section of the horn has an extension where its end-face is parallel to the XY plane (see Figure 50).

Figure 50 and Figure 51 show the radiation patterns of the offset-set fed reflectarray antenna. The realized gain is 33.94 dB and the 3-dB beamwidth in both planes are 3° . The aperture efficiency of this reflectarray design is 57.14%, which is slightly lesser than the center-fed configuration (61.3%). The lower efficiency in this case can be attributed to blockage by the feed

as well as the illumination and spillover effects. The sidelobe levels in the E-plane and H-plane are -22 dB and -20.9 dB, respectively. The bandwidth of the offset-fed configuration is also similar to the center-fed configuration at around 5.4% as shown in Figure 52.

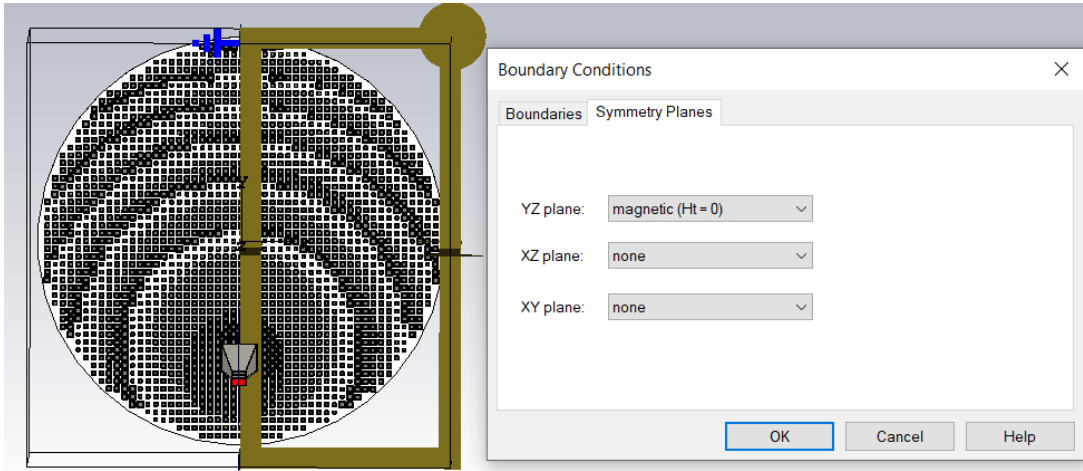


Figure 49: Symmetry planes for offset-fed reflectarray.

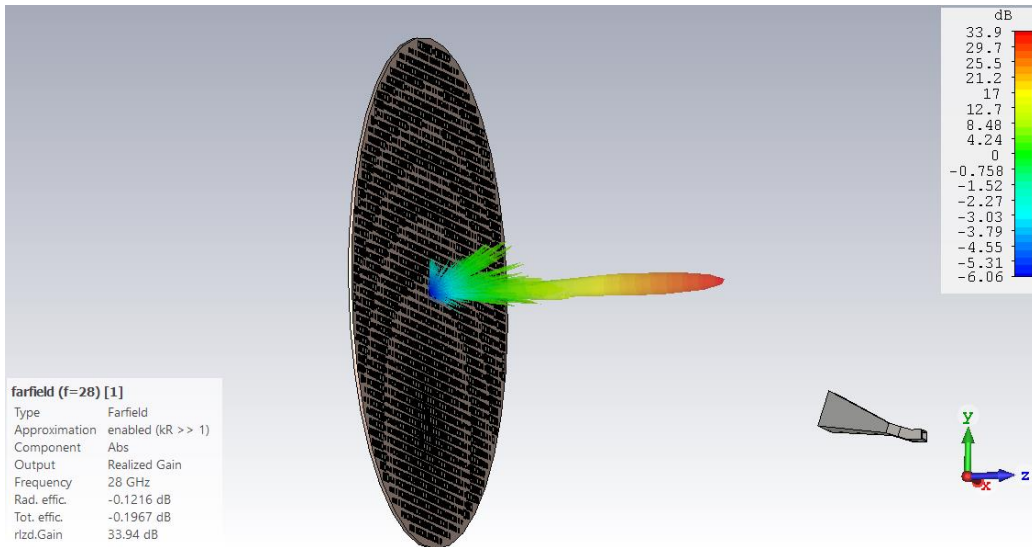


Figure 50: 3D radiation pattern for square ring patch element design - offset fed configuration @ 28GHz.

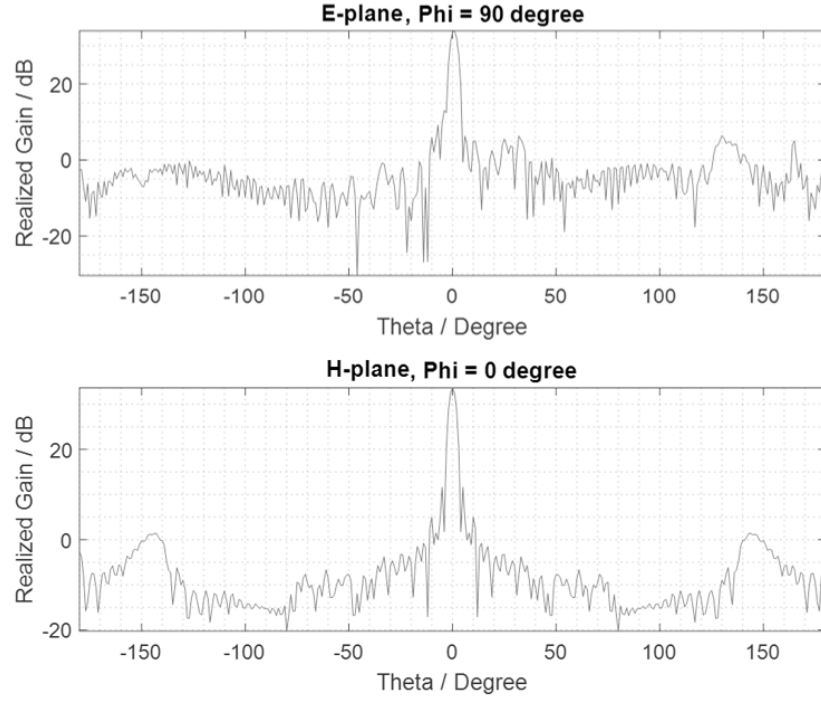


Figure 51: 2D radiation pattern for the square ring patch element design - offset fed configuration @ 28GHz, E-plane (top), H-plane (bottom).

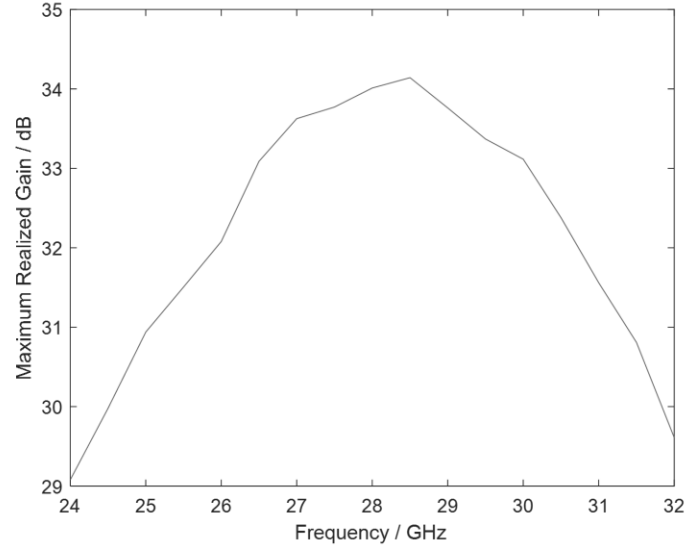


Figure 52: Maximum Realized Gain vs Frequency for offset fed reflectarray.

Comparing the sidelobe levels, the offset-fed case performs better than the center-fed case although it is not very significant. Furthermore, the effect due to the supporting structure of the feed in both cases has not been taken into account.

Figure 53 and Figure 54 show the radiation patterns when the supporting structure for the center-fed square ring patch reflectarray is included. The sidelobes in the H-plane has significantly increased from -21 dB to -16.4 dB. Moreover, the gain has fallen from 34.2 dB to 33.5 dB. These degradations are the reasons for using an offset configuration.

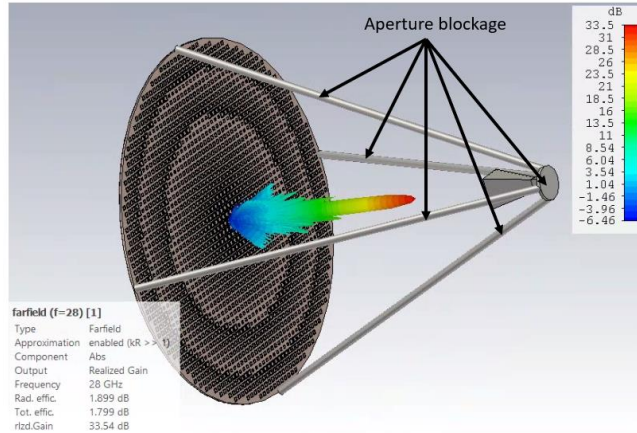


Figure 53: 3D radiation pattern for square ring patch element design center fed with structure @28GHz.

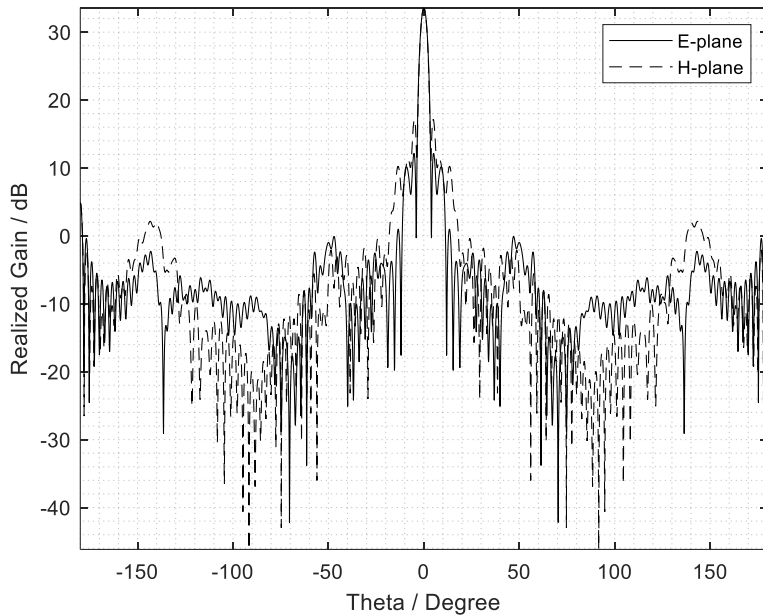


Figure 54: 2D radiation pattern for square ring patch element design center fed with structure @28GHz.

6.2 OFFSET CONFIGURATION WITH TILTED BEAM

Another common configuration when engineers design offset-fed configuration is to introduce a “direction” to the main beam. Instead of the usual ($0^\circ, 0^\circ$) direction, the main beam is reflected in a mirror-like fashion with respect to feed angle as shown in Figure 55. In this offset-fed tiled-beam configuration, where the beam is directed to the opposite side of the feed, there is even less aperture blockage.

Using (10) with ($\theta_b = 17^\circ, \phi_b = 0^\circ$) to approximately match the “reflection” angle, we obtain the phase distribution in Figure 56. The phase distribution is very similar to that of the center-fed case. However, upon closer examination, the right side is more “squeezed” (around 3 rings) while the left side seems to be more “expanded” (around 2 rings). The reason is that the phase transition on the right side is much steeper compared to the left side. Another observation is that the “center” has shifted from the right to left.

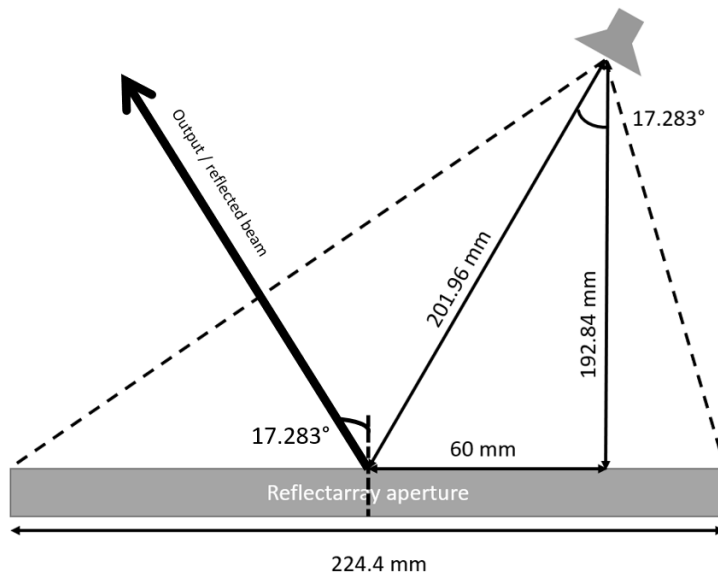


Figure 55: Geometry of the offset configuration for titled beam.

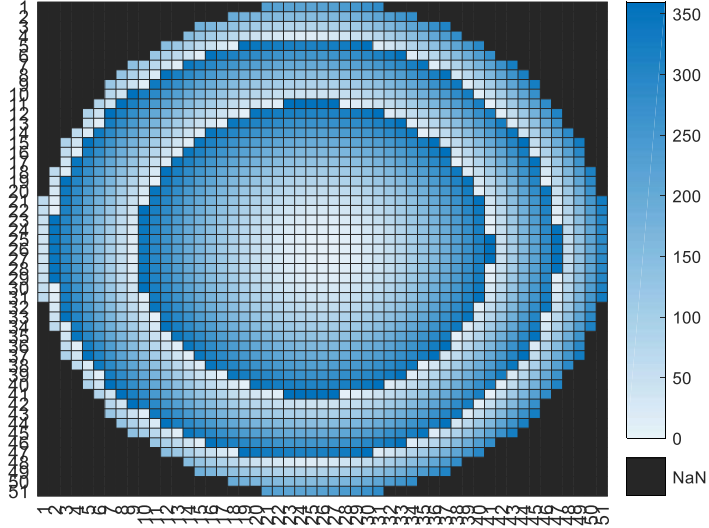


Figure 56: Offset feed with tilted beam @ 17° phase distribution.

Figure 57 and Figure 58 show the radiation patterns for the offset-fed tilted-beam reflectarray. The realized gain is 33.7 dB and directed at $\theta = 17^\circ$. The aperture efficiency is 54.1%, which is slightly less than that of the offset-set boresight beam configuration (57.14%) because the projected aperture is smaller. The sidelobe levels in the $\phi=90^\circ$ plane (or E-plane) is -21.6 dB, and -24.1 dB for the conical cut for $\theta = 17^\circ$.

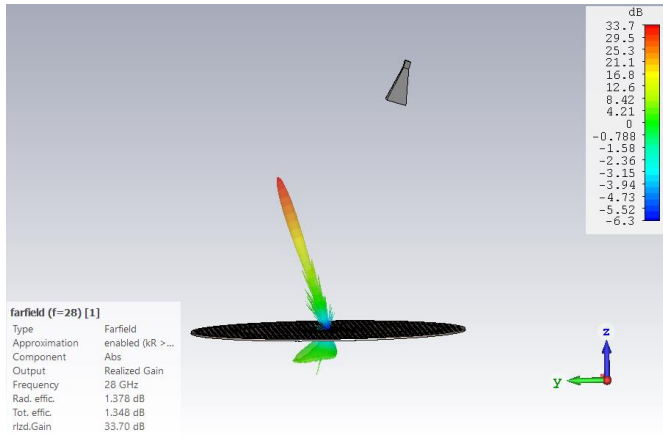


Figure 57: 3D radiation pattern for square ring patch element design - offset fed with tilted beam at -17° @ 28GHz.

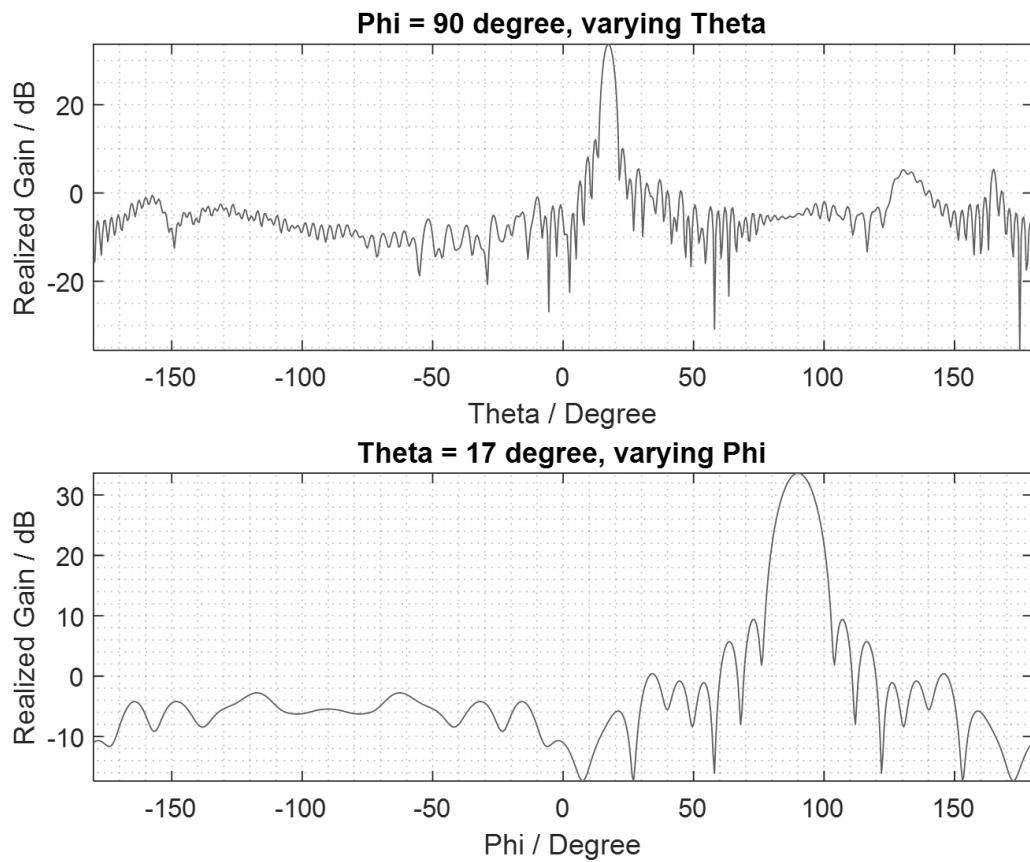


Figure 58: 2D radiation pattern for square ring patch element design - offset fed with tilted beam at -17° @ 28GHz.

7 REFLECTARRAY – WITH A SPLASH PLATE FEED

Using a splash plate feed is common for a parabolic reflector antenna because it is easier to install. Unlike the horn antenna, the splash plate is made of a waveguide and a reflector “blocking” the other end of the waveguide to reflect the wave towards the reflecting aperture (can think of it as a double reflector antenna). Designing a splash-plate requires many iterations as there is no standard way to designing one [13]. However, there are some general guidelines to follow. The splash plate is used in the following manner as shown in Figure 59.

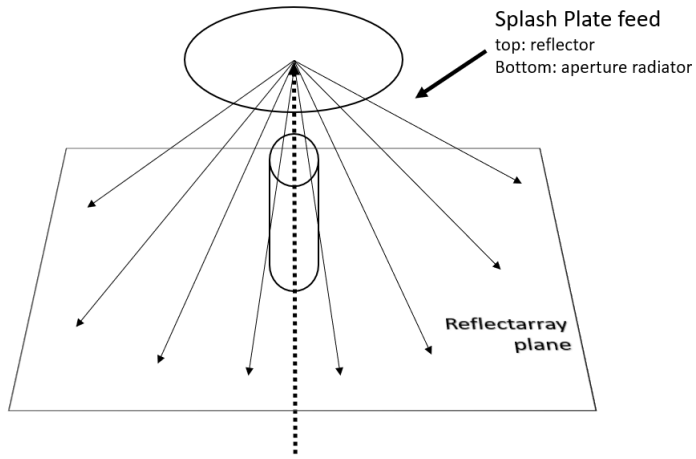


Figure 59: Visualization of the splash plate feed configuration.

Generally, a splash plate feed is not as efficient as a feed horn. However, it is easier to install and has a lower aperture blockage [13] as it can be designed not to have a supporting structure. In addition, the goal of using splash plate is usually to reduce the F/D for a lower profile antenna.

7.1 DESIGN APPROACH FOR A SPLASH PLATE

The flat splash plate can be designed using the Geometrical theory of diffraction (G.T.D) model. Since the reflector is in front of the feed and assuming the reflector is ideal, we can mirror the feed to the other side to predict how the signal is being reflected as shown in Figure 60. Using this property, the conventional feed design approach can be used.

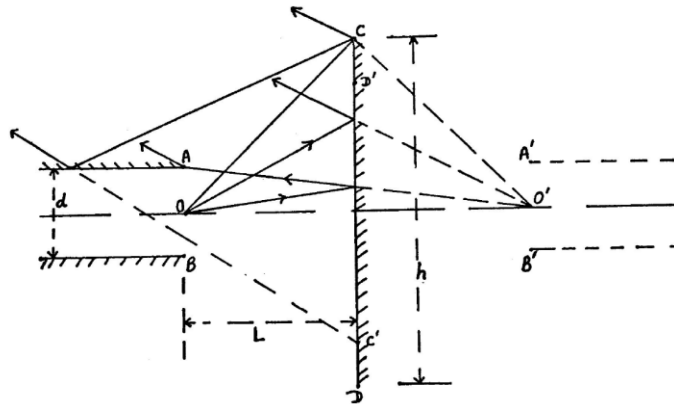


Figure 60: G.T.D Model [13].

According to [13], h should be about 4λ , L about 2λ , and the waveguide about 0.8λ wide. However, these guidelines give only the “basic” shape. Fine-tuning is still required to fit the reflectarray design.

The flat reflector of the splash plate is not good enough due to insufficient matching from the waveguide to the reflector to the free space, resulting in very low efficiency. In order to improve matching, a pointy tip and a dielectric (usually PTFE) is added at the reflecting end to achieve a better match (see Figure 61) [13]. The process takes time and intuition to produce a decent splash plate.

Using an existing 10 GHz splash plate design, some scaling (to 28 GHz) and fine-tuning are done to meet the reflectarray design criteria. Figure 62 shows the resultant radiation pattern after fine-tuning. From this pattern, the beamwidth corresponds to a pyramidal horn antenna with a q value of 0.5 and a phase center at 6.562mm above the reflector of the splash plate.

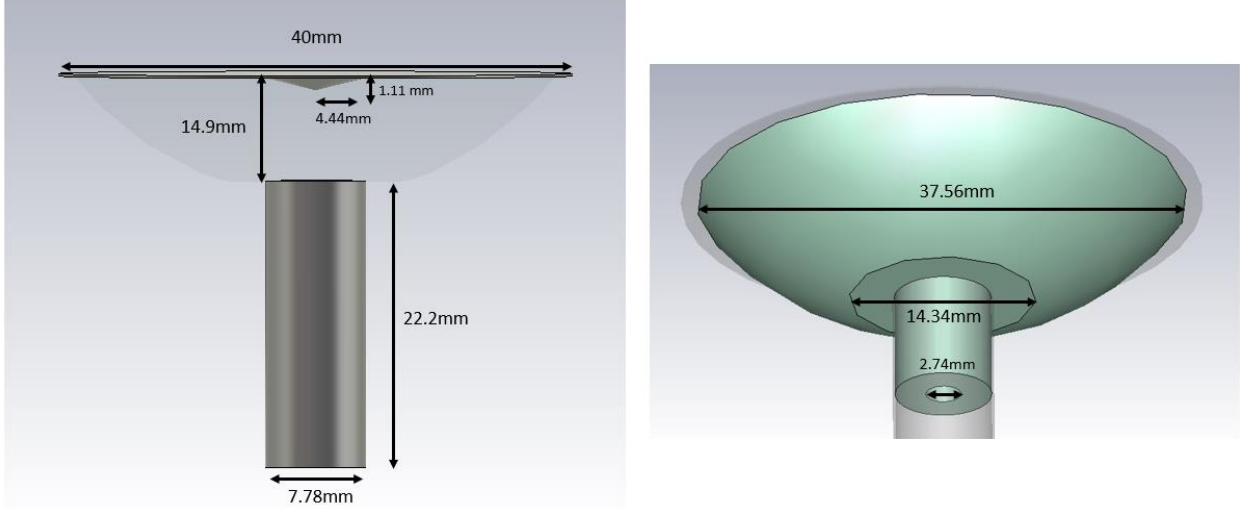


Figure 61: Geometry of the designed splash plate.

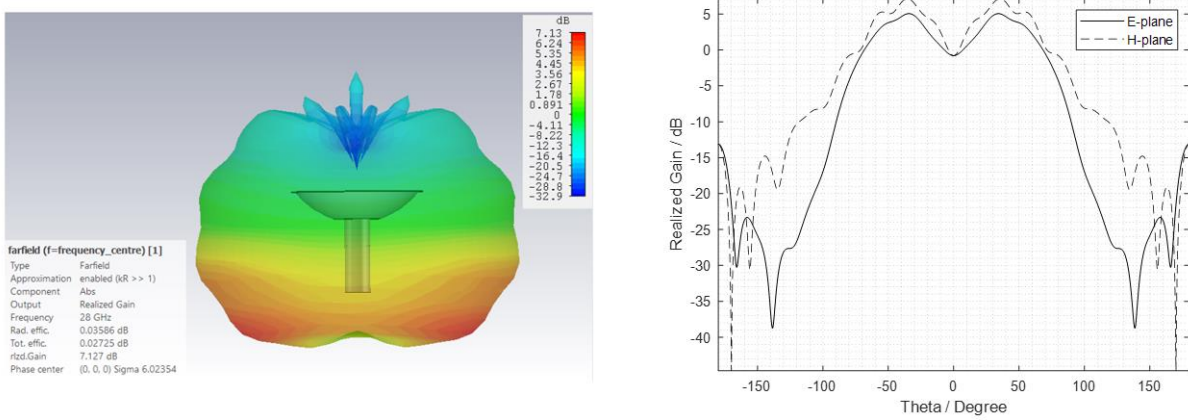


Figure 62: Radiation pattern of the splash plate.

It is quite obvious that with such a wide beamwidth, the focal point has to be lowered to illuminate the reflectarray aperture effectively. However, the peak of the F/D plot is lower than what it was before, which means using such a wide beamwidth feed may not be such a good idea as the optimal gain will be less compared to using a feed with a narrower beamwidth (compared to the previous F/D curve, the theoretical gain can more than 70%). Nevertheless, this reflectarray will be much more compact than the one before as the F/D is around 0.3 (see Figure 63).

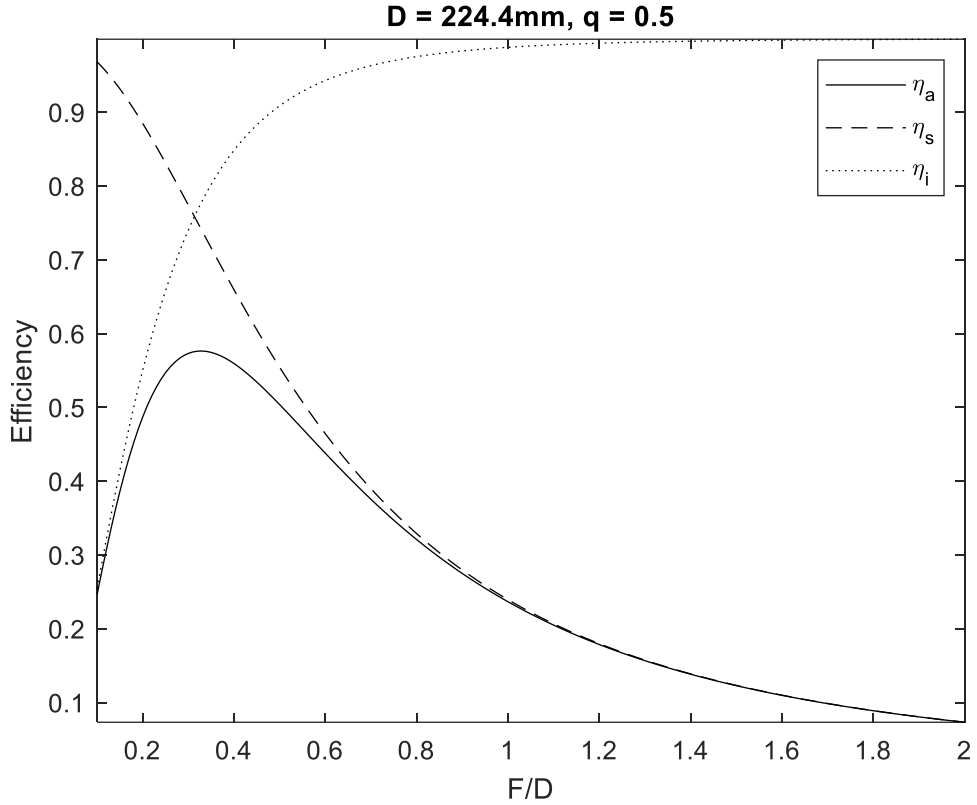


Figure 63: F/D plot for the splash plate configuration.

Figure 64 and Figure 65 show the radiation patterns for the splash-plate reflectarray. The realized gain is 32.6 dB and the 3-dB beamwidth is 3°. The aperture efficiency of this reflectarray is 42%, which is not as good as all the previous configurations. The sidelobe levels are rather high, about -17.6 dB in the E-plane and -14.6 dB in the H-plane. The sidelobe levels are higher than in previous configurations. Beyond the first sidelobe, the subsequent sidelobe level is very low.

Based on its performance, this splash plate reflectarray may not be a suitable. However, it has a smaller profile which also makes it more portable. Moreover, this advantage will become more prominent for larger reflectarray apertures because the splash plate does not require any supporting structure. It will also scale very well with size. As the funding is limited for this FYP, fabricating a splash plate is more expensive than buying a ready-made horn.

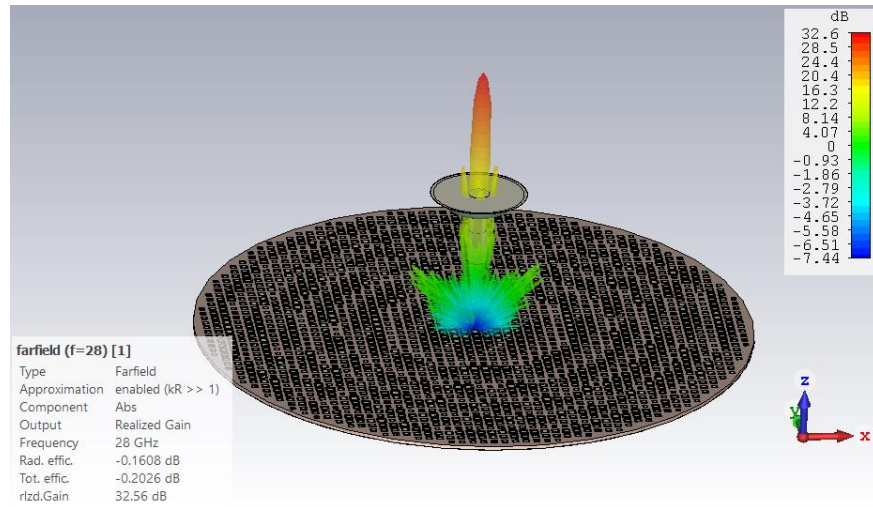


Figure 64: 3D radiation pattern for square ring patch element design with splash plate feed @ 28GHz.

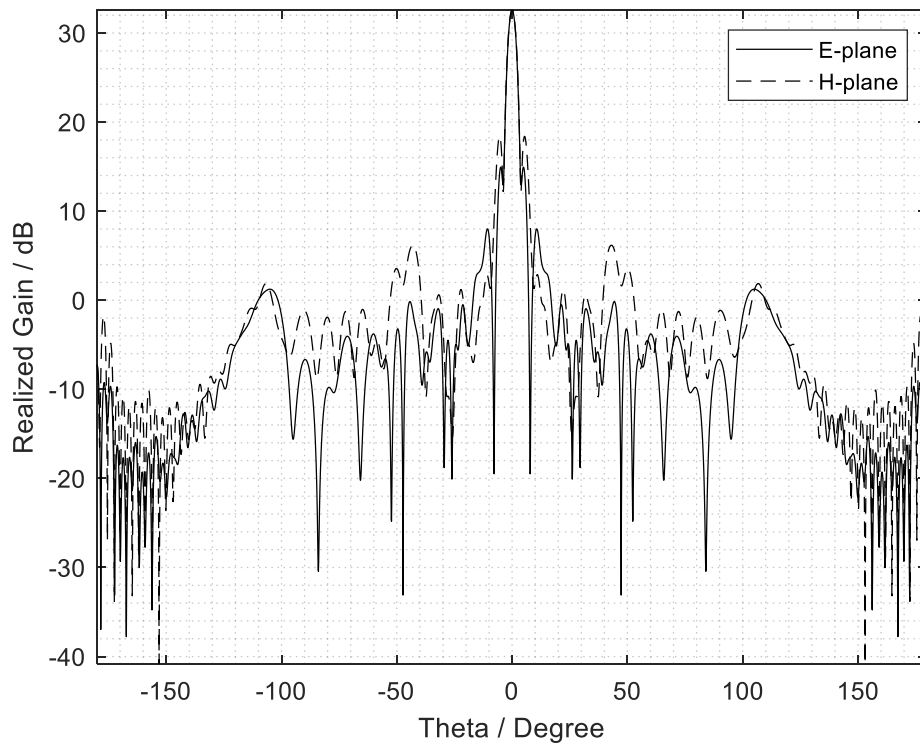


Figure 65: 2D radiation pattern for square ring patch element design with splash plate feed @ 28GHz.

7.2 NARROW BEAMWIDTH SPLASH PLATE

Another way to amalgamate the splash plate into a reflectarray more effectively is to design a splash plate with a narrower beamwidth to achieve a higher F/D ratio. A narrow beamwidth splash plate is uncommon because designing one may result in high level of back lobe. However, using the previous design with a slight twist, the dielectric and matching tip is able to redirect and reduce the beamwidth with negligible side effect.

Figure 66 shows the splash plate used to generate a narrower beamwidth to illuminate the reflectarray. Its radiation pattern is shown in Figure 67. The pattern corresponds to a pyramidal horn antenna with a q value of 4.5. Compared to the previous design, the beamwidth has decreased significantly from 178° to 80° (-10 dB beamwidth average).

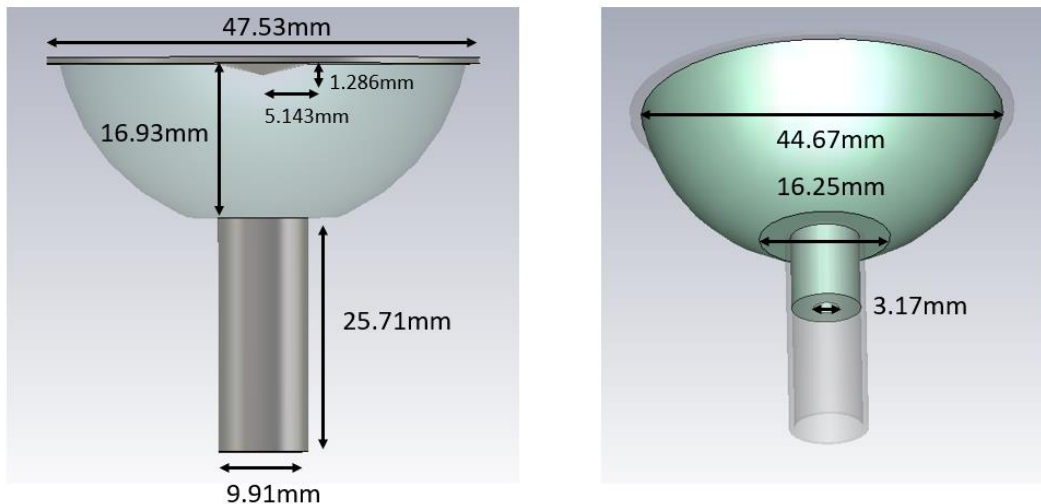


Figure 66: Geometry of the narrow beamwidth splash plate.

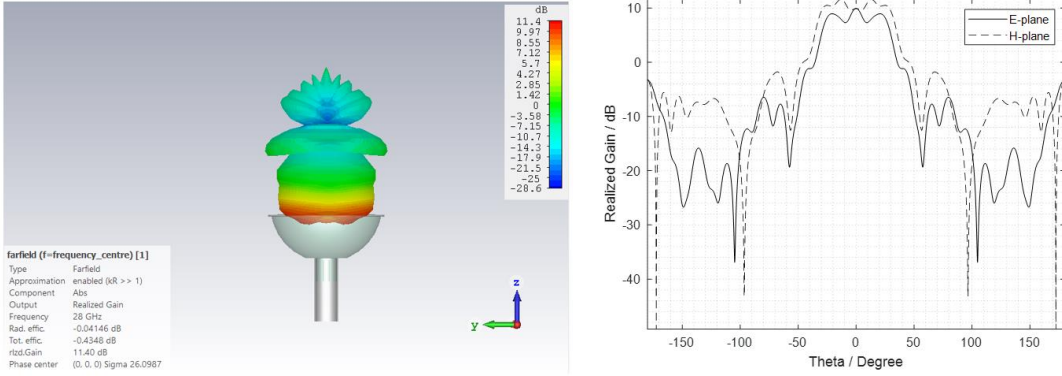


Figure 67: Radiation pattern of the narrow-beamwidth splash plate.

With the q value, the theoretical efficiency is significantly improved from the measly 57% to 73.9% as shown in Figure 68. With a beamwidth of 80° , the splash plate has to be placed higher than before with F/D of about 0.7.

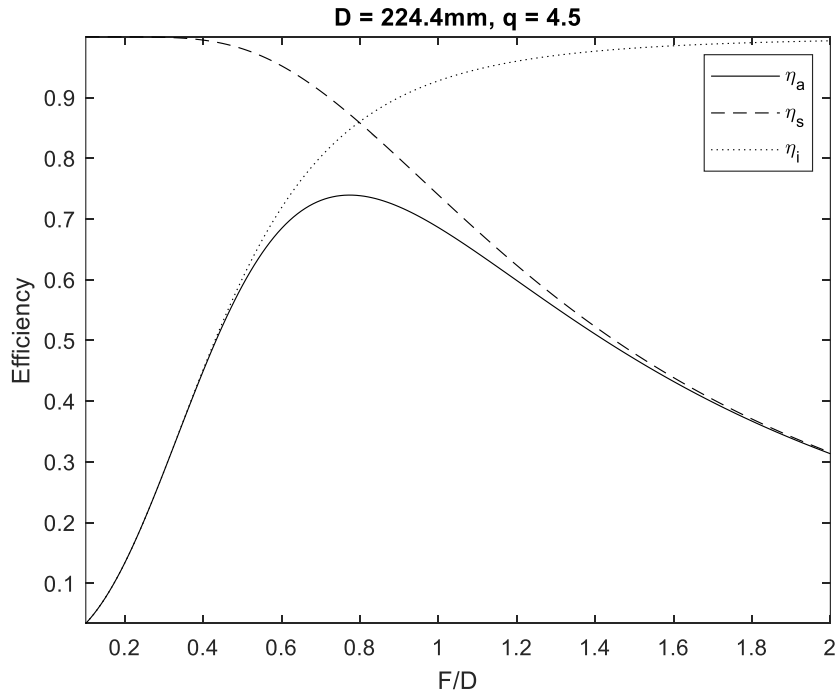


Figure 68: F/D plot for the narrow beamwidth splash plate configuration.

Figure 69 and Figure 70 show the radiation patterns for the new splash-plate reflectarray. The realized gain is 33.9 dB, higher than the 32.6 dB in the previous design. The 3-dB beamwidth remains at 3° as expected. The aperture efficiency of the new reflectarray design is 56.6%

compared to 43% in the previous design. The aperture efficiency is almost on par with the offset feed design. The sidelobe levels are -13.5 dB and -16.5 dB in the E-plane and H-plane, respectively. Although there is significant improvement in the gain, the sidelobe levels are still quite similar gain to the previous design.

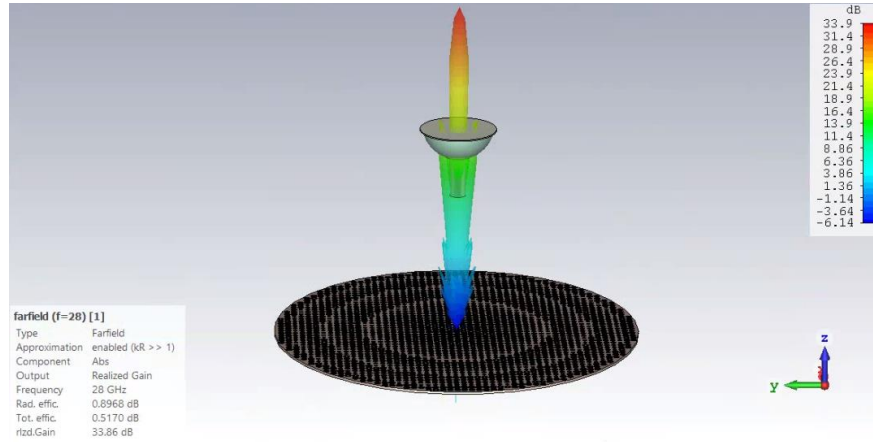


Figure 69: 3D radiation pattern for square ring patch element design with narrow beamwidth splash plate feed @ 28GHz.

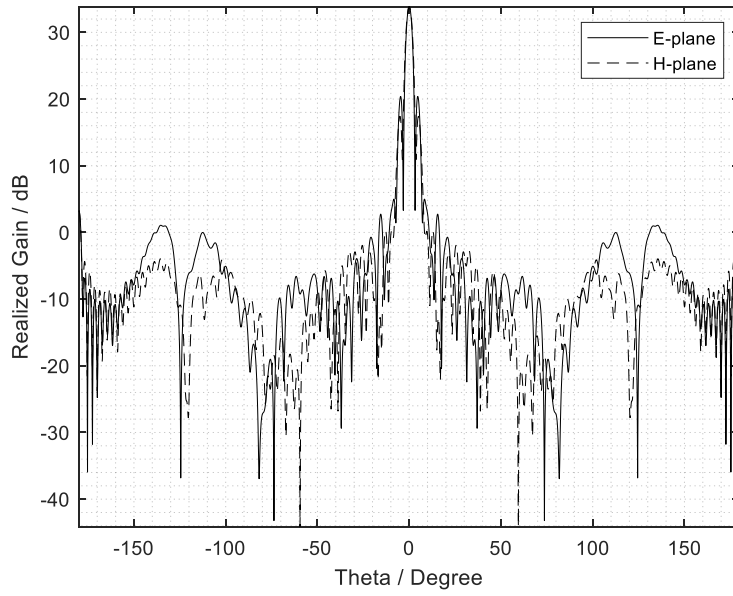


Figure 70: 2D radiation pattern for square ring patch element design with narrow beamwidth splash plate feed @ 28GHz.

8 FABRICATION & MEASUREMENT RESULTS

After exploring and assessing the various designs, the selected configuration for fabrication and testing is the offset square ring patch design with boresight main beam (Chapter 6.1). The support structure is drawn in CST and sent for 3D printing (see Figure 71). The reflectarray aperture is sent for PCB fabrication.

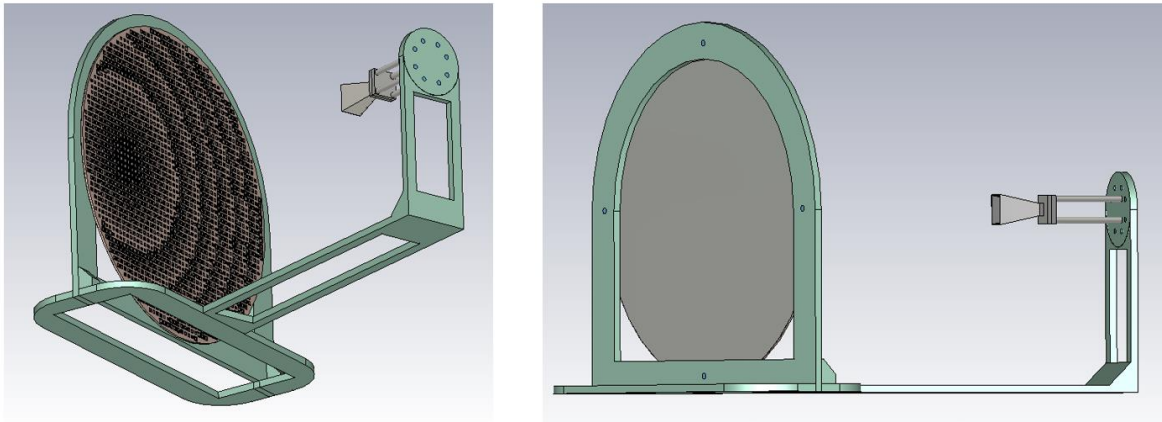


Figure 71: Model of the reflectarray with the holding structure.

The support structure is designed with a lot of “gaps”. Firstly, the cost of 3D printing is not based on complexity but material. Secondly, the gaps will reduce reflections from the structure although it has a low reflective index (plastic material). There are also screw holes used to hold reflectarray in place. Plastic screws are used in place of metallic ones because metallic screws have high reflective index. The fabricated antenna is as shown in Figure 72.

The fabricated reflectarray antenna was tested in a compact range. The boresight is carefully calibrated to achieve accurate result. The measurement used 0.1° step angle and 0.1 GHz step frequency from 26 to 31 GHz, measuring along the E-plane.

The measured radiation pattern is shown in Figure 73. The measured result agrees with the simulated result quite closely, albeit with slightly higher sidelobe on both sides. Note that the

simulation does not consider the holding structure of the reflectarray. The maximum gain is also slightly lower (by $\sim 1\text{dB}$) than the simulated result.



Figure 72: Fabricated reflectarray antenna tested in microwave chamber (left) & compact range (right).

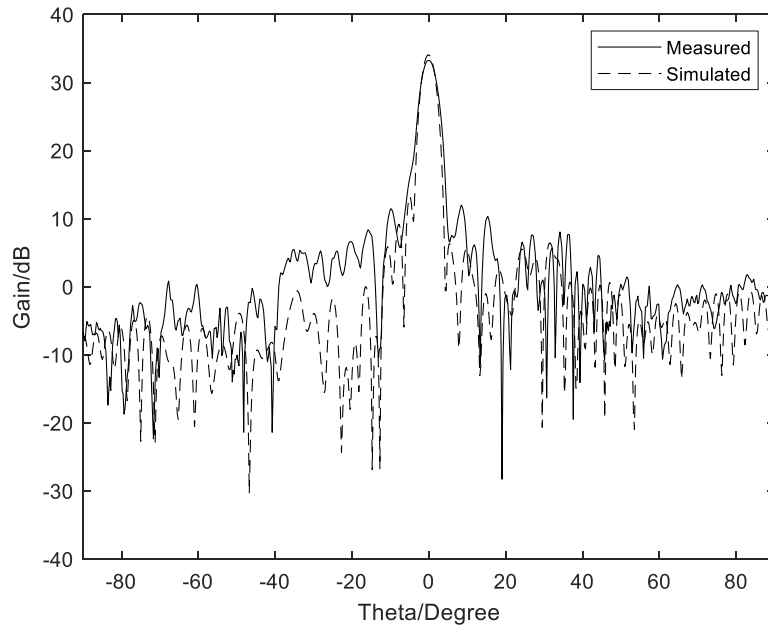


Figure 73: Measured vs simulated result @ 28GHz.

The measured gain-bandwidth performance is compared to the simulation result in Figure 74. Although the gain is lower than the simulation, its 1-dB bandwidth (from 26.4 to 30.7 GHz) of

7.53% is greater than the simulated result of 5.93% (from 26.55 to 29.9 GHz). Overall, the fabricated reflectarray antenna achieved the desired result and goal of this project.

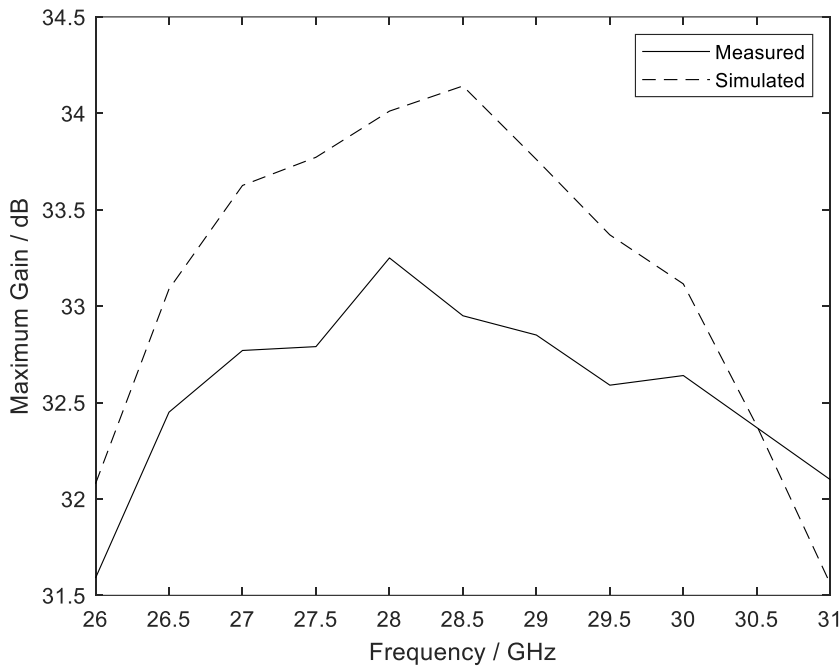


Figure 74: Measured maximum gain over frequencies.

9 CONCLUSION AND FUTURE WORK

Overall, the entire project has been successful with a working fabricated antenna in the end to verify against with simulation result. The main take-away of this work is a gain in general knowledge of how a reflectarray is designed. The thesis had also explored several element designs, showing the improvement from single to multi-resonating elements; the reflectarray phase distribution and different feed configuration. In conclusion, the author had comprehensively covered the core aspect in designing a reflectarray antenna.

Some exploratory work had also been done as shown in the bonus section of this thesis, where a dual band/frequency reflectarray was studied (**which is beyond the scope of this project**). The future work can improve on the design of the dual band/frequency reflectarray.

Lastly, a fully automated reflectarray design software (standalone application) was developed by the author to provide a teaching platform to people with no experience in creating a reflectarray of their own. Anybody interested in the software may contact xuewen@u.nus.edu to download and try out the software.

10 BONUS & EXPLORATION WORK

10.1 DUAL FREQUENCY/BAND REFLECTARRAY FOR 5G COMMUNICATION (28/38GHZ)

10.1.1 Introduction

Recently, the reflectarray antennas are being sought after for its reduced mass, volume and ease of fabrication with high-gain characteristics. However, reflectarray antenna suffers a major drawback of narrowband performance especially when the reflectarray gets larger in size [5]. The bandwidth is limited by two factors: the microstrip patch elements and the differential spatial phase delay [6].

Despite the limitations, the microstrip reflectarray can be adapted for dual-band/frequency purposes. Several methods have been explored to achieve this function such as stacking multiple layers of different-sized elements as seen in [14] and using frequency selective surface (FSS) - backed layers [15] to achieve dual-band characteristics. However, these multi-layering approaches increase weight, volume and fabrication complexity. Single-layer design involves multiple elements on the same surface where accommodation constraints are more prominent hence proper element arrangement is important for this configuration. Several single-layer designs are presented such as the triband reflectarray using three types of elements in [16] and dual-band reflectarray using two crossed dipoles of different frequency band in [17].

5G communications are going to be the future inevitably to meet the demand for high data rate. However, the millimeter-wave frequencies (mm-wave) have propagation limitations due to high path loss, which lead to very short communication distances. The current industry is looking into suitable high gain antenna in order to overcome this problem. Reflectarray antennas are suitable for this application because mm-waves for 5G does not affect the size of the antenna due to its short wavelength [18]. Moreover, reflectarray antenna has less design complexity and is also

more adaptable with shorter wavelength compared to massive MIMO systems. The goal of this chapter is to present a design that operates on the 28/38 GHz that overlaps with the 5G band.

10.1.2 Element Design

The objective of this section is to design different phasing elements that can co-exists together on the same surface. Hence, element shape is an important consideration. The 28 GHz phasing element is a cross-dipole element while the 38 GHz phasing element is a square ring patch element. The 28 and 38 GHz phasing elements have a grid size of 5mm and 2.5mm respectively. The element arrangement is described in Figure 75. The elements are printed on a Rogers 4003C substrate with thickness of 30mil (0.813mm), dielectric constant of 3.55 and loss tangent of 0.0027, backed by a conducting ground plane. Both the element is within the $0.3\sim0.5 \lambda_0$ range in order to reduce grating lobes [5]. The 28/38 GHz phasing elements are simulated independently with CST microwave studio 2018 using the plane wave Floquet mode approach.

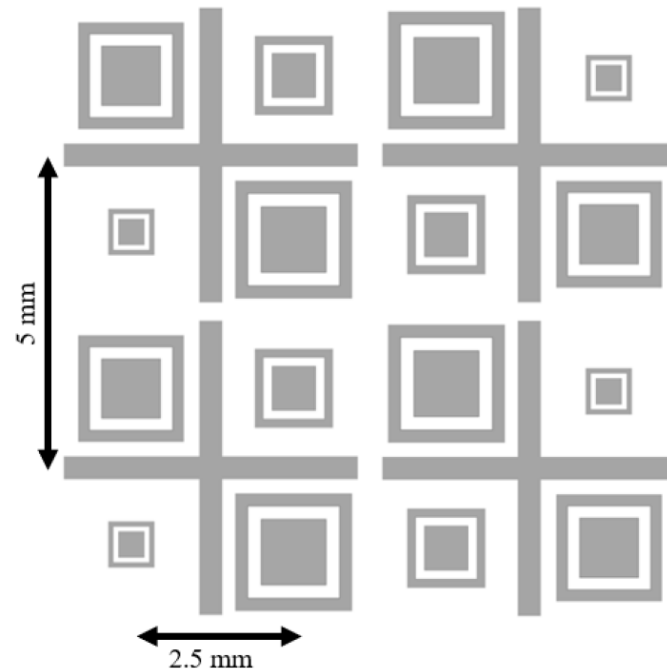


Figure 75: Reflecting surface geometry of a single-layer dual-frequency reflectarray antenna.

The proposed element for the 28 GHz phasing element is made up of dipoles with a fixed thickness of 0.5mm and is arranged in a square lattice with periodicity of 5mm as shown in Figure 76a. The phase variation is controlled by the length of the dipole (L1). The proposed element for the 38 GHz phasing element is made up of square ring patches, a multi-resonator element. However, the maximum size (R1) of the square ring patch can only be less than 2mm because some space has to be reserved for accommodating the dipole. For this paper, the maximum size is chosen to be 1.8mm to prevent the 28 GHz and 38 GHz phasing elements being too close to one another, which might lead to increase mutual coupling between the elements. The phase variation is controlled by the length of the outer square (R1) and has a geometry of $R2=K1\times R1$, $w=K2\times R1$ as shown in Figure 76b, where K1 and K2 are determined to be 0.7 and 0.2 respectively. The reflection phase versus dimension for the phasing elements are shown in Figure 77(a) and (b). Both the elements also demonstrate close to a full cycle phase variation.

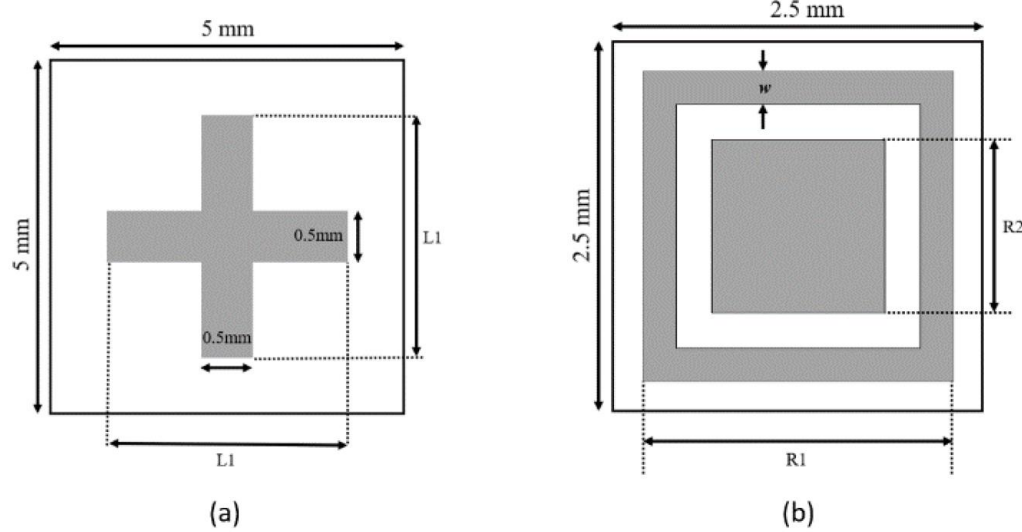


Figure 76: Geometry of the a) 28 GHz cross dipole & b) 38 GHz square ring patch phasing element, $R2=K1\times R1$, $w=K2\times R1$.

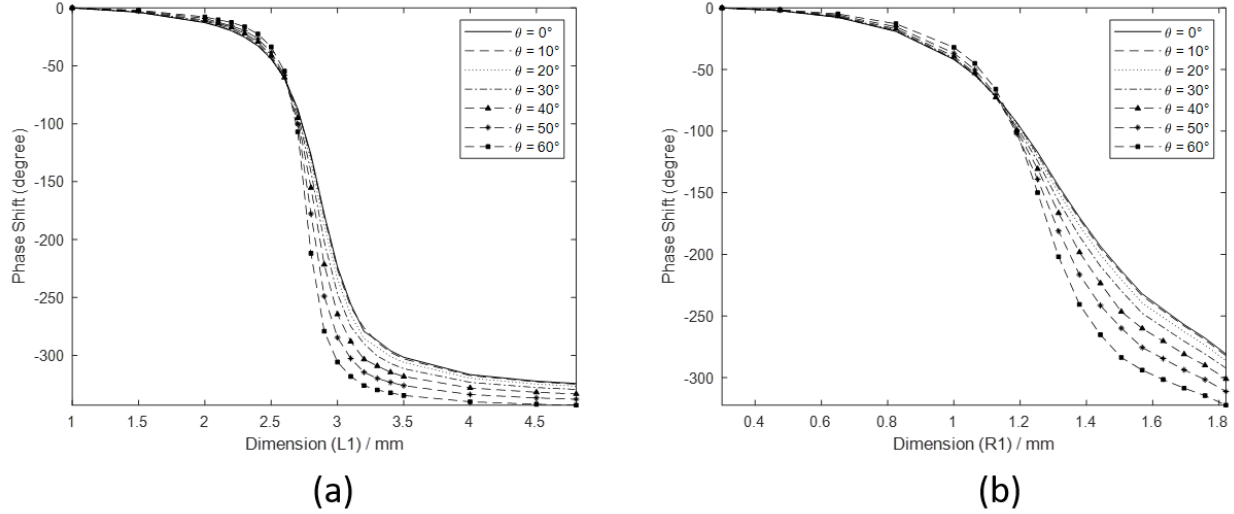


Figure 77: Reflected phase response versus dimension a) Dipole (L_1) & b) Square ring patch (R_1).

10.1.3 System Design

For this section, an offset fed configuration is considered to reduce aperture blockage by the feed and holding structure. The effect is usually more significant in small reflectarray where the feed has a similar proportion to the aperture. Aperture blockage will lead to increase in sidelobe level and reduction in antenna gain. The reflectarray aperture is square shape with side length of 135mm with 27×27 28GHz & 54×54 35GHz elements. It is illuminated by a pyramidal horn with an offset angle of 29.59° . The horn has a q-value of 11.5 at 38 GHz and 6.4 at 28 GHz. The F/D value is determined analytically, using the method introduced in [7]. The F/D plot is being plotted for each q-value in Figure 78. An F/D ratio of 0.9 is chosen. The desired main beam is tilted 30° away from the boresight of the reflectarray aperture for 28GHz and 0° for 38 GHz. The partial reason for this configuration is to make sure there is a good distribution between the large and small elements and to further decrease the mutual coupling (e.g. if both frequencies have the same desired main beam, most of the bigger elements will be placed in the middle). The phase distribution curve for both 28 GHz and 38 GHz are shown in Figure 79 and the schematic drawing of the reflectarray is given in Figure 80.

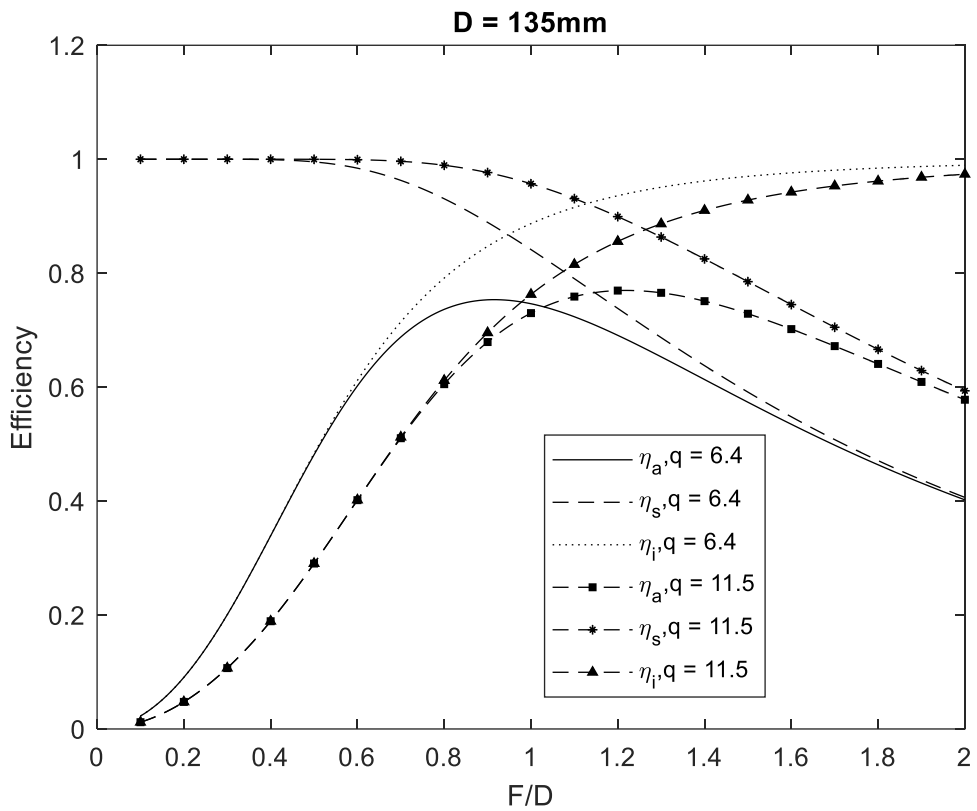


Figure 78: F/D curve for the proposed design.

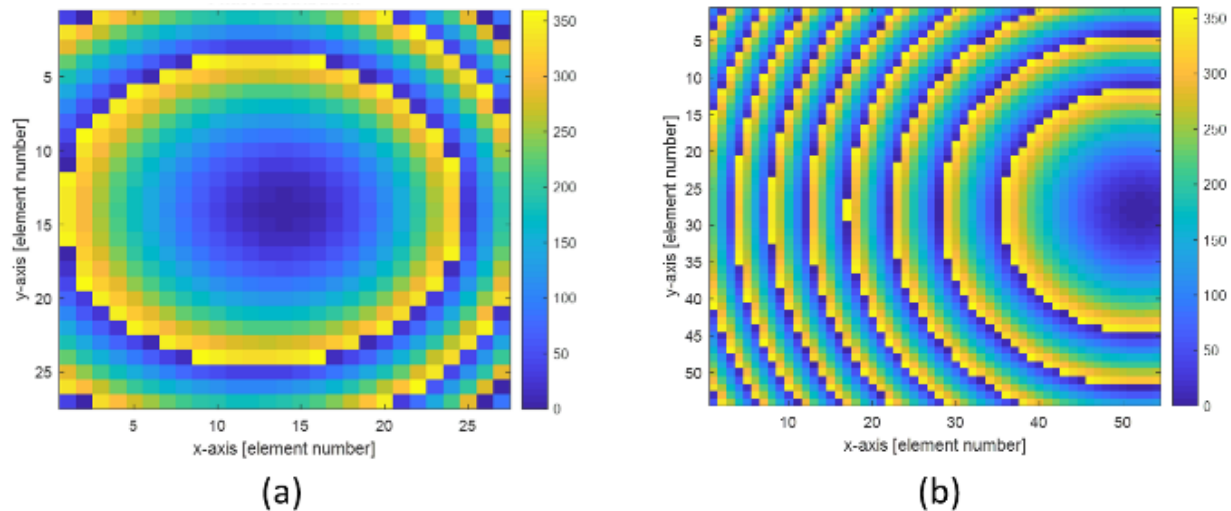


Figure 79: Phase distribution curve for a) 28 GHz & b) 38 GHz.

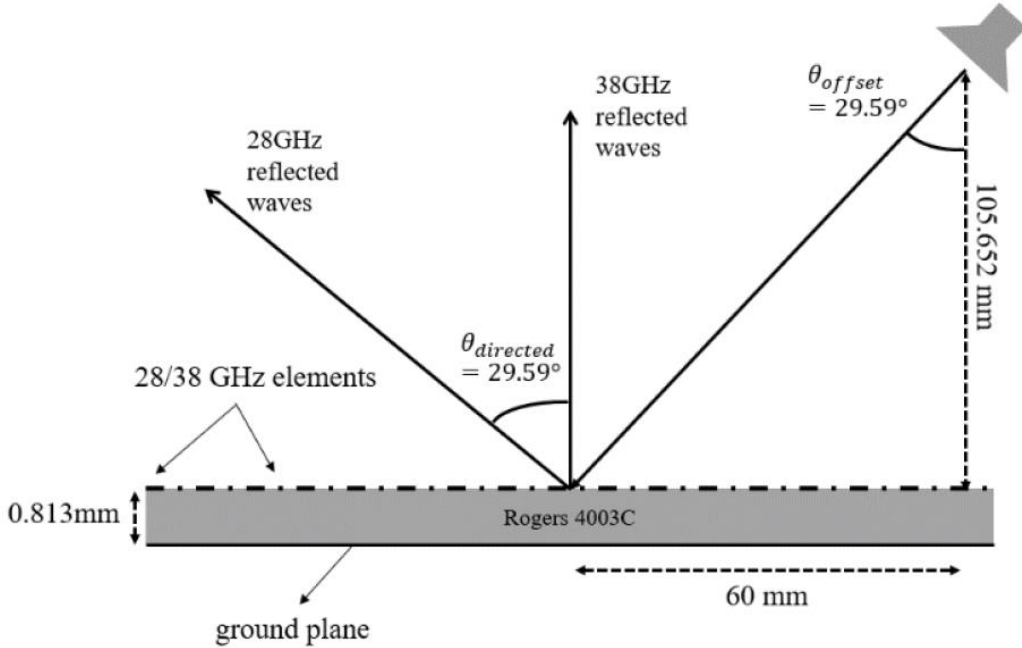


Figure 80: Schematic view of the dual-frequency reflectarray.

10.1.4 Full-wave Simulation Result

The designed reflectarray is analyzed using CST Microwave studio TLM solver. The simulated radiation patterns at 28 and 38 GHz are plotted along the E-plane as shown in Figure 81a. At 28GHz, the sidelobe levels are -14.5 dB and -21.0 dB, while at 38 GHz the sidelobe levels are -20.1 and -24.0 dB. Another noticeable trait is at 38GHz, the gain at around 30° is slightly higher than the other angle probably due to the slight reflection from the 28GHz elements. Other than its operating frequency, a broadband performance is also accomplished in this design especially at the higher frequency range where it reaches the Q-band. As the frequency increases, the gain of an aperture antenna usually also increases, hence it is more appropriate to check the antenna performance by using aperture efficiency instead. The antenna aperture efficiency and realized gain are plotted against frequency in Figure 81b. Figure 82 is a 3D radiation pattern plot for both 28 and 38 GHz.

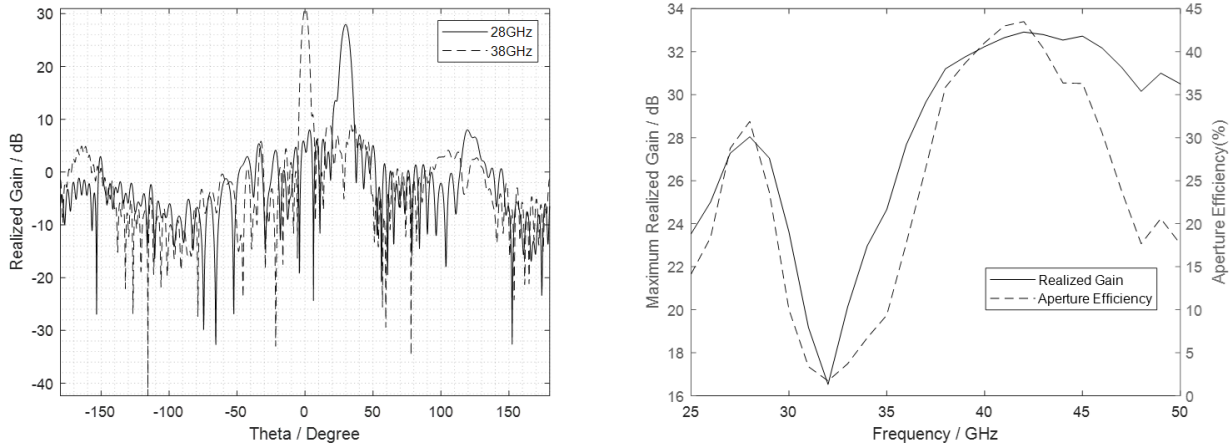


Figure 81: a) Simulated radiation patterns at 28 GHz and 38 GHz; b) Simulated gain and aperture efficiency in frequency band.

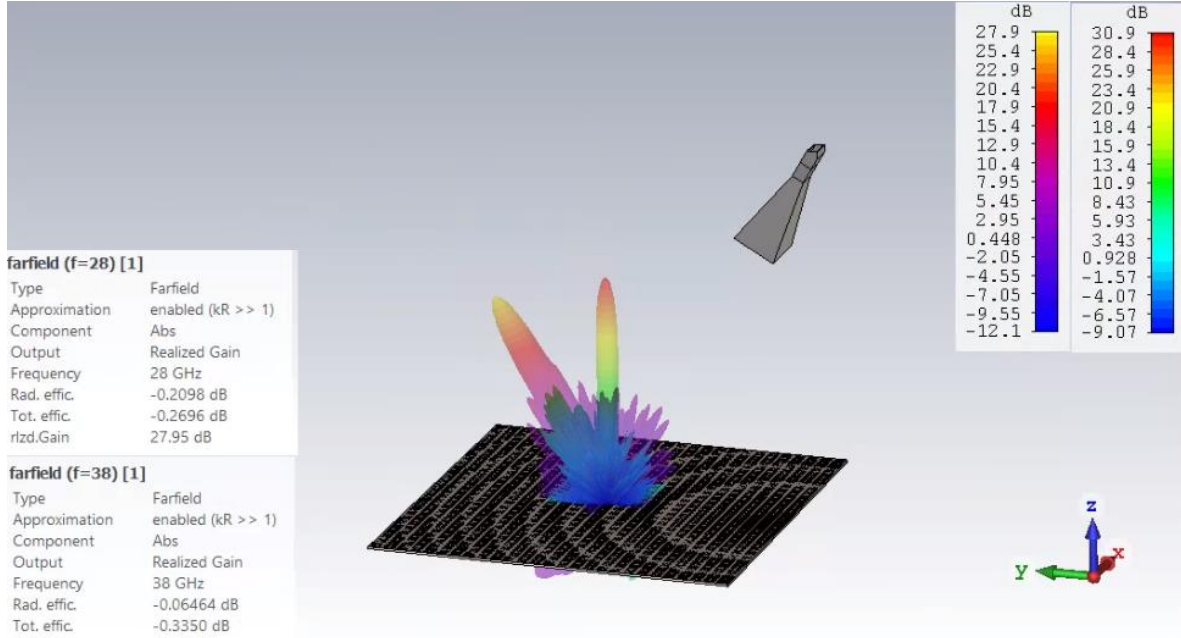


Figure 82: 3D radiation pattern for both 28GHz and 38GHz stacked together.

A dual-frequency reflectarray is achieved at both 28GHz and 38GHz. The full-wave simulated result has shown that the gains are 28.08 dB at 28 GHz and 31.04 dB at 38GHz with decent aperture efficiency of 32.17% and 34.53% respectively. Other than its operating frequency, the proposed antenna can also be used in Q-Band frequency with a peak aperture efficiency of 43.5% at 42 GHz.

10.2 AUTOMATED REFLECTARRAY DESIGN APP

A software was developed as a side-project while doing this FYP. The software can be used for professional antenna design or a teaching platform to introduce the reflectarray antenna concept to people with zero experience for this topic. Everything was designed and programmed by the author. A rough illustration of the software is as shown here:

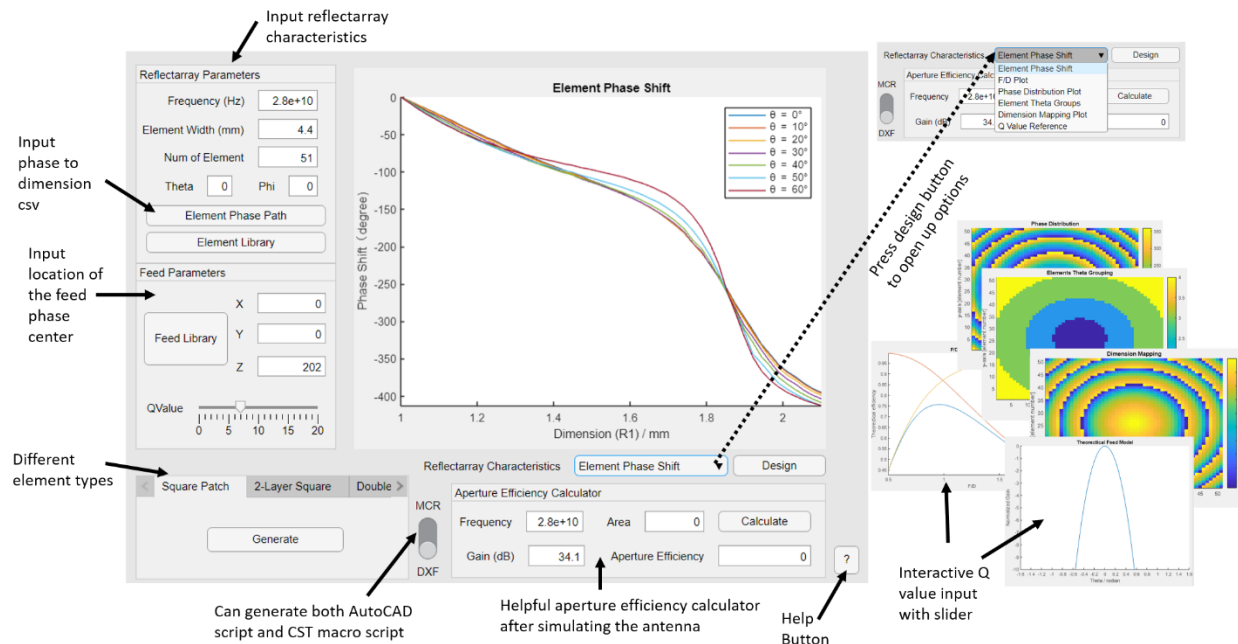


Figure 83: Graphics user interface of the reflectarray design application.

The author had also used the software to experiment with different kind of reflectarray configuration and had achieved consistent results. An element library is also given to guide users on how to format the csv file before feeding it into the reflectarray application. A feed library of various pyramidal horns is also given to allow users to try out different F/D. MCR script automation is also provided, if the user does not have AutoCAD. This script will draw in the CST software directly but at slightly slower speed than importing the dxf format from AutoCAD. Interactive q value slider was also programmed to let the user play with different q value to see the change in the theoretical feed model (for q value reference) and F/D plot will also be updated.

10.3 RADIATION ANALYSIS TECHNIQUES

With recent improvement in personal computer's computational power, this analysis is optional. However, at times when simulation software is unavailable or computer does not have the necessary hardware to compute the radiation pattern, this approach can provide quick insights to the radiation pattern of the reflectarray. The analysis is based on Array Theory provided by [4]. The main idea behind this concept is to sum up all the element's radiation. The author has programmed a tool to predict the radiation of the reflectarray based on the Array Theory. Note that the prediction does not account for the coupling effect. Figure 84 shows the comparison between Array Theory and CST simulation for a 27×27 offset-fed reflectarray at 28GHz. Even though, the prediction does not 100% matched with the CST simulation, the main beam pattern is quite similar. Unlike the CST simulation, Array Theory prediction takes less than 10 seconds compared to hours.

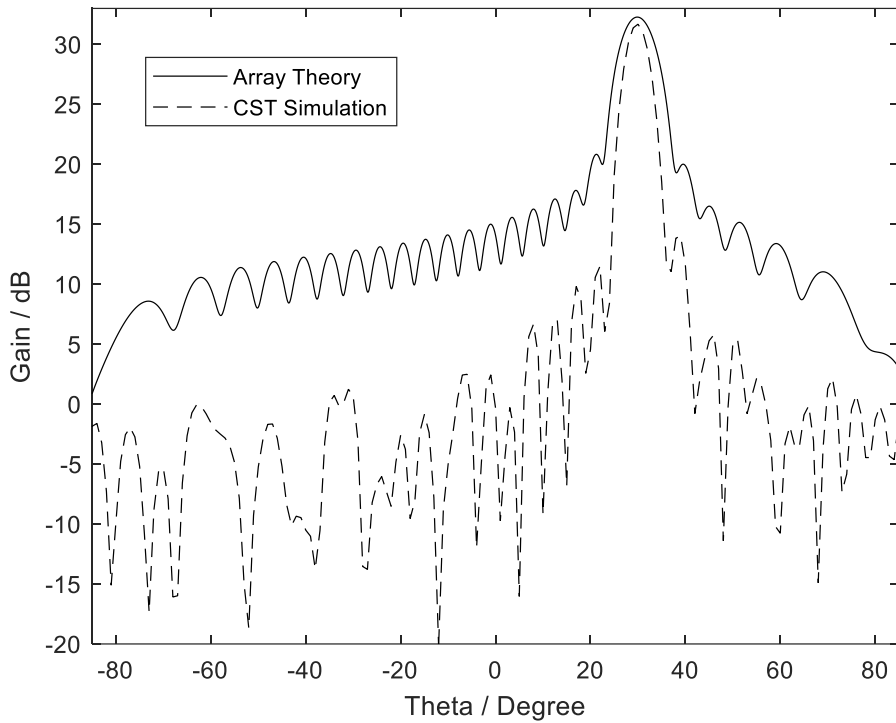


Figure 84: Array Theory vs CST Simulation radiation pattern.

REFERENCES

- [1] Dassault Systemes, "CST - Computer Simulation Technology," [Online]. Available: <https://www.cst.com/products/cstmws>.
- [2] C. A. Balanis, Antenna Theory Analysis And Design Fourth Edition, New Jersey: Wiley, 2016.
- [3] D. G. Berry, R. G. Malech and W. A. Kennedy, "The reflectarray antenna," *IEEE Trans.Antennas Propagat.*, Vols. AP - 11, pp. 645-651, 1963.
- [4] P. Nayeri, F. Yang and A. Z. Elsherbini, Reflectarray Antennas: Theory, Designs, and Applications, Wiley IEEE Press, 2018.
- [5] J. Huang and J. A. Encinar, Reflectarray Antennas, New Jersey: John Wiley & Sons, 2008.
- [6] J. Huang, "Bandwidth study of microstrip reflectarray and a novel phased reflectarray concept," *IEEE AP-S/URSI symposium*, pp. 1134-1137, 1998.
- [7] A. Yu, F. Yang, A. Z. Elsherbini, J. Huang and Y. Rahmat-Samii, "APERTURE EFFICIENCY ANALYSIS OF REFLECTARRAY," *MICROWAVE AND OPTICAL TECHNOLOGY LETTERS*, vol. 52, no. 2, pp. 364-372, 2010.
- [8] E. Carrasco, M. Barba and J. Encinar, "Aperture-coupled reflectarray element with wide range of phase delay," *ELECTRONICS LETTERS*, vol. 42, no. 12, 2006.
- [9] J. Encinar and J. Zornoza, "Broadband design of three-layer printed reflectarrays," *IEEE Transactions on Antennas and Propagation*, vol. 51, no. 7, pp. 1662 - 1664, 2003.
- [10] M. E. Bialkowski and K. H. Sayidmarie, "Investigations Into Phase Characteristics of a Single-Layer Reflectarray Employing Patch or Ring Elements of Variable Size," *IEEE Transactions on Antennas and Propagation*, vol. 56, no. 11, pp. 3366-3372, 2008.
- [11] A - INFO, *LB-28-15 Datasheet*, China: A-INFO.
- [12] P. J. Bevelacqua, "The Parabolic Reflector Antenna (Satellite Dish)," Antenna-Theory.com, [Online]. Available: <http://www.antenna-theory.com/antennas/reflectors/dish.php>. [Accessed 2019 February 2019].
- [13] D.P.S.Malik and G. James, "Splash Plate Feed Design," *5th European Microwave Conference*, pp. 41-45, 1975.
- [14] C. Han, C. Rodenbeck, J. Huang and K. Chang, "A C/Ka dual frequency dual layer circularly polarized reflectarray antenna with microstrip ring elements," *IEEE Trans Antennas Propag*, vol. 52, no. 11, pp. 2871-2876, 2004.
- [15] M. R. Chaharmir, J. Shaker and H. Legay, "Dual-band Ka/X reflectarray with broadband loop elements," *Microw. Antennas Propag*, vol. 4, pp. 225-231, 2010.

- [16] F. Yang, Y. Kim, J. H. A. Yu and A. E. Elsherbeni, "A Single Layer Reflectarray Antenna for C/X/Ka," in *ICEAA*, Italy, 2007.
- [17] R. Chaharmir, J. Shaker and M. Cuhaci, "Development of dual-band circularly polarised reflectarray," *Inst. Elect. Eng. Proc., Microw. Antennas Propag.*, vol. 153, no. 1, pp. 49-54, 2003.
- [18] M. H. Dahri, M. H. Jamaluddin, M. I. Abbasi and M. R. Kamarudin, "A Review of Wideband Reflectarray Antennas for 5G Communication," *IEEE Access*, vol. 5, pp. 17803-17815, 2017.

APPENDIX A – REFLECTARRAY AUTOMATION APP ALGORITHM

Reflectarray Phase Distribution (Snippets)

```
function RAApertureScript(app)
    OpFreq = app.FrequencyHzEditField.Value;
    NumElement1axis = app.NumofElementEditField.Value;
    ElementSize_mm = app.ElementWidthmmEditField.Value;
    Feedpos =
    [app.XEditField.Value,app.YEditField.Value,app.ZEditField.Value]; %x,y,z
    Radius = ElementSize_mm*NumElement1axis/2;

    app.Element = zeros(NumElement1axis,NumElement1axis);
    TotalElement = NumElement1axis*NumElement1axis;
    app.ElementCoord = zeros(TotalElement,2);
    Counter = 1;
    XStart = -((floor(NumElement1axis/2))*ElementSize_mm); %1st Element
    YStart = ((floor(NumElement1axis/2))*ElementSize_mm);
    YSteps = 0;
    XSteps = 0;
    YCoord = 0;
    XCoord = 0;
    GridWidth = ElementSize_mm;
    Wavelength = 299792458/OpFreq;
    WaveNumber = (2*pi)/Wavelength; %K0
    PhaseConstant = 0;
    %PhaseConstant = 168*pi/180;
    %PhaseConstant = -84.01*pi/180;
    ElementNum = zeros(TotalElement,2);
    app.ElementAngle = zeros(TotalElement,1);

    %Direction of the beam
    %Since it is all perpendicular to plane hence all 0
    theta = app.ThetaEditField.Value * pi/180; %theta0
    phi = app.PhiEditField.Value * pi/180; %theta0

    for j = 1:1:NumElement1axis
        YCoord = YStart - YSteps;
        for i = 1:1:NumElement1axis
            XCoord = XStart + XSteps;
            DistFeed = sqrt((XCoord-Feedpos(1))^2 + (YCoord-Feedpos(2))^2
+ (0-Feedpos(3))^2);
            DistFeed = DistFeed*0.001; %Ri in meter
            PhaseRA = WaveNumber * (DistFeed - sin(theta) *
(XCoord*0.001*cos(phi) + YCoord*0.001*sin(phi))) + PhaseConstant;
            PhaseRA = PhaseRA*(180/pi); %Convert to degree
            app.Element(j,i) = PhaseRA;
            app.ElementCoord(Counter,1) = XCoord;
            app.ElementCoord(Counter,2) = YCoord;
        end
        Counter = Counter + 1;
    end
```

```
    app.ElementAngle(Counter,1) =
acos((Feedpos(3)*0.001)/DistFeed)*180/pi;
    ElementNum(Counter,1) =i ;
    ElementNum(Counter,2) =j ;
    Counter = Counter + 1;
    XSteps = XSteps + GridWidth;
end
XSteps = 0;
YSteps = YSteps + GridWidth;
end
PhaseConstant = min(min(app.Element));
app.Element = app.Element - PhaseConstant;
app.Element = rem(app.Element, 360);

end
```

Reflectarray F/D Calculations (Snippets)

```
function FDPlot(app)
    ElemWidth = app.ElementWidthmmEditField.Value;
    NumElem = app.NumofElementEditField.Value;
    %F/D Code
    %Spillover Efficiency
    app.HDRatio = 0.1:0.01:2;
    HDLength = length(app.HDRatio);
    app.NsMat = zeros(1,HDLength);
    D = ElemWidth*NumElem;
    q = app.qvalue;
    Id = (2*pi)/(2*q + 1);
    %Square
    for i = 1:1:HDLength
        HDR = app.HDRatio(i);
        H = HDR*D;
        r0 = H;
        Pr = @(x,y)
        (H./((sqrt(x.^2+y.^2+H^2)).^3)).*((r0^2+(sqrt(x.^2+y.^2+H^2)).^2-
        (sqrt(x.^2+y.^2)).^2)./(2*r0*(sqrt(x.^2+y.^2+H^2))).^(2*q));
        In = integral2(Pr,-(D/2),(D/2),-(D/2),(D/2), 'Method', 'iterated');
        Ns = In/Id;
        app.NsMat(i) = Ns;
    end
    %Illumination Efficiency
    %Square
    qe = 1;
    app.NiMat = zeros(1,HDLength);
    for i = 1:1:HDLength
        HDR = app.HDRatio(i);
        H = HDR*D;
        r0 = H;
        I_D = @(x,y)
        (((H^qe)./(sqrt(x.^2+y.^2+H^2)).^(1+qe))).*((r0^2+(sqrt(x.^2+y.^2+H^2)).^2-
        (sqrt(x.^2+y.^2)).^2)./(2*r0.*sqrt(x.^2+y.^2+H^2))).^(q)).^2;
        Denominator = integral2(I_D,-(D/2),(D/2),-
        (D/2),(D/2), 'Method', 'iterated');
        I_N = @(x,y)
        (((H^qe)./(sqrt(x.^2+y.^2+H^2)).^(1+qe))).*((r0^2+(sqrt(x.^2+y.^2+H^2)).^2-
        (sqrt(x.^2+y.^2)).^2)./(2*r0.*sqrt(x.^2+y.^2+H^2))).^(q));
        Norminator = (abs(integral2(I_N,-(D/2),(D/2),-
        (D/2),(D/2), 'Method', 'iterated')))^2;
        Aa = D*D;
        Ni = (1/Aa)*(Norminator/Denominator);
        app.NiMat(i) = Ni;
    end
    %Efficiency
    app.NMat = app.NsMat.*app.NiMat; end;
```

Reflectarray Element Mapping (Snippets)

```
function Mapping(app)
    Counter = 1;
    UnitPhase = app.ProcessedReport;
    Dim = UnitPhase(:,1);
    [~,Numplot] = size(UnitPhase);
    for i = 2:1:Numplot
        DataTheta(:,i-1) = UnitPhase(:,i) - min(UnitPhase(:,i));
    end

    NumElement1axis = app.NumofElementEditField.Value;
    ElementDim = zeros(NumElement1axis,NumElement1axis);
    DistributionData = app.Element;

    for j = 1:1:NumElement1axis
        for i = 1:1:NumElement1axis
            if app.ElementAngle(Counter,1) > 60
                Dimension =
spline(DataTheta(:,7),Dim,DistributionData(j,i));
                if Dimension < min(Dim)
                    Dimension = min(Dim);
                end
                ElementDim(j,i) = Dimension;
            elseif app.ElementAngle(Counter,1) > 50
                Dimension =
spline(DataTheta(:,6),Dim,DistributionData(j,i));
                if Dimension < min(Dim)
                    Dimension = min(Dim);
                end
                ElementDim(j,i) = Dimension;
            elseif app.ElementAngle(Counter,1) > 40
                Dimension =
spline(DataTheta(:,5),Dim,DistributionData(j,i));
                if Dimension < min(Dim)
                    Dimension = min(Dim);
                end
                ElementDim(j,i) = Dimension;
            elseif app.ElementAngle(Counter,1) > 30
                Dimension =
spline(DataTheta(:,4),Dim,DistributionData(j,i));
                if Dimension < min(Dim)
                    Dimension = min(Dim);
                end
                ElementDim(j,i) = Dimension;
            elseif app.ElementAngle(Counter,1) > 20
                Dimension =
spline(DataTheta(:,3),Dim,DistributionData(j,i));
                if Dimension < min(Dim)
```

```

        Dimension = min(Dim);
    end
    ElementDim(j,i) = Dimension;
elseif app.ElementAngle(Counter,1) > 10
    Dimension =
spline(DataTheta(:,2),Dim,DistributionData(j,i));
    if Dimension < min(Dim)
        Dimension = min(Dim);
    end
    ElementDim(j,i) = Dimension;
else
    Dimension =
spline(DataTheta(:,1),Dim,DistributionData(j,i));
    if Dimension < min(Dim)
        Dimension = min(Dim);
    end
    ElementDim(j,i) = Dimension;
end
Counter = Counter + 1;
end
end
app.ElementDim2D = ElementDim;
app.ElementDim1D = ElementDim(:);

end

```

Reflectarray CAD Scripting for one of the elements (Double Circular)

```
Dimension = app.ElementDim1D;
Coordinates = app.ElementCoord;
K1 = app.K1EditField.Value;
K2 = app.K2EditField.Value;
NumElement1axis = app.NumofElementEditField.Value;

TotalElement = NumElement1axis*NumElement1axis;
Radius = NumElement1axis*app.ElementWidthmmEditField.Value/2;
f = uifigure('Position',[300 300 400 120]);
d = uiprogressdlg(f,'Title','Scripting in Progress',...
    'Indeterminate','on','Cancelable','on');

if app.ScriptFormatSwitch.Value == "DXF"
    Script =
fopen('OneStopRA/DoubleCircularRing/DoubleCircular.scr','w');
W = K2*(Dimension(:,1));
OuterRingInner = 2*(Dimension(:,1)-W);
OuterRingOuter = 2*(Dimension(:,1));
InnerRingOuter = 2*K1*(Dimension(:,1));
InnerRingInner = 2*(K1*(Dimension(:,1))-W);

Report = cat(2,Coordinates,Dimension);
Report = cat(2,Report,InnerRingInner);
Report = cat(2,Report,InnerRingOuter);
Report = cat(2,Report,OuterRingInner);
Report = cat(2,Report,OuterRingOuter);

for i = 1:1:TotalElement

    xi = Report(i,1);
    yi = Report(i,2);
    ElementDist = sqrt(xi^2 + yi^2);

    if ElementDist > Radius
        continue;
    end

    fprintf(Script,'DONUT\n');
    fprintf(Script,'%f\n',Report(i,4));
    fprintf(Script,'%f\n',Report(i,5));
    fprintf(Script,'%f',Report(i,1));
    fprintf(Script,'%f\n',Report(i,2));
    fprintf(Script,'\n');

    fprintf(Script,'DONUT\n');
    fprintf(Script,'%f\n',Report(i,6));
    fprintf(Script,'%f\n',Report(i,7));
```

```

        fprintf(Report,'%f',Report(i,1));
        fprintf(Report,'%f\n',Report(i,2));
        fprintf(Report,'\n');
    end

    fclose(Report);

elseif app.ScriptFormatSwitch.Value == "MCR"
    Script =
fopen('OneStopRA/DoubleCircularRing/DoubleCircular.mcr','w');
    fprintf(Report,'Sub Main ()\n');
    fprintf(Report,'Component.New "Ring"\n');
    W = K2*(Dimension(:,1));
    OuterRingInner = (Dimension(:,1)-W);
    OuterRingOuter = (Dimension(:,1));
    InnerRingOuter = K1*(Dimension(:,1));
    InnerRingInner = (K1*(Dimension(:,1))-W);

    Report = cat(2,Coordinates,Dimension);
    Report = cat(2,Report,InnerRingInner);
    Report = cat(2,Report,InnerRingOuter);
    Report = cat(2,Report,OuterRingInner);
    Report = cat(2,Report,OuterRingOuter);

    for i = 1:1:TotalElement

        xi = Report(i,1);
        yi = Report(i,2);
        ElementDist = sqrt(xi^2 + yi^2);

        if ElementDist > Radius
            continue;
        end
        fprintf(Report,'With Cylinder\n');
        fprintf(Report,'    .Reset\n');
        fprintf(Report,'    .Name "Outer %d"\n',i);
        fprintf(Report,'    .Component "Ring"\n');
        fprintf(Report,'    .Material "PEC"\n');
        fprintf(Report,'    .OuterRadius "%f"\n',0.5*Report(i,7));
        fprintf(Report,'    .InnerRadius "%f"\n',0.5*Report(i,6));
        fprintf(Report,'    .Axis "z"\n');
        fprintf(Report,'    .Zrange "0", "0"\n');
        fprintf(Report,'    .Xcenter "%f"\n',0.5*Report(i,1));
        fprintf(Report,'    .Ycenter "%f"\n',0.5*Report(i,2));
        fprintf(Report,'    .Segments "0"\n');
        fprintf(Report,'    .Create\n');
        fprintf(Report,'End With\n');

    end

```

```

for i = 1:1:TotalElement

    xi = Report(i,1);
    yi = Report(i,2);
    ElementDist = sqrt(xi^2 + yi^2);

    if ElementDist > Radius
        continue;
    end
    fprintf(Report,'With Cylinder\n');
    fprintf(Report,'    .Reset\n');
    fprintf(Report,'    .Name "Inner %d"\n',i);
    fprintf(Report,'    .Component "Ring"\n');
    fprintf(Report,'    .Material "PEC"\n');
    fprintf(Report,'    .OuterRadius "%f"\n',0.5*Report(i,5));
    fprintf(Report,'    .InnerRadius "%f"\n',0.5*Report(i,4));
    fprintf(Report,'    .Axis "z"\n');
    fprintf(Report,'    .Zrange "0", "0"\n');
    fprintf(Report,'    .Xcenter "%f"\n',0.5*Report(i,1));
    fprintf(Report,'    .Ycenter "%f"\n',0.5*Report(i,2));
    fprintf(Report,'    .Segments "0"\n');
    fprintf(Report,'    .Create\n');
    fprintf(Report,'End With\n');

end
fprintf(Report,'End Sub');
fclose(Report);
end

```

Reflectarray Radiation Pattern Analysis (Snippets)

```
GridSize = app.GridWidthEditField.Value*1e-3;
    NumElement = app.ElementPerAxisEditField.Value;
    xPos = app.xEditField.Value*1e-3;
    yPos = app.yEditField.Value*1e-3;
    zPos = app.zEditField.Value*1e-3;
    Feedpos = [xPos,yPos,zPos]; %X Y Z
%Initiate
YSteps = 0;
XSteps = 0;
%Reflectarray Parameters
OpFreq = app.FreqEditField.Value * 1e9;
Wavelength = 299792458/OpFreq;
k = (2*pi)/Wavelength; %K0
theta_b = app.Theta_bEditField.Value * pi/180; %theta0
phi_b = app.Phi_bEditField.Value * pi/180;
qf = app.qfEditField.Value;
qe = app.qeEditField.Value;
Phi = app.ObservationPhiEditField.Value * pi/180;
Counter_Temp = 0;

for Theta = -1.5:0.001:1.5
    XStart = -((floor(NumElement/2))*GridSize);
    YStart = (floor(NumElement/2))*GridSize;
    YSteps = 0;
    EFieldSum = 0;
    Counter_Temp = Counter_Temp + 1;
    for j = 1:1:NumElement
        YCoord = YStart - YSteps; %Coord = coordinate of mnth element
        for i = 1:1:NumElement %This is where the real action is
            XCoord = XStart + XSteps;
            rfvec = Feedpos;
            rmnvec = [XCoord,YCoord,0]; %Center = 0,0,0
            rvec = rmnvec - rfvec;
            FeedHeight = Feedpos(3);
            Theta_e = acos(FeedHeight/norm(rvec));
            Theta_f = acos(((norm(rfvec))^2 + (norm(rvec))^2 -
            (norm(rmnvec))^2)/(2*norm(rfvec)*norm(rvec)));
            XSteps = XSteps + GridSize;
            uvec = [sin(Theta)*cos(Phi), sin(Theta)*sin(Phi),
            cos(Theta)];
            Phi_mn = k * (norm(rvec) - sin(theta_b) *
            (XCoord*cos(phi_b) + YCoord*sin(phi_b)));
            EField_1element =
            (((cos(Theta))^qe)*((cos(Theta_f))^qf)/norm(rvec))...
                *exp(-sqrt(-1)*k*(norm(rvec)-dot(rmnvec,uvec)))...
                *((cos(Theta_e))^qe)*exp(sqrt(-1)*Phi_mn);
            EFieldSum = EFieldSum + EField_1element;
```

```
    end
    XSteps = 0;
    YSteps = YSteps + GridSize;
end
EFieldTotal(Counter_Temp) = 10*log10(abs(EFieldSum));
end
theta_rad = -1.5:0.001:1.5;
theta_deg = theta_rad*180/pi;
plot(app.UIAxes,theta_deg,EFieldTotal);
set(app.UIAxes,'xminorgrid','on','yminorgrid','on')
```

APPENDIX B – HEALTH & SAFETY

For this FYP, the main danger came from testing the antenna in the compact range as the author had to climb up to the testing platform in order to test his antenna. The testing platform was more than 3m tall hence a fall might cause serious injuries. In order to mitigate the danger, the author wore full covered shoes with good grip and made sure there were 2 more person to supervise and provide assistance.

Another danger came from using the testing equipment in the microwave lab. As the test equipment was highly sensitive, several measures were put in place to protect both users and the equipment. The author had to wear a lab coat and a “grounding” wristband before using the equipment.

Lastly, the author had also taken the compulsory safety quiz to ensure he is certified to operate in the lab safely.